Exchange of Volatile Organic Compounds at the Atmosphere-Soil Interface

Dissertation
zur Erlangung des Grades
'Doktor rerum naturalium (Dr. rer.nat.)'
im Promotionsfach Chemie
am Fachbereich Chemie, Pharmazie und Geowissenschaften
der Johannes Gutenberg-Universität in Mainz
Paul Crutzen Graduate School

Guo Li
geb. am 12.07.1985 in Xingtai/Hebei, China

Mainz, Germany, Aug. 2018

I hereby declare that I wrote the dissertation without any unauthorized external assistance. I used only sources acknowledged in the work. All textual passages which are appropriated verbatim or paraphrased from published and unpublished texts as well as all information obtained from oral sources are duly indicated and listed in accordance with bibliographical rules. In carrying out this research, I complied with the rules of standard scientific practice as formulated in the statutes of Johannes Gutenberg-University Mainz to insure standard scientific practice.

Abstract

Volatile organic compounds (VOCs) play a crucial role in atmospheric chemistry, contributing to the formation of ozone and secondary organic aerosols. Exchange processes at the atmosphere-soil interface can potentially affect the budget of VOCs in the atmosphere. Knowledge about VOC exchange at the atmosphere-soil interface, however, is still very limited. Thus, the main parts of the PhD project presented in this thesis are aimed at exploring the atmosphere-soil exchange properties and processes of different species of VOC.

The first two parts of this work cover laboratory experiments and field measurements. For both studies, a coated-wall flow tube technique is employed, which allows us to investigate the uptake and heterogeneous reaction kinetics of VOCs at soil surfaces. The lab experiment focuses on formaldehyde (HCHO), which is an important precursor of OH radical and a key intermediate of VOC oxidation reactions but has one or several missing sinks/sources to be identified. The observed uptake and re-emission of HCHO reveals a bi-directional exchange on soil surfaces, suggesting that soil could serve either as a source or a sink depending on ambient conditions and trace gas concentrations. Further kinetic analysis shows that HCHO uptake on soil is a partially reversible process involving both adsorption/desorption and chemical reactions. With co-existence of water molecules, water vapor can exert a competition effect for reactive sites on soil with HCHO molecules and therefore influence the exchange behavior of HCHO. The field measurement, which is performed at an urban background site in Beijing, is intended to investigate exchange properties of VOCs at the atmosphere-soil interface under ambient conditions. The derived uptake coefficients (γ) and corresponding deposition velocities (V_d) or surface resistances (R_c) exhibit different average values and temporal variabilities for different VOCs. Most of the VOCs show a long-term net deposition. However, formic acid is emitted from the soil. The correlation analysis suggests that the emitted formic acid is most probably arising from the heterogeneous oxidation of other deposited VOCs.

The last part is designed to optimize the usage of the coated-wall flow tube technique from a technical point of view. Coated-wall flow tube reactors are frequently used to investigate gas uptake and heterogeneous or multiphase reaction kinetics under laminar flow conditions. Coating surface roughness may potentially distort the laminar flow pattern, induce turbulence and introduce uncertainties in the calculated uptake coefficient based on molecular diffusion assumptions (e.g., Brown/CKD/KPS methods), which hasn't been sufficiently addressed in previous applications. Here, we suggest using a critical height δ_c to evaluate turbulence effects in the design and analysis of coated-wall flow tube experiments. When a geometric coating thickness δ_g is larger than δ_c, the roughness elements of the coating may cause local

turbulence and result in overestimation of the real uptake coefficient (γ). We further develop modified CKD/KPS methods (i.e., CKD-LT/KPS-LT) to account for roughness-induced local turbulence effects. By combination of the original methods and their modified versions, the maximum error range can be quantified and finally γ can be constrained. Additionally, the critical height δ_c can also be adjusted by optimizing flow tube configurations and operation conditions, to ensure not only unaffected laminar flow patterns but also other specific requirements of an individual flow tube experiment.

Contents

1. Introduction and Motivation

1.1 The atmospheric relevance of VOCs

Volatile organic compounds (VOCs) represent the entire set of vapor phase atmospheric organics excluding CO and CO_2 (Seinfeld and Pandis, 2016). Therefore, VOCs span a broad range of pure hydrocarbons (i.e., alkanes, alkenes, alkynes, and aromatics) and their derivatives, such as oxygenated (e.g., alcohols, aldehydes, and acids etc.) and halogenated hydrocarbons (e.g., CFCs, HCFCs, and HFCs etc.) (Seinfeld and Pandis, 2016). The vast array of VOCs can be originated from both biogenic and anthropogenic sources. On a global scale, the biogenic volatile organic compounds (BVOCs) are estimated to be 1150 Tg of carbon per year, accounting for 75-90% of the global total VOCs emissions, while the anthropogenic volatile organic compounds (AVOCs) contribute to the remaining fraction (Messina et al., 2016).

Once emitted into the atmosphere, VOCs can exert a crucial impact on local, regional and global atmospheric chemistry (Park et al., 2013a). They react with the atmospheric oxidants (e.g., OH and NO_3 radicals) and further produce other oxidative species such as HO_2 and RO_2 radicals to influence the oxidizing capacity of the atmosphere and thus affect the concentration and distribution of other reactive gas species (Thompson, 1992). They are also closely associated with the production and depletion of an important air pollutant, ozone (O_3), depending on the concentration levels of nitrogen oxides (NO_x = NO + NO_2) in the atmosphere (Trainer et al., 1987;Jacob and Wofsy, 1988;Atkinson, 2000;Chameides et al., 1988). Moreover, VOCs can generate secondary organic aerosols (SOAs) through homogeneous/heterogeneous reactions and these SOAs play central roles in climate change and atmospheric chemistry by means of providing cloud condensation nuclei, scattering sunlight and participating in heterogeneous chemical reactions (Andreae and Crutzen, 1997;Jang et al., 2002).

1.2 Exchange of VOCs between the atmosphere and soils

Understanding the budgets of VOCs in the atmosphere is essential to understand the VOCs-relevant transformation processes in atmospheric chemistry. The well-known sources of AVOCs include fossil fuel combustion, biomass burning, industrial processes, solvent use and road transportation (Wang et al., 2014;Wei et al., 2008;Li et al., 2014;Yuan et al., 2010;Niu et al., 2016), and the important contributors for BVOCs are vegetation and oceans (Guenther et al., 1995;Kesselmeier and Staudt, 1999). The removal processes of VOCs are mainly classified into three pathways: (1) oxidation to CO and CO_2; (2) transformation into SOAs and (3) dry and wet deposition on surfaces, such as vegetation, oceans and soils (Goldstein and Galbally, 2007). For these discussed processes influencing the budgets of VOCs, many of

them are closely linked to heterogeneous/multiphase reactions, for example, VOCs emissions from vegetation and deposition onto soils etc..

Due to the important roles of heterogeneous/multiphase processes in affecting the budgets of VOCs, many VOC exchange studies at the atmosphere-vegetation interface have been conducted, considering that vegetation is the largest source/sink of VOCs on a global scale (Gershenzon, 1994;Guenther et al., 1994;Fuentes et al., 1996;Fall et al., 1999;Schade and Goldstein, 2002;Seco et al., 2007;Karl et al., 2010;Park et al., 2013b;Gordon et al., 2014). However, in contrast to the efforts on vegetation-VOCs interactions, VOC exchange between the atmosphere and soils have received less attention (Lamb et al., 1987;Asensio et al., 2008;Guenther et al., 1995). Existing evidences show that soil can be either a source (Guenther, 1999) or a sink (Bender and Conrad, 1993;Asensio et al., 2007a) of atmospheric VOCs. The major contributors of VOC emissions from natural soils can be litter (Gray et al., 2010;Warneke et al., 1999;Hayward et al., 2001;Schade and Goldstein, 2001), roots (Janson, 1993;Chen et al., 2004;Lin et al., 2007) and microorganisms (Scholler et al., 2002), and the significance of each may depend on soil type and various environmental parameters such as ambient relative humidity (RH), soil water content, temperature (T), and VOC concentration, etc.. Meanwhile, VOCs in the atmosphere can be taken up by soils, in terms of adsorption and degradation by roots (Simonich and Hites, 1995;Newman et al., 1997;Cho et al., 2005), biodegradation by microorganisms (van Roon et al., 2005) and physical/chemical adsorption by soil particles (Pignatello and Xing, 1996;Li et al., 2016).

The potential effects of VOC exchange at the atmosphere-soil interface on atmospheric chemistry, are not well understood. For example, Asensio et al. (2007b) measured seasonal soil VOC exchange rates in a Mediterranean holm oak forest site and concluded that VOCs fluxes in soil might have greater impact on soil ecology than on atmospheric chemistry. But further measurements performed on a Mediterranean shrubland showed that soil uptake rates for some VOCs were comparable with foliar uptake rates (Asensio et al., 2008), and therefore further studies were suggested to elucidate possible importance of soil VOCs sink in regional chemistry-climate models. Warneke et al. (1999) and Gray et al. (2010) reported that soil and leaf litter contributed significantly to VOC budget in the atmosphere, especially in spring and fall when reduced solar radiation and temperatures reduced emissions from living vegetation. On the other hand, particles/SOAs formation potential of VOC emissions from soil and leaf litter, also during spring and fall, were studied and emphasized by several researchers (Mäkelä et al., 2000;Bigg, 2004;Faiola et al., 2014).

Given the to date discovered significance yet scarce available information of soil VOC exchange, more research work should be implemented to clarify the VOC exchange behaviors at the atmosphere-soil interface as well as their potential impact on atmospheric chemistry.

1.3 Techniques for investigating VOC exchange at the atmosphere-soil interface

Several techniques have been developed and employed to investigate the VOC exchange between the atmosphere and different types of soils. The eddy covariance (EC) method is considered the most reliable technique for studying VOC exchange between the atmosphere and biosphere (Park, 2012), and is also widely used to measure VOC fluxes at various soil surfaces (Karl et al., 2001;Ruuskanen et al., 2011;Aubinet et al., 2012;Baldocchi, 2014). However, because this method is based on directly and continuously turbulent flux measurements, fast gas analyzers with a high frequency of 10 – 20 Hz (e.g., proton-transfer-reaction time-of-flight mass spectrometer, PTR-TOF-MS) are required to achieve a high time resolution of the measured VOC concentrations (Rantala, 2016). On the basis of the EC method, a disjunct eddy covariance (DEC) method is further proposed by Rinne et al., (2001), which allows for a longer time period to analyze the VOC concentrations and thus makes EC measurements possible when using slower analyzers (Rinne et al., 2001;Warneke et al., 2002).

Chamber techniques have also been applied to measure VOC exchange fluxes on forest floors or grasslands (Pape et al., 2009;Kolari et al., 2012). According to the flow conditions inside chambers, the chamber techniques can be further divided into static chamber method (i.e., non-steady-state method) and dynamic flow-through chamber method (i.e., steady-state method) (Aaltonen, 2012). In the static chamber method, the chamber is fully closed and the air in the chamber headspace is kept static to achieve a stabilized gas concentration during the closure, then this gas concentration change inside the chamber is used for flux calculation (Hutchinson and Livingston, 2001;Livingston et al., 2005). While for the dynamic flow-through chamber method, zero or ambient air is continuously flushed through the chamber, and the gas concentration difference between the chamber inlet and outlet can be used to derive the corresponding flux (Pape et al., 2009;Kolari et al., 2012). Commonly, the dynamic flow-through chamber method is more frequently used than the static chamber method for VOC exchange studies, because with the former method it is possible to analyze larger sample volumes without introducing obvious gas concentration, pressure and temperature changes inside the soil samples (Aaltonen, 2012;Pape et al., 2009;Kolari et al., 2012).

Under some specific conditions, such as very low fluxes, fluxes decrease as the gas concentration increases within the chamber headspace, and gas exchanging within very porous samples, the use of chamber methods becomes complicated. In this case, the gradient method can be used as an alternative.

For example, Helming et al., (2009) measured VOC concentration gradients within and above an examined snowpack, and calculated the gas exchange fluxes at the soil-snow-atmosphere interface using the Fick's Law of diffusion. Their results demonstrated that the gradient method was a highly sensitive technique for elucidating gas exchange processes associated with porous samples (Helmig et al., 2009).

Coated-wall flow tube reactors are extensively employed for investigations of uptake and reaction kinetics of gases with reactive liquid/semisolid/solid surfaces (Howard, 1979;Kolb et al., 2010;Li et al., 2018b). Uptake and heterogeneous reactions of several trace gases (e.g., NO_2, HONO) on soil surfaces have been studied using the coated-wall flow tube technique (Stemmler et al., 2006;Wang et al., 2012;Donaldson et al., 2014;VandenBoer et al., 2015). Here, for our VOC exchange between soil and the atmosphere, this technique was firstly adopted to investigate the uptake of HCHO onto soil surfaces under controlled laboratory conditions (Li et al., 2016). Then it was futher developed to be used under a real-world case aiming at examing the exchange of 13 VOC species at the atmosphere-soil interface under ambient conditions at an urban background site in Beijing (Li et al., 2018a).

Normally, these methods are applied by coupling with fast-response and sensitive gas analyzers, which allow for monitoring one specific VOC species or several VOC species simultaneously.

1.4 Knowledge gaps and research objectives

As discussed above, investigations regarding VOC exchange at the atmosphere-soil interface are still lacking. The reported studies on VOC exchange span a wide range of soil types and field measurement conditions, which complicates the way to clearly understand substantial VOC exchange mechanisms. Actually, soils are a complex ecosystem including soil litter, plant roots, microorganisms and soil particles. The intrinsic complexity of soils and the diversity of the processes contributing to the production, consumption and accumulation of VOCs in soils result in the current situation that, assessment of the relative importance of each source and sink on the overall VOC exchange is difficult to be achieved in the field (Penuelas et al., 2014). Furthermore, measurements and quantifications of the relative contributions of biotic versus abiotic processes to soil VOC uptake/emission haven't been directly addressed so far. Most of the previous investigations reveal a bidirectional exchange behavior of VOCs at the atmosphere-soil interface, but the detailed reasons are not very well-known. Thus, understanding the explicit function of each soil component on VOC exchange may provide insights into the underlying uptake/emission mechanisms. On the other hand, information on the types and quantities of VOC exchange at the atmosphere-soil interface is still scarce and therefore needs to be further explored. Thus, this thesis intends to address the following knowledge gaps:

(1). Previous soil VOC exchange studies mainly focus on soils which encompasses both biotic (e.g., soil bacteria, plant roots) and abiotic (e.g., physicochemical reactions on soil surfaces and within soil pores) processes. These research results cannot distinguish the relative importance of biotic versus abiotic processes on VOC exchange. In addition, the variability of soil microorganisms and soil surface covering of different examined soil types makes the VOC exchange on one specific soil type unrepresentative. Hence, it is necessary to inspect the VOC exchange on one or several soil samples which could represent the common features of soils, in order to provide deeper insights into the VOC exchange mechanisms at the atmosphere-soil interface.

(2). Little information is available on the strength of soils as a VOC sink, and moreover the types and quantities of exchanged VOCs on soils under ambient conditions are rarely reported by previous researchers (Penuelas et al., 2014). It is therefore necessary to investigate the exchange of different types of VOCs on soils and meanwhile quantify their exchanging strength.

(3). Coated-wall flow tube reactors are frequently used to investigate gas uptake and heterogeneous or multiphase reaction kinetics under laminar flow conditions (Li et al., 2018b). Coating surface roughness may potentially distort the laminar flow pattern, induce turbulence and introduce uncertainties in the calculated uptake coefficient based on molecular diffusion assumptions (e.g., Brown/CKD/KPS methods). This case hasn't been sufficiently addressed in previous applications. Thus, evaluation of the potential effects of coating surface roughness on the calculated uptake coefficient and proposing one simple and feasible criterion to eliminate these effects are crucial for future flow tube experiments design.

In view of these knowledge gaps, in the main parts of this thesis, we will present our work from the following three topics, with their specific objectives being highlighted:

(a). Laboratory experiments

Atmospheric HCHO represents one of the most abundant carbonyls in the atmosphere and is a key intermediate in atmospheric hydrocarbon oxidation (Li et al., 2016). Budget analyses reveal large discrepancies between observed HCHO concentrations and those predicted from models (Jacob, 2000;Wagner et al., 2002). However, there are few studies concerning the contribution of soil to HCHO's budget. We therefore conducted a laboratory study to explore the exchange of HCHO on sterilized soil surfaces and identify the potential importance of soil on HCHO's budget. The soil sterilization treatment could exclude the biotic influences and allow us to focus on the impacts of physicochemical processes on HCHO exchange.

(b). Field measurements

To characterize the exchange of 13 VOC species at the atmosphere-soil interface under real world conditions and quantify their uptake/emission strength in terms of derived long-term average uptake coefficients. Similarly, sterilized soil was investigated to address physicochemical processes and heterogeneous/multiphase reactions independently from biological activity. The VOC exchange which are primarily influenced by physicochemical processes on soil (sterilized bare soil, mainly consisting of soil minerals), can represent the general features of VOC exchange on bare soils.

(c). Coated-wall flow tube technique optimization

To evaluate the potential effects of coating surface roughness on uptake coefficients derived from coated-wall flow tube experiments and further propose a method to eliminate the surface roughness effects.

2. Results and Conclusions

2.1 Overview

The main results of this PhD project are described in three first-author manuscripts which are attached in Appendix B. Two of these have already been published and one is currently undergoing public review and discussion in the journal Atmospheric Chemistry and Physics. Figure 2.1 provides an overview of the studies, and the main results and conclusions are summarized in the following sections.

In addition to the research and results presented in this thesis, the PhD project also comprises investigations of the atmospheric abundance and atmosphere-ocean exchange of nitrous acid (HONO) and cloud condensation nuclei (CCN) in the course of the ship measurement campaign AQABA (Air Quality and climate change in the Arabian Basin) and the development of new measurement techniques for the determination of gas uptake coefficients using a twin chamber system. These additional studies are still in progress and thus not included in this thesis.

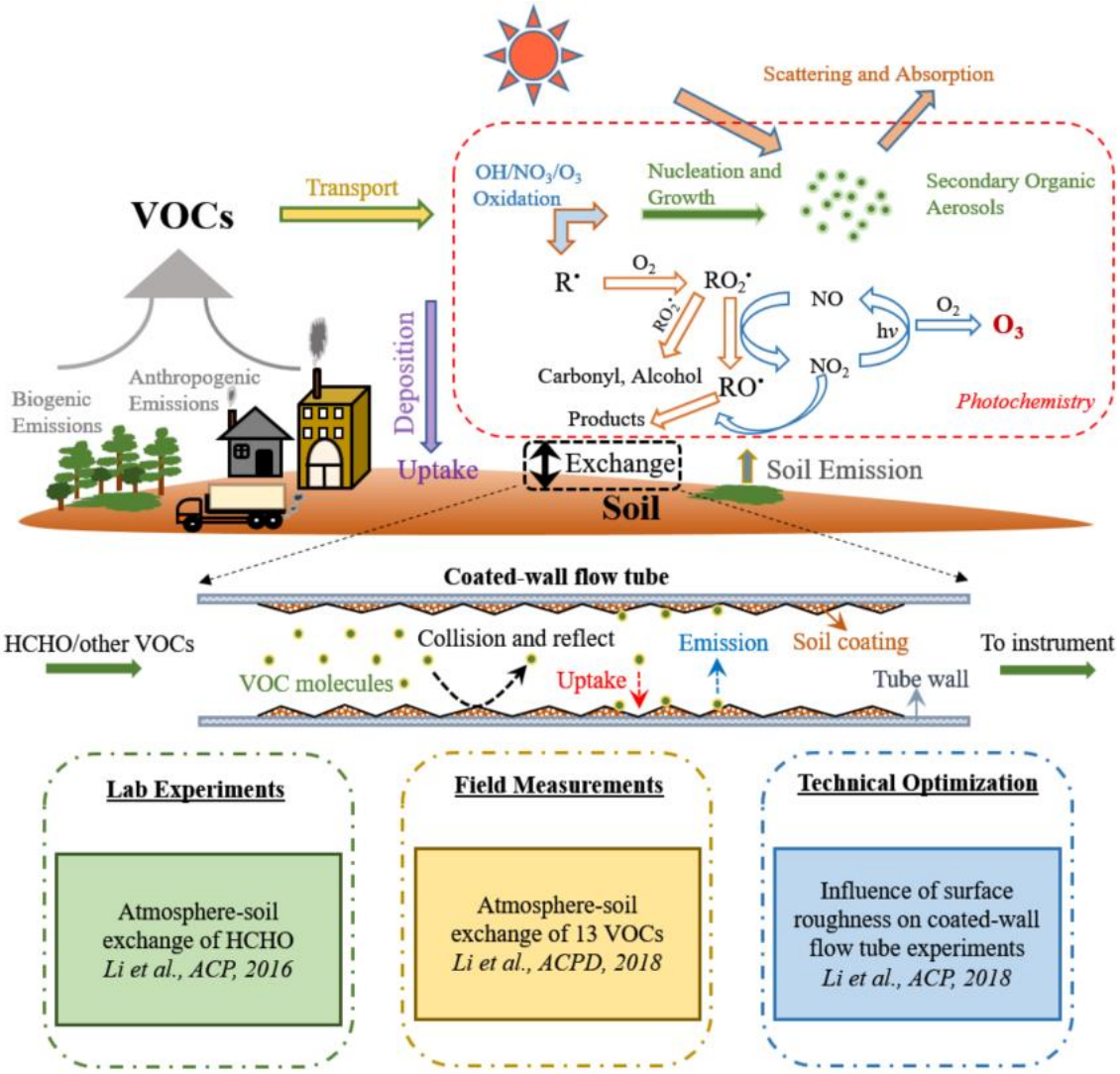

Figure 2.1 Structure of this thesis. The upper part shows the importance of VOCs in atmospheric chemistry and the exchange of VOCs at the atmosphere-soil interface can have a profound impact. The middle part describes the coated-wall flow tube technique used for investigations of the VOC exchange. The lower part summarizes the individual studies under the main topic of VOC exchange at the atmosphere-soil interface.

2.2 Individual studies

2.2.1 Atmosphere-soil exchange of HCHO in a coated-wall flow tube

Gaseous HCHO is an important precursor of OH radicals and a key intermediate molecule in the oxidation of atmospheric volatile organic compounds (VOCs). Budget analyses reveal large discrepancies between modeled and observed HCHO concentrations in the atmosphere. Through laboratory experiment, we investigated the HCHO uptake on soil surfaces by a coated-wall flow tube method. Under dry

conditions (relative humidity = 0%), an initial γ of (1.1 ± 0.05) × 10^{-4} is determined, which gradually drops to (5.5 ± 0.4) × 10^{-5} after 8-hour experiments. Experiments under wet conditions show a smaller γ that drops faster over time until reaching a plateau. The drop of γ with increasing relative humidity and over time can both be explained by the adsorption theory in which high surface coverage leads to a reduced uptake rate. The fact that γ stabilizes at a non-zero plateau suggests the involvement of irreversible chemical reactions. Further back-flushing experiments show that two thirds of the adsorbed HCHO can be re-emitted into the gas phase while the residual is retained by the soil. This partial reversibility confirms that HCHO uptake by soil is a complex process involving both adsorption/desorption and chemical reactions which must be considered in trace gas exchange (emission or deposition) at the atmosphere-soil interface. Our results suggest that soil and soil-derived airborne particles can either act as a source or a sink for HCHO, depending on ambient conditions and HCHO concentrations.

For more details, see Appendix B.1, Li et al., Atmos. Chem. Phys., 2016.

2.2.2 Atmosphere-soil exchange of VOCs in a differential coated-wall flow tube system operated with ambient air

In addition to HCHO, the exchange of other VOC species at the atmosphere-soil interface is not well quantified either (see Sect. 1.4). Therefore, we used a newly designed differential coated-wall flow tube system to investigate the long-term variability of bidirectional air-soil exchange of 13 common VOCs at ambient air conditions of an urban background site in Beijing. Sterilized soil was investigated to address physicochemical processes and heterogeneous/multiphase reactions independently from biological activity. Most VOCs revealed net deposition with average uptake coefficients (γ) in the range of 10^{-7} – 10^{-6} (referring to the geometric soil surface area), corresponding to deposition velocities (V_d) of 0.0013 – 0.01 cm s^{-1} and soil surface resistances (R_c) of 98 – 745 s cm^{-1}, respectively. Formic acid, however, was emitted at a long-term average rate of ~ 6 × 10^{-3} nmol m^{-2} s^{-1}, suggesting that it was formed and released upon heterogeneous oxidation of other VOCs. The soil-atmosphere exchange of one individual VOC species can be affected by both its surface degradation/depletion caused by surface reactions and by competitive uptake or heterogeneous formation/accommodation of other VOC species. Overall, the results show that physicochemical processing and heterogeneous oxidation on soil and soil-derived dust can act as a sink or as a source of atmospheric VOCs, depending on molecular properties and environmental conditions.

At ambient atmospheric conditions, both the relatively low uptake coefficients derived for the majority of VOC species and the emission of formic acid from the soil to some extent challenge the applicability of

models using uptake coefficients derived from laboratory-based uptake measurements, where single VOC species or simple mixtures are supplied using purging air devoid of oxidizing agents. Field measurements as presented here, with all relevant parameters changing in concert, may call attention for the existence of yet unknown interferences or synergetic effects.

For more details, see Appendix B.2, Li et al., Atmos. Chem. Phys. Discuss., 2018.

2.2.3 Influence of surface roughness on coated-wall flow tube experiments

Coated-wall flow tube reactors are frequently used to investigate gas uptake and heterogeneous or multiphase reaction kinetics under laminar flow conditions. Coating surface roughness may potentially distort the laminar flow pattern, induce turbulence and introduce uncertainties in the calculated uptake coefficient based on molecular diffusion assumptions (e.g., Brown/CKD/KPS methods), which hasn't been sufficiently addressed in previous applications. Thus, we investigated the influence of surface roughness and local turbulence on coated-wall flow tube experiments for gas uptake and kinetic studies. According to laminar boundary theory and considering the specific flow conditions in a coated-wall flow tube, we suggest using a critical height δ_c to evaluate turbulence effects in the design and analysis of coated-wall flow tube experiments. When a geometric coating thickness δ_g is larger than δ_c, the roughness elements of the coating may cause local turbulence and result in overestimation of the real uptake coefficient (γ). If a geometric coating thickness δ_g is larger than δ_c, the roughness elements of the coating may cause local turbulence and result in overestimation of the real uptake coefficient (γ). We further develop modified CKD/KPS methods (i.e., CKD-LT/KPS-LT) to account for roughness-induced local turbulence effects. By combination of the original methods and their modified versions, the maximum error range of γ_{CKD} (derived with the CKD method) or γ_{KPS} (derived with the KPS method) can be quantified and finally γ be constrained. When turbulence is generated, γ_{CKD} or γ_{KPS} can bear large difference compared to γ. Their difference becomes less for gas reactants with lower uptake (i.e., smaller γ), or/and for a smaller ratio of the geometric coating thickness to the flow tube radius (δ_g/R_0). On the other hand, the critical height δ_c can also be adjusted by optimizing flow tube configurations and operating conditions (i.e., tube diameter, length and flow velocity), to ensure not only unaffected laminar flow patterns but also other specific requirements for an individual flow tube experiment.

For more details, see Appendix B.3, Li et al., Atmos. Chem. Phys., 2018.

2.3 Conclusions and outlook

In this thesis, the exchange of VOCs at the atmosphere-soil interface is investigated by means of both laboratory experiments and field measurements. A coated-wall flow tube technique is employed to provide deep insights into the heteogeneous reaction kinetics on soil surfaces.

Under laboratory conditions, soil exhibits strong capacity for absorbing gaseous HCHO, with initial γ ranging from $(1.4 \pm 0.08) \times 10^{-4}$ at 0% relative humidity to $(3.0 \pm 0.3) \times 10^{-5}$ at 70% relative humidity based on the geometric soil surface. Because of simultaneously acting adsorption/desorption processes, γ shows a strong temporal dependence with an initial peak and subsequent decay until a steady state is reached. We also find a clear relative humidity dependence of γ, especially in the low relative humidity range (e.g., $\leq$ 30%, under ambient pressure and temperature conditions) and little relative humidity effect at relative humidity > 30%. The RH dependence of HCHO uptake can be explained by a transition of uptake pathways. Under low RH and water coverage (less than one monolayer) water molecules compete with gaseous HCHO for the adsorption sites on soil, while under high RH the soil surface is fully covered with water molecules providing a near constant amount of surface adsorption sites. Our results also show that HCHO uptake on soil is a partially reversible process involving both adsorption/desorption and chemical reactions. The adsorption/desorption reveals a bi-directional exchange on soil surfaces in which soil could serve either as a source or as a sink depending on ambient conditions and trace gas concentrations.

Under field situations, almost all the investigated VOCs show an average net deposition on the pre-treated sterilized soil, examined over an extended exposure of one month. The derived deposition velocities are found to be at the lower end of ranges reported for natural soil habitats, but were in fair agreement with models based on pure physicochemistry. Only formic acid displays a long-term emission. The emission of formic acid is solely due to physicochemical processes (i.e., heterogeneous transformations of absorbed VOC precursors) on soil, which represents an additional ground-based source of this organic acid.

Furthermore, in order to evaluate the influence of surface roughness and local turbulence on coated-wall flow tube experiments for gas uptake and kinetic studies, a new criterion is proposed to eliminate/minimize the potential effects of coating surface roughness on laminar flow in coated-wall flow tube experiments and therefore validate the application of conventional diffusion correction methods for uptake coefficient calculations. While keeping a coating film thickness well within the critical height δ_c to exclude potential surface roughness effects, flexible coated-wall flow tube design can also be achieved, i.e., one can increase δ_c by adjusting flow tube geometric parameters (i.e., tube diameter and tube length) or flow velocity V_{avg} to ensure not only an unaffected laminar flow pattern but also a flexible residence

time in flow tube reactors. We illustrate the application of this new criterion for previous investigations, and demonstrate its effectiveness in optimizing flow tube design and consolidating kinetic experimental results. Moreover, based on the CKD/KPS methods, their modified versions are proposed. The combinations of CKD/KPS and their modified versions can be used to quantify the maximum error of the calculated uptake coefficient (γ_{CKD} or γ_{KPS}) when roughness-induced local turbulence occurs. And the real uptake coefficient γ can be finally constrained.

Based on the work mentioned above, future work addressing the VOC exchange at the atmosphere-soil interface can be carried out from the following aspects:

(1). The exchange properties of more VOC species on different soil types need to be further investigated and, the strength of soil serving as a source or a sink for various VOC species should be further identified.

(2). As here we only focus on the physicochemical processes occurring in soil and considering the fact that soil is a complex system which encompasses both biotic and abiotic processes, further research work revealing the relative importance of biotic factors in affecting the VOC exchange features is helpful to have a profound understanding of the interactions between soil and the atmosphere.

3. References

Aaltonen, H.: Exchange of volatile organic compounds in the boreal forest floor, Ph.D, Department of Forest Sciences, University of Helsinki, Finland, 2012.

Andreae, M. O., and Crutzen, P. J.: Atmospheric Aerosols: Biogeochemical Sources and Role in Atmospheric Chemistry, Science, 276, 1052-1058, 10.1126/science.276.5315.1052, 1997.

Asensio, D., Penuelas, J., Filella, I., and Llusia, J.: On-line screening of soil VOCs exchange responses to moisture, temperature and root presence, Plant and Soil, 291, 249-261, 2007a.

Asensio, D., Peñuelas, J., Ogaya, R., and Llusià, J.: Seasonal soil VOC exchange rates in a Mediterranean holm oak forest and their responses to drought conditions, Atmospheric Environment, 41, 2456-2466, http://dx.doi.org/10.1016/j.atmosenv.2006.05.007, 2007b.

Asensio, D., Penuelas, J., Prieto, P., Estiarte, M., Filella, I., and Llusia, J.: Interannual and seasonal changes in the soil exchange rates of monoterpenes and other VOCs in a Mediterranean shrubland, European Journal of Soil Science, 59, 878-891, 2008.

Atkinson, R.: Atmospheric chemistry of VOCs and NOx, Atmospheric Environment, 34, 2063-2101, http://dx.doi.org/10.1016/S1352-2310(99)00460-4, 2000.

Aubinet, M., Vesala, T., and Papale, D.: Eddy Covariance: A Practical Guide to Measurement and Data Analysis, Springer, 2012.

Baldocchi, D.: Measuring fluxes of trace gases and energy between ecosystems and the atmosphere – the state and future of the eddy covariance method, Global Change Biology, 20, 3600-3609, 10.1111/gcb.12649, 2014.

Bender, M., and Conrad, R.: Kinetics of Methane Oxidation in Oxic Soils, Chemosphere, 26, 687-696, 1993.

Bigg, E. K.: Gas emissions from soil and leaf litter as a source of new particle formation, Atmospheric Research, 70, 33-42, http://dx.doi.org/10.1016/j.atmosres.2003.10.003, 2004.

Chameides, W., Lindsay, R., Richardson, J., and Kiang, C.: The role of biogenic hydrocarbons in urban photochemical smog: Atlanta as a case study, Science, 241, 1473-1475, 10.1126/science.3420404, 1988.

Chen, F., Ro, D. K., Petri, J., Gershenzon, J., Bohlmann, J., Pichersky, E., and Tholl, D.: Characterization of a root-specific Arabidopsis terpene synthase responsible for the formation of the volatile monoterpene 1,8-cineole, Plant Physiology, 135, 1956-1966, 2004.

Cho, C. W., Sung, K., Coapcioglu, M. Y., and Drew, M.: Influence of water content and plants on the dissipation of chlorinated volatile organic compounds in soil, Water Air and Soil Pollution, 167, 259-271, 2005.

Donaldson, M. A., Berke, A. E., and Raff, J. D.: Uptake of Gas Phase Nitrous Acid onto Boundary Layer Soil Surfaces, Environmental Science & Technology, 48, 375-383, 2014.

Faiola, C. L., VanderSchelden, G. S., Wen, M., Elloy, F. C., Cobos, D. R., Watts, R. J., Jobson, B. T., and VanReken, T. M.: SOA Formation Potential of Emissions from Soil and Leaf Litter, Environmental Science & Technology, 48, 938-946, 10.1021/es4040045, 2014.

Fall, R., Karl, T., Hansel, A., Jordan, A., and Lindinger, W.: Volatile organic compounds emitted after leaf wounding: On-line analysis by proton-transfer-reaction mass spectrometry, J Geophys Res-Atmos, 104, 15963-15974, 1999.

Fuentes, J. D., Wang, D., Neumann, H. H., Gillespie, T. J., DenHartog, G., and Dann, T. F.: Ambient biogenic hydrocarbons and isoprene emissions from a mixed deciduous forest, Journal of Atmospheric Chemistry, 25, 67-95, 1996.

Gershenzon, J.: Metabolic Costs of Terpenoid Accumulation in Higher-Plants, J Chem Ecol, 20, 1281-1328, 1994.

Goldstein, A. H., and Galbally, I. E.: Known and Unexplored Organic Constituents in the Earth's Atmosphere, Environmental Science & Technology, 41, 1514-1521, 10.1021/es072476p, 2007.

Gordon, M., Vlasenko, A., Staebler, R. M., Stroud, C., Makar, P. A., Liggio, J., Li, S. M., and Brown, S.: Uptake and emission of VOCs near ground level below a mixed forest at Borden, Ontario, Atmos Chem Phys, 14, 9087-9097, 2014.

Gray, C. M., Monson, R. K., and Fierer, N.: Emissions of volatile organic compounds during the decomposition of plant litter, Journal of Geophysical Research-Biogeosciences, 115, 2010.

Guenther, A., Zimmerman, P., and Wildermuth, M.: Natural Volatile Organic-Compound Emission Rate Estimates for United-States Woodland Landscapes, Atmospheric Environment, 28, 1197-1210, 1994.

Guenther, A., Hewitt, C. N., Erickson, D., Fall, R., Geron, C., Graedel, T., Harley, P., Klinger, L., Lerdau, M., McKay, W. A., Pierce, T., Scholes, B., Steinbrecher, R., Tallamraju, R., Taylor, J., and Zimmerman, P.: A global model of natural volatile organic compound emissions, Journal of Geophysical Research: Atmospheres, 100, 8873-8892, 10.1029/94JD02950, 1995.

Guenther, A.: Modeling biogenic volatile organic compound emissions to the atmosphere, in: Reactive Hydrocarbons in the Atmosphere, edited by: Hewitt, C. N., Academic Press, San Diego, 97-118, 1999.

Hayward, S., Muncey, R. J., James, A. E., Halsall, C. J., and Hewitt, C. N.: Monoterpene emissions from soil in a Sitka spruce forest, Atmospheric Environment, 35, 4081-4087, 2001.

Helmig, D., Apel, E., Blake, D., Ganzeveld, L., Lefer, B. L., Meinardi, S., and Swanson, A. L.: Release and uptake of volatile inorganic and organic gases through the snowpack at Niwot Ridge, Colorado, Biogeochemistry, 95, 167-183, 10.1007/s10533-009-9326-8, 2009.

Howard, C. J.: Kinetic measurements using flow tubes, The Journal of Physical Chemistry, 83, 3-9, 10.1021/j100464a001, 1979.

Hutchinson, G. L., and Livingston, G. P.: Vents and seals in non-steady-state chambers used for measuring gas exchange between soil and the atmosphere, European Journal of Soil Science, 52, 675-682, 10.1046/j.1365-2389.2001.00415.x, 2001.

Jacob, D. J., and Wofsy, S. C.: Photochemistry of biogenic emissions over the Amazon forest, Journal of Geophysical Research: Atmospheres, 93, 1477-1486, 10.1029/JD093iD02p01477, 1988.

Jacob, D. J.: Heterogeneous chemistry and tropospheric ozone, Atmospheric Environment, 34, 2131-2159, 2000.

Jang, M., Czoschke, N. M., Lee, S., and Kamens, R. M.: Heterogeneous Atmospheric Aerosol Production by Acid-Catalyzed Particle-Phase Reactions, Science, 298, 814-817, 10.1126/science.1075798, 2002.

Janson, R. W.: Monoterpene Emissions from Scots Pine and Norwegian Spruce, Journal of Geophysical Research-Atmospheres, 98, 2839-2850, 1993.

Karl, T., Guenther, A., Lindinger, C., Jordan, A., Fall, R., and Lindinger, W.: Eddy covariance measurements of oxygenated volatile organic compound fluxes from crop harvesting using a redesigned proton-transfer-reaction mass spectrometer, Journal of Geophysical Research: Atmospheres, 106, 24157-24167, 10.1029/2000JD000112, 2001.

Karl, T., Harley, P., Emmons, L., Thornton, B., Guenther, A., Basu, C., Turnipseed, A., and Jardine, K.: Efficient Atmospheric Cleansing of Oxidized Organic Trace Gases by Vegetation, Science, 330, 816-819, 2010.

Kesselmeier, J., and Staudt, M.: Biogenic Volatile Organic Compounds (VOC): An Overview on Emission, Physiology and Ecology, Journal of Atmospheric Chemistry, 33, 23-88, 10.1023/a:1006127516791, 1999.

Kolari, P., Bäck, J., Taipale, R., Ruuskanen, T. M., Kajos, M. K., Rinne, J., Kulmala, M., and Hari, P.: Evaluation of accuracy in measurements of VOC emissions with dynamic chamber system, Atmospheric Environment, 62, 344-351, http://dx.doi.org/10.1016/j.atmosenv.2012.08.054, 2012.

Kolb, C. E., Cox, R. A., Abbatt, J. P. D., Ammann, M., Davis, E. J., Donaldson, D. J., Garrett, B. C., George, C., Griffiths, P. T., Hanson, D. R., Kulmala, M., McFiggans, G., Poschl, U., Riipinen, I., Rossi, M. J., Rudich, Y., Wagner, P. E., Winkler, P. M., Worsnop, D. R., and O' Dowd, C. D.: An overview of current issues in the uptake of atmospheric trace gases by aerosols and clouds, Atmos Chem Phys, 10, 10561-10605, 2010.

Lamb, B., Guenther, A., Gay, D., and Westberg, H.: A National Inventory of Biogenic Hydrocarbon Emissions, Atmospheric Environment, 21, 1695-1705, 1987.

Li, G., Su, H., Li, X., Kuhn, U., Meusel, H., Hoffmann, T., Ammann, M., Pöschl, U., Shao, M., and Cheng, Y.: Uptake of gaseous formaldehyde by soil surfaces: a combination of adsorption/desorption equilibrium and chemical reactions, Atmos. Chem. Phys., 16, 10299-10311, 10.5194/acp-16-10299-2016, 2016.

Li, G., Cheng, Y., Kuhn, U., Xu, R., Yang, Y., Meusel, H., Ma, N., Wu, Y., Li, M., Williams, J., Hoffmann, T., Ammann, M., Pöschl, U., Shao, M., and Su, H.: Physicochemical uptake and release of volatile organic compounds by soil in coated-wall flow tube experiments with ambient air, Atmos. Chem. Phys. Discuss., 2018, 1-47, 10.5194/acp-2018-683, 2018a.

Li, G., Su, H., Kuhn, U., Meusel, H., Ammann, M., Shao, M., Pöschl, U., and Cheng, Y.: Technical note: Influence of surface roughness and local turbulence on coated-wall flow tube experiments for gas uptake andÂ kineticÂ studies, Atmos. Chem. Phys., 18, 2669-2686, 10.5194/acp-18-2669-2018, 2018b.

Li, M., Zhang, Q., Streets, D. G., He, K. B., Cheng, Y. F., Emmons, L. K., Huo, H., Kang, S. C., Lu, Z., Shao, M., Su, H., Yu, X., and Zhang, Y.: Mapping Asian anthropogenic emissions of non-methane volatile organic compounds to multiple chemical mechanisms, Atmos. Chem. Phys., 14, 5617-5638, 10.5194/acp-14-5617-2014, 2014.

Lin, C., Owen, S. M., and Penuelas, J.: Volatile organic compounds in the roots and rhizosphere of Pinus spp., Soil Biology & Biochemistry, 39, 951-960, 2007.

Livingston, G. P., Hutchinson, G. L., and Spartalian, K.: Diffusion theory improves chamber-based measurements of trace gas emissions, Geophysical Research Letters, 32, n/a-n/a, 10.1029/2005GL024744, 2005.

Mäkelä, J. M., Maso, M. D., Pirjola, L., Keronen, P., Laakso, L., Kulmala, M., and Laaksonen, A.: Characteristics of the atmospheric particle formation events observed at a borel forest site in southern Finland., Boreal Environ. Res., 5, 299−313, 2000.

Messina, P., Lathière, J., Sindelarova, K., Vuichard, N., Granier, C., Ghattas, J., Cozic, A., and Hauglustaine, D. A.: Global biogenic volatile organic compound emissions in the ORCHIDEE and MEGAN models and sensitivity to key parameters, Atmos. Chem. Phys., 16, 14169-14202, 10.5194/acp-16-14169-2016, 2016.

Newman, L. A., Strand, S. E., Choe, N., Duffy, J., Ekuan, G., Ruszaj, M., Shurtleff, B. B., Wilmoth, J., Heilman, P., and Gordon, M. P.: Uptake and biotransformation of trichloroethylene by hybrid poplars, Environmental Science & Technology, 31, 1062-1067, 1997.

Niu, H., Mo, Z., Shao, M., Lu, S., and Xie, S.: Screening the emission sources of volatile organic compounds (VOCs) in China by multi-effects evaluation, Frontiers of Environmental Science & Engineering, 10, 1, 10.1007/s11783-016-0828-z, 2016.

Pape, L., Ammann, C., Nyfeler-Brunner, A., Spirig, C., Hens, K., and Meixner, F. X.: An automated dynamic chamber system for surface exchange measurement of non-reactive and reactive trace gases of grassland ecosystems, Biogeosciences, 6, 405-429, 10.5194/bg-6-405-2009, 2009.

Park, J.-H., Goldstein, A. H., Timkovsky, J., Fares, S., Weber, R., Karlik, J., and Holzinger, R.: Active Atmosphere-Ecosystem Exchange of the Vast Majority of Detected Volatile Organic Compounds, Science, 341, 643-647, 10.1126/science.1235053, 2013a.

Park, J. H.: Quantifying the ecosystem-scale emission and deposition fluxes of biogenic volatile organic compounds (BVOC) and their oxidation products above plant canopies, Ph.D, University of California, Berkeley, Berkeley, 2012.

Park, J. H., Goldstein, A. H., Timkovsky, J., Fares, S., Weber, R., Karlik, J., and Holzinger, R.: Active Atmosphere-Ecosystem Exchange of the Vast Majority of Detected Volatile Organic Compounds, Science, 341, 643-647, 2013b.

Penuelas, J., Asensio, D., Tholl, D., Wenke, K., Rosenkranz, M., Piechulla, B., and Schnitzler, J. P.: Biogenic volatile emissions from the soil, Plant Cell Environ, 37, 1866-1891, 2014.

Pignatello, J. J., and Xing, B. S.: Mechanisms of slow sorption of organic chemicals to natural particles, Environmental Science & Technology, 30, 1-11, 1996.

Rantala, P.: Ecosystem scale measurements of surface-atmosphere volatile organic compound exchange, Ph.D, Department of Physics, University of Helsinki, Finland, 2016.

Rinne, H. J. I., Guenther, A. B., Warneke, C., de Gouw, J. A., and Luxembourg, S. L.: Disjunct eddy covariance technique for trace gas flux measurements, Geophysical Research Letters, 28, 3139-3142, 10.1029/2001GL012900, 2001.

Ruuskanen, T. M., Müller, M., Schnitzhofer, R., Karl, T., Graus, M., Bamberger, I., Hörtnagl, L., Brilli, F., Wohlfahrt, G., and Hansel, A.: Eddy covariance VOC emission and deposition fluxes above grassland using PTR-TOF, Atmos. Chem. Phys., 11, 611-625, 10.5194/acp-11-611-2011, 2011.

Schade, G. W., and Goldstein, A. H.: Fluxes of oxygenated volatile organic compounds from a ponderosa pine plantation, Journal of Geophysical Research-Atmospheres, 106, 3111-3123, 2001.

Schade, G. W., and Goldstein, A. H.: Plant physiological influences on the fluxes of oxygenated volatile organic compounds from ponderosa pine trees, J Geophys Res-Atmos, 107, 2002.

Scholler, C. E. G., Gurtler, H., Pedersen, R., Molin, S., and Wilkins, K.: Volatile metabolites from actinomycetes, Journal of Agricultural and Food Chemistry, 50, 2615-2621, 2002.

Seco, R., Penuelas, J., and Filella, I.: Short-chain oxygenated VOCs: Emission and uptake by plants and atmospheric sources, sinks, and concentrations, Atmospheric Environment, 41, 2477-2499, 2007.

Seinfeld, J. H., and Pandis, S. N.: Atmospheric Trace Constituents, in: Atmospheric Chemistry and Physics: from Air Pollution to Climate Change, 3rd ed., John Wiley & Sons, Inc., Hoboken, New Jersey, 2016.

Simonich, S. L., and Hites, R. A.: Organic Pollutant Accumulation in Vegetation, Environmental Science & Technology, 29, 2905-2914, 1995.

Stemmler, K., Ammann, M., Donders, C., Kleffmann, J., and George, C.: Photosensitized reduction of nitrogen dioxide on humic acid as a source of nitrous acid, Nature, 440, 195-198, http://www.nature.com/nature/journal/v440/n7081/suppinfo/nature04603_S1.html, 2006.

Thompson, A. M.: The Oxidizing Capacity of the Earth's Atmosphere: Probable Past and Future Changes, Science, 256, 1157-1165, 10.1126/science.256.5060.1157, 1992.

Trainer, M., Williams, E. J., Parrish, D. D., Buhr, M. P., Allwine, E. J., Westberg, H. H., Fehsenfeld, F. C., and Liu, S. C.: Models and observations of the impact of natural hydrocarbons on rural ozone, Nature, 329, 705-707, 1987.

van Roon, A., Parsons, J. R., Krap, L., and Govers, H. A. J.: Fate and transport of monoterpenes through soils. Part II: Calculation of the effect of soil temperature, water saturation and organic carbon content, Chemosphere, 61, 129-138, 2005.

VandenBoer, T. C., Young, C. J., Talukdar, R. K., Markovic, M. Z., Brown, S. S., Roberts, J. M., and Murphy, J. G.: Nocturnal loss and daytime source of nitrous acid through reactive uptake and displacement, Nat Geosci, 8, 55-60, 2015.

Wagner, V., von Glasow, R., Fischer, H., and Crutzen, P. J.: Are CH2O measurements in the marine boundary layer suitable for testing the current understanding of CH4 photooxidation?: A model study, J Geophys Res-Atmos, 107, 2002.

Wang, H. L., Lou, S. R., Huang, C., Qiao, L. P., Tang, X. B., Chen, C. H., Zeng, L. M., Wang, Q., Zhou, M., Lu, S. H., and Yu, X. N.: Source Profiles of Volatile Organic Compounds from Biomass Burning in Yangtze River Delta, China, Aerosol Air Qual Res, 14, 818-828, 2014.

Wang, L., Wang, W. G., and Ge, M. F.: Heterogeneous uptake of NO2 on soils under variable temperature and relative humidity conditions, J Environ Sci-China, 24, 1759-1766, 2012.

Warneke, C., Karl, T., Judmaier, H., Hansel, A., Jordan, A., Lindinger, W., and Crutzen, P. J.: Acetone, methanol, and other partially oxidized volatile organic emissions from dead plant matter by abiological processes: Significance for atmospheric HOx chemistry, Global Biogeochemical Cycles, 13, 9-17, 1999.

Warneke, C., Luxembourg, S. L., de Gouw, J. A., Rinne, H. J. I., Guenther, A. B., and Fall, R.: Disjunct eddy covariance measurements of oxygenated volatile organic compounds fluxes from an alfalfa field before and after cutting, Journal of Geophysical Research: Atmospheres, 107, ACH 6-1-ACH 6-10, 10.1029/2001JD000594, 2002.

Wei, W., Wang, S., Chatani, S., Klimont, Z., Cofala, J., and Hao, J.: Emission and speciation of non-methane volatile organic compounds from anthropogenic sources in China, Atmospheric Environment, 42, 4976-4988, http://dx.doi.org/10.1016/j.atmosenv.2008.02.044, 2008.

Yuan, B., Liu, Y., Shao, M., Lu, S., and Streets, D. G.: Biomass Burning Contributions to Ambient VOCs Species at a Receptor Site in the Pearl River Delta (PRD), China, Environmental Science & Technology, 44, 4577-4582, 10.1021/es1003389, 2010.

A. Personal List of Publications

Journal Articles

1. Li, G., Su, H., Kuhn, U., Meusel, H., Hoffmann, T., Ammann, M., Pöschl, U., Shao, M., and Cheng, Y.: Uptake coefficient determination using a twin chamber system, *in preparation*.

2. Li, G., Cheng, Y., Kuhn, U., Xu, R., Yang Y., Meusel, H., Ma, N., Wu, Y., Li, M., Williams, J., Hoffmann, T., Ammann, M., Pöschl, U., Shao, M., and Su, H.: Physicochemical uptake and release of volative organic compounds by soil in coated-wall flow tube experiments with ambient air, Atmos. Chem. Phys. Discuss., 2018, 1-47, https://doi.org/10.5194/acp-2018-683, 2018.

3. Li, G., Su, H., Kuhn, U., Meusel, H., Ammann, M., Shao, M., Pöschl, U., and Cheng, Y.: Technical Note: Influence of surface roughness and local turbulence on coated-wall flow tube experiments for gas uptake and kinetic studies, Atmos. Chem. Phys., 18, 2669-2686, https://doi.org/10.5194/acp-18-2669-2018, 2018.

4. Meusel, H., Elshorbany, Y., Kuhn, U., Bartels-Rausch, T., Reinmuth-Selzle, K., Kampf, C. J., Li, G., Wang, X., Lelieveld, J., Pöschl, U., Hoffmann, T., Su, H., Ammann, M., and Cheng, Y.: Light-induced protein nitration and degradation with HONO emission, Atmos. Chem. Phys., 17, 11819-11833, https://doi.org/10.5194/acp-17-11819-2017, 2017.

5. Li, G., Su, H., Li, X., Kuhn, U., Meusel, H., Hoffmann, T., Ammann, M., Pöschl, U., Shao, M., and Cheng, Y.: Uptake of gaseous formaldehyde by soil surfaces: a combination of adsorption/desorption equilibrium and chemical reactions, Atmos. Chem. Phys., 16, 10299-10311, https://doi.org/10.5194/acp-16-10299-2016, 2016.

Oral Presentations

1. Li, G.: Ambient flow-tube study of VOC exchange at the atmosphere-soil interface in Beijing, General Assembly of the European Geoscience Union, Vienna, Austria, 9-13 April 2018.

2. Li, G.: Uptake of gaseous formaldehyde by soil surfaces: a combination of adsorption/desorption equilibrium and chemical reactions, The 4th Annual Conference of the VOCs Pollution Prevention Professional Committee, Shijiazhuang, China, 20-21 August 2016.

3. Li, G.: Uptake of gaseous HCHO onto soil surfaces, a coated-wall flow tube study, MPGS Days 2016, Mainz, Germany, 17-18 March 2016.

4. Li, G.: Uptake of gaseous HCHO onto soil surfaces, a coated-wall flow tube study, Doktorandenseminar DoSe, Mainz, Germany, 20 October 2015.

5. Li, G.: Uptake of gaseous HCHO onto soil surfaces, a coated-wall flow tube study, General Assembly of the European Geoscience Union, Vienna, Austria, 12-17 April 2015.

Poster Presentations

1. Li, G.: Exchange of VOCs at the atmosphere-soil interface under ambient conditions, a coated-wall flow tube study, American Geophysical Union Falling Meeting, San Francisco, California, USA, 12-16 December 2016.

B. Selected Publications

1. Li, G., Su, H., Li, X., Kuhn, U., Meusel, H., Hoffmann, T., Ammann, M., Pöschl, U., Shao, M., and Cheng, Y.: Uptake of gaseous formaldehyde by soil surfaces: a combination of adsorption/desorption equilibrium and chemical reactions, Atmos. Chem. Phys., 16, 10299-10311, https://doi.org/10.5194/acp-16-10299-2016, 2016.

2. Li, G., Cheng, Y., Kuhn, U., Xu, R., Yang Y., Meusel, H., Ma, N., Wu, Y., Li, M., Williams, J., Hoffmann, T., Ammann, M., Pöschl, U., Shao, M., and Su, H.: Physicochemical uptake and release of volative organic compounds by soil in coated-wall flow tube experiments with ambient air, Atmos. Chem. Phys. Discuss., 2018, 1-47, https://doi.org/10.5194/acp-2018-683, 2018.

3. Li, G., Su, H., Kuhn, U., Meusel, H., Ammann, M., Shao, M., Pöschl, U., and Cheng, Y.: Technical Note: Influence of surface roughness and local turbulence on coated-wall flow tube experiments for gas uptake and kinetic studies, Atmos. Chem. Phys., 18, 2669-2686, https://doi.org/10.5194/acp-18-2669-2018, 2018.

B.1 Li *et al.*, Atmos. Chem. Phys., 2016

Uptake of gaseous formaldehyde by soil surfaces: a combination of adsorption/desorption equilibrium and chemical reactions

Guo Li[1,2], Hang Su[1], Xin Li[3], Uwe Kuhn[1], Hannah Meusel[1], Thorsten Hoffmann[4], Markus Ammann[5], Ulrich Pöschl[1], Min Shao[2,*], Yafang Cheng[1,*]

[1]Multiphase Chemistry Department, Max Planck Institute for Chemistry, Mainz, Germany

[2]College of Environmental Sciences and Engineering, Peking University, Beijing, China

[3]Institute for Energy and Climate Research, IEK-8, Research Center Jülich, Jülich, Germany

[4]Institute of Inorganic Chemistry and Analytical Chemistry, Johannes Gutenberg University Mainz, Mainz, Germany

[5]Laboratory of Radiochemistry and Environmental Chemistry, Paul Scherrer Institute, 5232 Villigen, Switzerland

Correspondence to: Y. Cheng (yafang.cheng@mpic.de) or M. Shao (mshao@pku.edu.cn)

Atmospheric Chemistry and Physics, 16, 10299-10311, 2016

DOI: 10.5194/acp-16-10299-2016, 2016.

Author contributions:

HS, YC and GL designed the research.

GL performed the experimental study.

GL, HS, YC, XL, UK, HM, TH, MA, UP and MS discussed the results.

GL, HS, UK and YC wrote the paper.

Atmos. Chem. Phys., 16, 10299–10311, 2016
www.atmos-chem-phys.net/16/10299/2016/
doi:10.5194/acp-16-10299-2016

Atmospheric Chemistry and Physics Open Access EGU

Uptake of gaseous formaldehyde by soil surfaces: a combination of adsorption/desorption equilibrium and chemical reactions

Guo Li[1,2], Hang Su[1], Xin Li[3], Uwe Kuhn[1], Hannah Meusel[1], Thorsten Hoffmann[4], Markus Ammann[5], Ulrich Pöschl[1], Min Shao[2], and Yafang Cheng[1]

[1]Multiphase Chemistry Department, Max Planck Institute for Chemistry, Mainz, Germany
[2]College of Environmental Sciences and Engineering, Peking University, Beijing, China
[3]Institute for Energy and Climate Research, IEK-8, Research Center Jülich, Jülich, Germany
[4]Institute of Inorganic Chemistry and Analytical Chemistry, Johannes Gutenberg University Mainz, Mainz, Germany
[5]Laboratory of Radiochemistry and Environmental Chemistry, Paul Scherrer Institute, 5232 Villigen, Switzerland

Correspondence to: Yafang Cheng (yafang.cheng@mpic.de) and Min Shao (mshao@pku.edu.cn)

Received: 30 March 2016 – Published in Atmos. Chem. Phys. Discuss.: 18 April 2016
Revised: 14 July 2016 – Accepted: 28 July 2016 – Published: 15 August 2016

Abstract. Gaseous formaldehyde (HCHO) is an important precursor of OH radicals and a key intermediate molecule in the oxidation of atmospheric volatile organic compounds (VOCs). Budget analyses reveal large discrepancies between modeled and observed HCHO concentrations in the atmosphere. Here, we investigate the interactions of gaseous HCHO with soil surfaces through coated-wall flow tube experiments applying atmospherically relevant HCHO concentrations of $\sim$10 to 40 ppbv. For the determination of uptake coefficients (γ), we provide a Matlab code to account for the diffusion correction under laminar flow conditions. Under dry conditions (relative humidity = 0 %), an initial γ of $(1.1 \pm 0.05) \times 10^{-4}$ is determined, which gradually drops to $(5.5 \pm 0.4) \times 10^{-5}$ after 8 h experiments. Experiments under wet conditions show a smaller γ that drops faster over time until reaching a plateau. The drop of γ with increasing relative humidity as well as the drop over time can be explained by the adsorption theory in which high surface coverage leads to a reduced uptake rate. The fact that γ stabilizes at a non-zero plateau suggests the involvement of irreversible chemical reactions. Further back-flushing experiments show that two-thirds of the adsorbed HCHO can be re-emitted into the gas phase while the residual is retained by the soil. This partial reversibility confirms that HCHO uptake by soil is a complex process involving both adsorption/desorption and chemical reactions which must be considered in trace gas exchange (emission or deposition) at the atmosphere–soil interface. Our results suggest that soil and soil-derived airborne particles can either act as a source or a sink for HCHO, depending on ambient conditions and HCHO concentrations.

1 Introduction

Atmospheric HCHO represents one of the most abundant carbonyls in the atmosphere and is a key intermediate in atmospheric hydrocarbon oxidation. It is one of the major primary sources of HO_x ($HO_x = HO + HO_2$) radicals (Lowe and Schmidt, 1983; Fried et al., 1997; Hak et al., 2005; Seinfeld and Pandis, 2006) and it also serves as a large source in the global budget of H_2 and CO (Price et al., 2007). Around 90 % of global tropospheric HCHO is produced by the oxidation of methane (CH_4) and non-methane volatile organic compounds (NMVOCs), while direct emissions from biomass burning and fossil fuel combustion contribute to the remaining fraction (Carlier et al., 1986; Lee et al., 1998; Andreae and Merlet, 2001; Parrish et al., 2012). The known removal processes of HCHO include reaction with OH radicals, photolysis, deposition and aerosol uptake, of which the first two pathways are supposed to dominate (Zhou et al., 1996; Tie et al., 2001; Fried et al., 2003).

Budget analyses, however, reveal large discrepancies between observed HCHO concentrations and those predicted from models (Jacob, 2000; Wagner et al., 2002). Overpredictions of HCHO have been reported in a series of studies since the mid-1990s (Liu et al., 1992; Heikes et al., 1996;

Jacob et al., 1996; Zhou et al., 1996). For example, a recent model study at a semi-rural site in southern China by Li et al. (2014) showed 2–5 times higher HCHO than observations. On the other hand, underpredictions have also been found in a few studies (Ayers et al., 1997; Jaegle et al., 2000; Weller et al., 2000; Kormann et al., 2003). The disagreement between model calculations and observations suggests an inadequate understanding of the HCHO budget and the existence of additional source/sink terms. For example, neglecting uptake of HCHO by aerosols/clouds (Zhou et al., 1996; Tie et al., 2001; Fried et al., 2003) may result in an overestimation, while insufficient consideration of NMVOCs oxidation processes may lead to underestimated production of HCHO (Wagner et al., 2002). So far the imbalance in the HCHO budget remains inconclusive.

Soil and soil-derived mineral dust could represent an important kind of surface regulating the budget of several trace gases and aerosols in the atmosphere (Usher et al., 2003; Kulmala and Petaja, 2011; Su et al., 2011; Oswald et al., 2013; Donaldson et al., 2014a). Understanding the interactions of HCHO with soil surfaces may help to explain the discrepancies and improve our understanding of the HCHO budget. Some field flux measurements have found HCHO emission from soil surfaces (DiGangi et al., 2011) while other studies suggested a net HCHO deposition on soil surfaces (Gray et al., 2014).

In this study, we investigate the HCHO uptake on soil surfaces using a coated-wall flow tube method. The experiments are performed under conditions relevant to the atmosphere, i.e., HCHO concentrations of ~ 10 to 40 ppbv and relative humidities (RHs) of 0 to 70 %. The uptake coefficients γ are determined by numerically solving the Cooney-Kim-Davis equation, which describes the loss of a trace species to the flow tube wall at laminar flow conditions (Murphy and Fahey, 1987). The results are discussed along with its underlying mechanisms and atmospheric implications.

2 Methods

2.1 Sample preparation

Soil samples were collected at a depth of 0–5 cm from a cultivated field site in Mainz, Germany (49°59′ N, 8°13′ E). The soil pH was ~ 7.5 (1 : 2 soil / water (v/v), Thermo Scientific, OrionStar A211 pH meter). The soil texture comprised 15 % sand, 69 % silt and 16 % clay (wet sieving method) and the soil humus content was 3 % (loss on ignition method) as analyzed by Envilytix GmbH (Wiesbaden, Germany). The collected samples were air-dried in the laboratory prior to grinding and sieving with a 120 mesh soil sieve. The sieved soil was autoclaved for 20 min at 394 K right before the flow tube coating procedure.

Different soil types are inhabited by different microbial communities being very sensitive to soil properties (e.g., soil water content, pH, temperature, etc.). The applied wide range of changes in relative humidity within our experiments affects the soil water content, with respective impact on microbial activity. For a natural soil probe, the apportionment between the soil microbiological trace gas exchange and soil physicochemical effects would become vague, specifically in view of time-dependent patterns of microbial activity after changes in soil water content. The soil sterilization treatment eliminates the effects of microbiological activity on trace gas uptake/emission mechanism. The soil samples used in our study may serve as a soil proxy to study the physicochemical side of trace gas exchange, constituting a key element in regulating trace gas exchange at the atmosphere–soil interface (Donaldson et al., 2014b; VandenBoer et al., 2015). However, our results on sterilized soil samples cannot necessarily be considered representative for other and/or natural types of soils.

The coating procedure is one of the challenges in flow tube experiments. Manually coating the tube could be time consuming, and the coating thickness and homogeneity strongly depend on the operator. Here, an air-dried continuous rotating coating tool (ACRO) was developed to standardize the coating procedure and improve reproducibility and homogeneity (Fig. S1 in the Supplement). During the coating procedure, the tube was installed into the ACRO through two cylindrical fittings. One fitting was fixed to the inlet of the tube promoting tube rotation by means of a motor and a driving belt, while the other at the tube's outlet served only as a supporter not being fixed to the tube. The flow tube was normally placed horizontally but could also be tilted by adjusting the slope of ACRO (through a positioning screw). A drying air stream was piloted into the tube through a duct at the inlet connector. Before coating, we prepared a soil slurry by mixing dry soil with sterilized deionized water obtained from a Milli-Q system (18.2 MΩ cm, Millipore). The slurry was uniformly injected into an internally sandblasted glass tube which was then installed into the ACRO. The coated tube was rotated with a speed of 14 rpm and dried overnight with a flow rate of $\sim 0.5\,\mathrm{L\,min^{-1}}$ of pure N_2 (RH = 0 %). The coating thickness/mass had been found to affect the trace gases uptake in earlier studies (Donaldson et al., 2014a). As the coating thickness increases, the uptake rate also increases due to enhanced number of surface sites available for gas uptake. Then the uptake rate moves up to a threshold level, where further increase in coating thickness doesn't affect the gas uptake. In order to exclude the influence of coating thickness, a relatively thick coating of $\sim 500\,\mu\mathrm{m}$ was chosen for our experiments. Figure 1 shows the homogeneous soil cover thickness and structural details of the soil surface topography derived by scanning electron microscope (SEM). The good reproducibility of the experimental results as shown later also confirms the fair homogeneity and reproducibility of the coating.

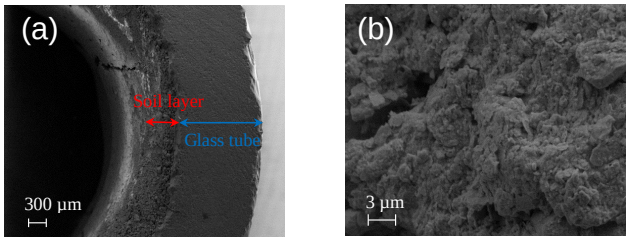

Figure 1. Characteristic morphology of coated soil layer observed by means of SEM (scanning electron microscope). **(a)** Flow tube cross-section view: the red arrow indicates the thickness of the soil layer and the blue arrow denotes the thickness of the glass tube. **(b)** View of the soil surface structure from above.

2.2 Flow tube experiments

The uptake of HCHO onto soil surfaces was measured by employing a coated-wall flow tube system (see Fig. 2). The system consisted of four parts: (1) a HCHO generator; (2) a humidification unit; (3) a flow tube and reference tube unit; and (4) a detection unit. HCHO was generated from a solid permeation tube (formaldehyde-para, rate: 91 ng min^{-1} at 60 °C, VICI Metronics Inc. USA) with N_2 ($\geq$ 99.999 %) as the carrier gas. The RH was controlled by mixing humidified N_2 with generated HCHO gas.

Two glass tubes (inner surface sandblasted) with identical dimensions (length: 250 mm, i.d.: 7 mm) were used for the uptake experiments. One tube was coated with soil samples and the other remained uncoated as a reference. Both tubes were placed in a cooling jacket in which a temperature of 296 $\pm$ 1 K was maintained during the experiments. HCHO concentrations were measured by an AL 4021 HCHO monitor (detection range: 100 ppt–3 ppm, noise: 2 % full scale, AERO LASER, Germany). It is an online HCHO analyzer for gaseous and liquid samples, based on the Hantzsch reaction. Gaseous HCHO is transferred into a liquid phase through a stripping coil, prior to reacting with Hantzsch reagents (ammonium acetate: for analysis, Merck, Germany; acetyl acetone: for analysis, Merck, Germany; and acetic acid (glacial): 100 %, Merck, Germany). The products show a strong fluorescence at 510 nm, which is measured by a photomultiplier. The operation principle is described in detail elsewhere (Dasgupta et al., 1988). This analyzer has been used for field measurements and has shown high stability (Preunkert et al., 2013, 2015). The flow rate used for our lab experiments was 1 L STP min^{-1}. The analyzer was operated with liquid calibration gas measurement mode and was calibrated using standard HCHO solutions (37 wt % in H_2O, Sigma-Aldrich, USA).

Several flow tube experiments were carried out to examine different aspects of the uptake processes, e.g., reproducibility, RH dependence, and bi-directional exchange, etc. In each experiment, we adopted the following procedure: (1) flushing the freshly coated tube with pure N_2; (2) flushing the uncoated reference tube with HCHO; (3) flushing the freshly coated tube with HCHO. The first step was to detect background HCHO emission from soil. While the second step allowed for identification of potential uptake of HCHO on clean glass surface, the third step was dedicated to investigate HCHO uptake by the soil surface, from which uptake coefficients can be derived. To check the stability of the HCHO monitor and generator, we also performed zero calibrations for the monitor and measured the generated HCHO concentrations before and after each experiment. As a wide range of RH conditions (0–70 %) was applied in the uptake experiments, the potential effect of water molecules on the generated HCHO concentration and background (zero air) concentration was examined. At the outlet of the stripping coil, the sample air was saturated to 100 % RH at 10 °C. Depending on the inlet air RH (at room temperature) the stripping solution would gain (condensation) or lose (evaporation) water according to the gas/liquid phase equilibrium (Junkermann and Burger, 2006). The bias in calculated HCHO concentrations was within $\pm$3 %. To check the RH effect on measured HCHO concentration under varying RH conditions, we occasionally compared the observed concentrations with data derived from the certified permeation rate of the permeation tube and the measured gas flow rate (gas phase calibration method). The observed total bias, assumed to characterize the instrument's accuracy was within $\pm$5 %. Moreover, the instrument's zero air background was observed to increase gradually when increasing RH from 0 to 50 %, and decreased when further increasing RH beyond 70 %. This could be due to the RH effect on the measurement principle, inlet surface effects, or aging of peristaltic tubes, stripping solution and Hantzsch solution (Kaiser et al., 2014). To account for the influence of changed background on measured HCHO concentration, the background was checked at the beginning and end of each experiment and the measured HCHO concentrations were corrected based on observed background values. On the other hand, well-known ozone interferences (Rodier and Birks, 1994; Kormann et al., 2003) were not of any concern for our studies, as the applied carrier gas was free of ozone.

2.3 Determination of uptake coefficients

The goal of our kinetic experiments is to determine the uptake coefficients γ. The parameter γ is defined as the fraction of effective collisions between HCHO and the soil surface that leads to loss of HCHO due to physical or chemical processes. For investigations on trace gas uptake kinetics using flow tubes, a method, designated the CKD solution (Murphy and Fahey, 1987), is commonly applied to account for radial and axial diffusion effects. Here we develop a new method rather than using the interpolated values provided in CKD method. As our method is based on the CKD, it can be specified as a CKD-based method (CKD-B). For the details of CKD-B, see Appendix A. In our experiment,

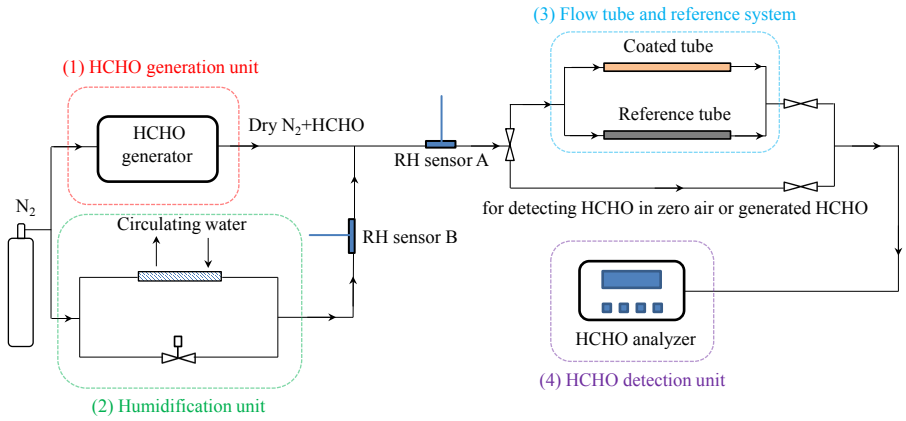

Figure 2. Schematic of the experimental setup. For details see text.

the Reynolds number Re is ~ 200 ensuring the laminar flow conditions which require $Re < \sim 2100$ (Murphy and Fahey, 1987). The total flow tube length is 25 cm and full development of laminar flow is achieved within ~ 5 cm for our setup. The uptake coefficients reported here are based on the geometric surface area of the soil sample, considering that in atmospheric models soil microstructure is not taken into account. In order to facilitate modelling, the calculated uptake coefficients as a function of initial HCHO concentration, relative humidity and uptake time period are summarized in Table S1 in the Supplement. The specific surface area of the soil sample, however, was also measured using a water vapor adsorption method based on the Brunauer-Emmett-Teller (BET) adsorption theory (Brunauer et al., 1938) being $18.9 \pm 1.3\ m^2\ g^{-1}$. For calculating this BET surface area, the mass of the adsorbed water on soil sample after equilibrium with pre-defined RH levels was determined by a non-dispersive infrared (NDIR) gas analyzer (type: Li-6262, LI-COR Biosciences Inc.) operated in differential mode. This BET surface area is comparable to that in other reports on similar soil types, e.g., 12–15 $m^2\ g^{-1}$ (Kahle et al., 2002) and 8–19 $m^2\ g^{-1}$ (Punrattanasin and Sariem, 2015). Accounting for the BET surface area would decrease γ by a factor of 10^4 in our case.

3 Results and discussion

3.1 HCHO uptake reproducibility on soil

Chamber experiments have often been used to investigate the soil emission or uptake of trace gases. A common problem of chamber studies is that the results are not reproducible. Even for the same soil samples and experimental setup, the results may still differ from each other. This lack of reproducibility deteriorates the interpretation, extrapolation and application of experimental results.

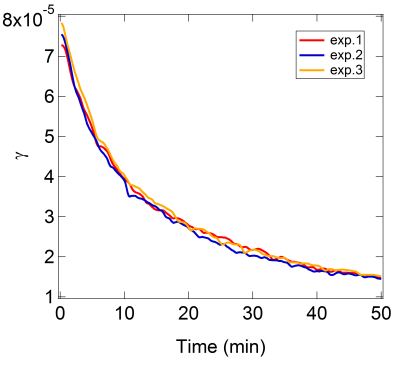

Figure 3. Effect of repeated uptake and emission on soil uptake coefficients within the uptake time range of 50 min at 50 % RH.

The change of soil microbiological activities and soil micro-structure seems to be the two most probable reasons leading to non-reproducible results. If that's the case, sterilized soil with a well-defined structure/geometry can avoid these influences and present reproducible results. To test it, we performed three uptake experiments for the same soil sample under the same RH conditions. Before each experiment, the coated flow tube was flushed with pure N_2 (HCHO-free) until HCHO release ceased.

As shown in Fig. 3, almost identical uptake coefficients are determined from three experiments (each lasted for 50 min) at RH of 50 % and HCHO concentration of ~ 35 ppbv. The reproducibility gives confidence in the kinetic parameter γ determined from the flow tube approach.

3.2 HCHO uptake on soil and temporal variation

Variation of uptake coefficients with time is a key question for evaluating the atmospheric relevance of surface uptake. Fast initial uptake can be unimportant if it quickly slows down due to consumption or occupation of reactive sites on surfaces (Kalberer et al., 1999). In this work, two 8 h uptake

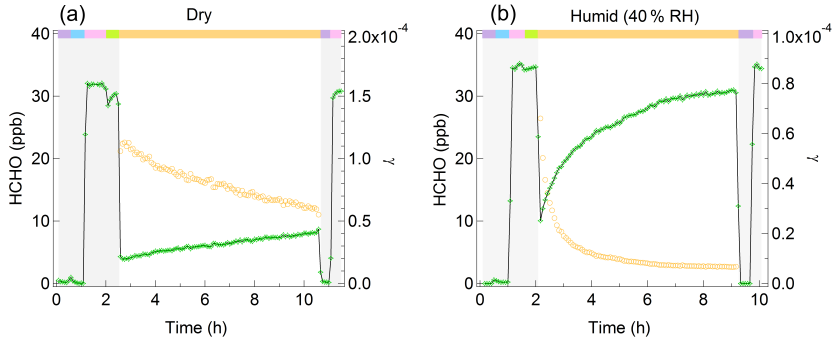

Figure 4. Observed HCHO (green diamonds) at the flow tube outlet and uptake coefficients (orange circles) as **(a)** ∼ 32 ppb of HCHO is exposed to soil at 0 % RH and **(b)** ∼ 35 ppb of HCHO is exposed to soil at 40 % RH. The bars with different colors indicate the time periods corresponding to different gas supply: purple bars (N_2), blue bar (N_2 after flowing through the soil-coated tube), pink bars (generated HCHO), green bar (HCHO after flowing through reference tube), orange bar (HCHO after flowing through soil-coated tube).

experiments were performed to check the temporal variability of the HCHO uptake coefficients.

We first investigated the case under dry conditions (RH of ∼ 0 %), in which ∼ 32 ppb of HCHO supplied by the HCHO generator was flushed through the flow tube. As shown in Fig. 4a, the largest HCHO uptake and decrease of HCHO concentration are found in the beginning of the uptake experiment. Within the 8 h experiment, γ is reduced from $(1.1 \pm 0.05) \times 10^{-4}$ to $(5.5 \pm 0.4) \times 10^{-5}$. To extend the generality of such dependence, we also conducted the same experiment but at RH of 40 %. As shown in Fig. 4b, the result reveals an even faster decay of γ over time suggesting an important role of water vapor in controlling the trace gas exchange at the atmosphere–soil interface.

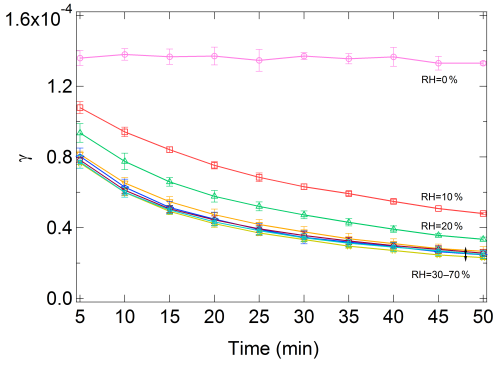

Figure 5. Uptake coefficients variation as a function of uptake time, under different RHs. The error bars represent the standard deviation of three replicate experiments.

3.3 Relative humidity (RH) effect

Water vapor has been suggested to influence the surface uptake for a variety of surface materials. On the one hand, it may compete for the reactive sites with other species and reduce their uptake (Ruiz et al., 1998; Goss et al., 2004; Donaldson et al., 2014a). On the other hand, the condensed water may attract more water-soluble or hydrophilic molecules and enhance the uptake (Pei and Zhang, 2011). To better understand the role of water molecules, we examined the RH dependence of uptake coefficients. Each experiment lasted for 50 min with the same setup as the aforementioned 8 h experiments.

Figure 5 shows the dependence of uptake coefficients of HCHO under different RHs. The highest value is achieved at dry conditions (RH of ∼ 0 %) and doesn't decrease much within the 50-min experiment. Increasing RH results in a sharp decrease of γ, until reaching a RH threshold level of ∼ 30 %. Above 30 % RH, γ becomes almost independent of RH. This RH effect could be expected for a longer uptake time period (e.g., 8 h), as the uptake coefficients always show a large difference between dry and humid conditions during the 8 h uptake experiments (Fig. 4a and b). For the detailed mechanism of the RH influence on HCHO uptake, see Sect. 3.6.

3.4 Concentration effect

We also investigated the dependence of the uptake coefficients on initial HCHO concentrations, under dry and humid conditions (Fig. 6). Under dry conditions, higher HCHO concentrations (20–40 ppb) lead to significantly reduced uptake coefficients. The HCHO molecules themselves exert a competition for reactive sites. This effect almost ceases under humidified conditions. As the number of water molecules is far more than that of HCHO and they both show competitive adsorption behavior on soil, it is conceivable that this concentration effect is weakened by increasing RH to 40 %, further confirming the strong influence of water on the HCHO uptake.

Such a dependence on the initial concentrations of analytes under low RH conditions had already been reported by other researchers. Sassine et al. (2010) investigated the HCHO uptake kinetics on TiO_2 mineral coatings and found that the

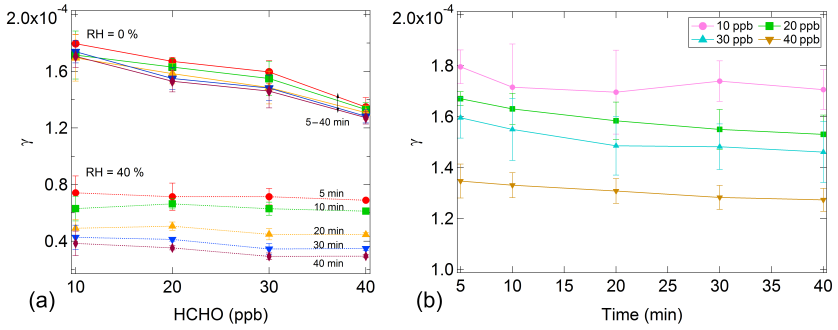

Figure 6. Dependence of uptake coefficients on initial HCHO concentrations at 0 and 40 % RH, after uptake time periods of 5 min (red), 10 min (green), 20 min (orange), 30 min (blue) and 40 min (purple) **(a)**; and uptake coefficients as a function of uptake time period at 0 % RH **(b)**; both under ambient pressure and 296 K. The error bars represent the standard deviation of three replicate experiments.

inverse of the uptake rate depended linearly on the inverse of the HCHO inlet concentrations. Wang et al. (2012) measured the uptake of NO_2 onto soil using a coated-wall flow tube and also observed that uptake coefficients were negatively dependent on NO_2 gas phase concentrations. They both gave explanations based on the Langmuir–Hinshelwood mechanism, in which gas molecules compete for the adsorption sites and the adsorbed molecules undergo following reactions. At higher HCHO concentrations (20–40 ppb) or/and higher water vapor partial pressure (RH = 40 %), the soil surface becomes more easily covered by adsorbed HCHO or/and H_2O molecules that had not yet reacted, resulting in lower probability of successful collisions between HCHO and the soil surface and thus a lowering of the uptake coefficient.

3.5 Reversibility of HCHO uptake

The decay of initial uptake is a common feature for trace gas uptake on different surfaces. It can be explained by different mechanisms, e.g., a process dominated by adsorption and chemical reactions; or a process governed by surface and bulk reactions. To explore the underlying mechanism, we conducted a back-flushing experiment and investigated the reversibility of HCHO uptake.

We first performed a standard experiment by flushing HCHO through a coated flow tube with RH of 50 %. Then the same tube was flushed with pure N_2 (HCHO free) and the amount of HCHO released elucidated potential uptake reversibility. Figure 7 shows that indeed the HCHO adsorbed by soil can be released back to the gas phase. The areas enclosed by the uptake and emission curves (orange area S_a and yellow area S_e) represent the amount of HCHO adsorbed and re-emitted by the soil, respectively. S_a and S_e could be calculated by curve fitting and integration. As the emission curve doesn't end with infinitely approaching the zero air signal, a fitted curve is used to consider this infinite decrease of HCHO signal and infer the total amount of re-emitted HCHO, reflected by S_e. Two functions are tested for emission curve fitting (parameters as detailed in Table 1). These fitting functions are derived on the basis of HCHO mass conservation in the flow tube, that is, the increase in gas flow HCHO concentration equals the HCHO released from the soil due to desorption and/or oligomer dissociation at the same time. The mass decay rate of HCHO on the soil which is determined by HCHO mass M and the net rate coefficient k can be expressed as $dM/dt = -k \times M^n$ (k reflects the net effect of emission rate and dissociation reaction rate on the soil surface; n means the apparent order of reactions between HCHO molecules (e.g., oligomerization), if $n = 1$, no reactions between HCHO molecules). Note that the HCHO mass decay mentioned here only takes into account processes which could re-emit HCHO into the gas phase (reversible reactions) rather than those converting HCHO into other products (irreversible reactions), as the emission curve in Fig. 7 only represents the reversible fraction. By solving the above differential equation and further taking the derivative of $M(t)$, the HCHO concentration C in the gas flow can be identified as a function of time t, as shown in Table 1 ($C = f(x)$, $t = x$). Table 1 compares two fitting functions, with the first one only accounting for zero and first order reactions and the second one further involving second order reactions. The latter provides better fitting results, implying the existence of physical/chemical interactions between adsorbed HCHO molecules on the soil surface (e.g., hydration and oligomerization). Thus, the second fitting function is applied to infer the total amount of re-emitted HCHO. The re-emitted HCHO is (70 ± 15) % ((average $\pm$ 1 standard deviation) %) of that adsorbed in the uptake experiment (Fig. 7), while the residual (30 ± 15) % remains in the soil. This partial reversibility suggests that HCHO uptake on soil is a combination of adsorption/desorption and chemical reactions.

To further explore the reasons for this partial reversibility, we conducted an energy dispersive X-ray (EDX) analysis of the soil sample. As shown in Fig. S2, inorganic elements (mainly exist as minerals) dominate the soil composition and the low fraction of carbon is consistent with the measurement of soil organic matter (Sect. 2.1). Among the inorganic elements, silicon is most abundant followed by alu-

Table 1. Parameters of fitting functions.

Functions	Coefficients (with 95 % confidence bounds)					Goodness of fit
	a	b	c	d	e	R^2
$f(x) = a + b \times \exp(-c \times x)$	-1.18×10^{-8}	39.7 (38.35, 41.04)	0.616 (0.607, 0.625)			0.944
$f(x) = a + b \times \exp(-c \times x) + d \times (e - d \times x)^{-2}$	-1.15×10^{-4} (−0.456, 0.455)	3.13 (2.35, 3.91)	0.214 (0.094, 0.333)	0.140 (0.121, 0.160)	0.264 (0.221, 0.308)	0.998

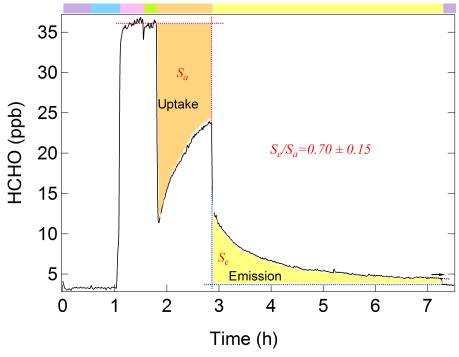

Figure 7. Reversible uptake of HCHO onto soil at 50 % RH. The yellow bar represents the time period when flushing with N_2 just after the uptake experiment; other color bars as in Fig. 4.

minium, calcium and iron, with their contents (wt %) being ∼ 64, ∼ 13, ∼ 6.3 and ∼ 5.7 %, respectively. The partial reversibility can be interpreted by the different uptake ability of various components. Carlos-Cuellar et al. (2003) reported that HCHO uptake was completely reversible on SiO_2 but only partly (< 1–15 %) reversible on α-Al_2O_3 and α-Fe_2O_3. Xu et al. (2011) investigated the heterogeneous reactions of HCHO on the surface of γ-Al_2O_3 particles and concluded that the adsorbed HCHO was firstly oxidized to dioxymethylene and further to formate. The fraction of silicon of ∼ 70 % (silicon content divided by the total amount of all inorganic elements) in the soil investigated here closely resembles the fraction of HCHO desorbed ((70 ± 15) %) from soil at zero air conditions.

Since mineral particles occupy the major volume (approximately 45–49 %) of soils (DeGomez et al., 2015) and silicon minerals (e.g., silicon oxides) are fairly common in mineral particles, the partial reversibility of HCHO uptake as shown in Fig. 7 may be expected as a general feature for other similar types of soils.

3.6 Uptake mechanism

Pore diffusion and surface processes could both account for the uptake of HCHO by soils. For pore diffusion within soils, the time scale depends on the thickness of the soil layer and the specific diffusion coefficients. Morrissey and Grismer (1999) reported typical macroscopic diffusion coefficients of VOCs ranging from 10^{-2} to 10^{-4} $cm^2\,min^{-1}$ for clay minerals. However, the effective diffusion coefficients of VOCs in soils depend on soil properties, e.g., soil porosity, pore geometry, grain size, soil water content etc. and on VOCs characteristics, e.g., molecular size, Henry's law constant, solubility etc. (Batterman et al., 1996). Adopting the above range and utilizing Fick's second law of diffusion for our experimental case, we estimate a time scale for HCHO diffusing through the soil layer from tens of seconds to several minutes. This time scale is much less than that for our uptake experiments (8 h), indicating that pore diffusion is not the limiting factor of uptake. In this sense, the uptake of HCHO by soil could be described by a mechanism including both adsorption/desorption and reactions of adsorbed HCHO on the soil surface.

For the adsorption process (Reaction R1), gas phase HCHO, HCHO(g), can react with a reactive site S on the soil surface and become adsorbed by soil. The adsorbed HCHO(ads) can desorb into gas phase and release the reactive site. Once adsorbed, individual HCHO molecules may react with adsorbed water (hydration) and/or further combine with other HCHO to form oligomers (Toda et al., 2014). On the other hand, HCHO(ads) can also be converted to other products through chemical reactions (Reaction R2).

$$\mathrm{HCHO(g)} + S \underset{k_d}{\overset{k_a}{\rightleftarrows}} \mathrm{HCHO(ads)} \underset{k_p}{\overset{k_o}{\rightleftarrows}} \mathrm{oligomers} \quad \text{(R1)}$$

$$\mathrm{HCHO(ads)} \xrightarrow{k_r} \mathrm{products} \quad \text{(R2)}$$

$$\mathrm{H_2O} + S \underset{k'_d}{\overset{k'_a}{\rightleftarrows}} \mathrm{H_2O(ads)} \quad \text{(R3)}$$

H_2O would also undergo adsorption/desorption processes (Reaction R3), occupy the reactive site and compete with HCHO. The competing effect of water molecules depends on the number of water monolayers on the soil surface. Ong and Lion (1991a) classified such effect into three regimes in their study of trichloroethylene (TCE) sorption on soil minerals. According to this mechanism, the first regime (regime I) is from dry conditions to one monolayer coverage of water on

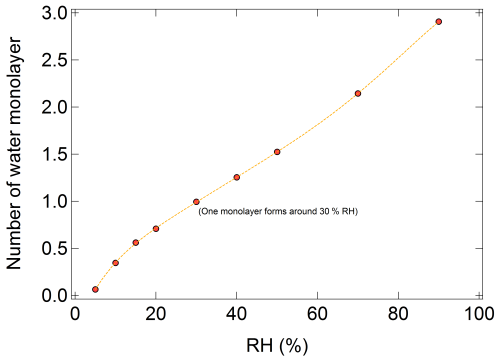

Figure 8. Number of soil surface water monolayers, based on gravimetric analysis of water uptake and soil surface area determined by the BET method.

the soil surface, where direct soil-gas sorption is evident with strong competition between water and HCHO for adsorption sites on soil. The second regime (regime II) corresponds to one to five monolayers of water molecules, with likely interactions between HCHO and water including sorption of HCHO onto surface-bound water that may lead to hydration and further oligomerization of HCHO, and limited dissolution into these monolayers. The third regime (regime III) starts from approximately five layers of water molecules up to the water holding capacity of soil, where the sorption of HCHO is dominated by condensed water on soil with respective dependence on Henry's law. In this regime, HCHO hydrates into methylene glycol or into polyoxymethylene glycols (oligomerization; Toda et al., 2014) which might further enhance the uptake of HCHO on soil.

Based on our BET experiment, one water monolayer forms at $\sim 30\,\%$ RH (Fig. 8) which is consistent with those values (20–30 %) reported by Donaldson et al. (2014a), Lammel (1999) and Goss (1993) retrieved across different soil types. For RH $\leq 30\,\%$, the HCHO sorption lies in the regime I, and water molecules show a large competing effect with HCHO as demonstrated by the strong negative dependence of γ on the RH (Fig. 5). For RH $> 30\,\%$, the water effect moves to the regime II. In this regime the adsorbed water is highly structured and modified by interactions with the soil mineral surface (Goss, 1992), and the surface area available for gas sorption is also kept constant (Goss et al., 2004). The constant surface area could explain the relatively stable uptake coefficients of HCHO observed between 30 and 70 % RH as shown in Fig. 5. We haven't reached regime III in our experiment (which would require a RH $> 90\,\%$). According to Ong and Lion (1991a), the uptake in regime III follows Henry's law. So increasing RH will increase the solvent volume (or number of water molecules) on the soil surface and thus increase the adsorption capacity.

In addition to the interactions between HCHO and water molecules in different regimes mentioned above, the rates

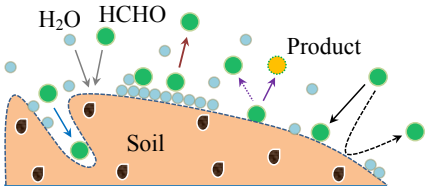

Figure 9. Schematic of HCHO uptake by soil surfaces.

of adsorption/desorption vs. the chemical reaction rates also come into play in the net exchange of HCHO.

During the uptake process, the rate expression for HCHO loss from the gas phase can be given by the following:

$$-\frac{\mathrm{d[HCHO(g)]}}{\mathrm{d}t} = k_a[\mathrm{HCHO(g)}][S] - k_d[\mathrm{HCHO(ads)}]. \quad (1)$$

From the point of kinetic gas theory, this loss rate could also be described as follows:

$$-\frac{\mathrm{d[HCHO(g)]}}{\mathrm{d}t} = \frac{\gamma_{\mathrm{HCHO}}\omega_{\mathrm{HCHO}}}{4} \times \frac{A_\mathrm{s}}{V} \times [\mathrm{HCHO(g)}] = \frac{\gamma_{\mathrm{HCHO}}\omega_{\mathrm{HCHO}}}{2r}[\mathrm{HCHO(g)}], \quad (2)$$

where γ_{HCHO} is the uptake coefficient of HCHO, ω_{HCHO} is the thermal velocity of HCHO, A_s is the geometric surface area of the soil, V and r are the volume and radius of the flow tube, respectively. Equating Eqs. (1) and (2) yields a positive correlation between $[S]$ and γ_{HCHO}. Increase of RH would decrease $[S]$ due to Reaction (R3) and thus further reduce the value of γ_{HCHO}. This further explains the RH dependence of γ as shown in Sect. 3.3.

For the variation of adsorbed HCHO on soil surface during the uptake, the adsorption/desorption, oligomerization/dissociation and chemical reactions are all considered and the rate is given as follows:

$$\frac{\mathrm{d[HCHO(ads)]}}{\mathrm{d}t} = k_a[\mathrm{HCHO(g)}][S] - k_d[\mathrm{HCHO(ads)}] + (k_p - k_o)[\mathrm{oligomers}] - k_r[\mathrm{HCHO(ads)}]. \quad (3)$$

At the start of uptake, [HCHO(ads)] is zero and only the forward reaction of adsorption is relevant. HCHO adsorbed onto the soil surface would accumulate and increase the rates of desorption, oligomerization and chemical reactions. [HCHO(ads)] will continuously grow until a steady state is established, in which case $\mathrm{d[HCHO(ads)]}/\mathrm{d}t = 0$ and the net loss of HCHO in the gas phase is dominated by chemical reactions on soil. Meanwhile, the oligomerization of adsorbed HCHO may serve as a temporary buffer, storing or releasing HCHO on soil. On the other hand, the emission of HCHO from soil can also be limited by dissociation of these oligomers and dehydration of HCHO hydrates, this may explain the prolonged emission curve found in Fig. 7.

4 Conclusions

We investigated the HCHO uptake on soil surfaces by a coated-wall flow tube method. Soil exhibits strong capacity for absorbing gaseous HCHO, with initial γ ranging from $(1.4 \pm 0.08) \times 10^{-4}$ at 0 % RH to $(3.0 \pm 0.3) \times 10^{-5}$ at 70 % RH based on the geometric soil surface. Because of simultaneously acting adsorption/desorption processes, γ shows a strong temporal dependence with an initial peak and subsequent decay until a steady state is reached. We also find a clear RH dependence of γ, especially in the low RH range (e.g., ≤ 30 %, under ambient pressure and temperature conditions) and little RH effect at RH > 30 %. The RH dependence of HCHO uptake can be explained by a transition of uptake pathways. Under low RH and water coverage (less than one monolayer) water molecules compete with gaseous HCHO for the adsorption sites on soil, while under high RH the soil surface is fully covered with water molecules providing a near constant amount of surface adsorption sites. Besides HCHO, a similar effect of RH had been reported for the soil uptake of other VOCs (Chiou and Shoup, 1985; Smith et al., 1990; Ong and Lion, 1991b, a; Pennell et al., 1992; Goss, 1993; Unger et al., 1996; Ruiz et al., 1998).

Our results also show that HCHO uptake on soil is a partially reversible process involving both adsorption/desorption and chemical reactions (see Fig. 9). The adsorption/desorption reveals a bi-directional exchange on soil surfaces in which soil could serve either as a source or as a sink depending on ambient conditions and trace gas concentrations. Because of the strong diurnal variability of ambient HCHO concentrations, soil water content, temperature and hence relative humidity, HCHO exchange at soil surfaces may quickly change its sign in a diurnal course as suggested for other trace gases such as HONO (Su et al., 2011; VandenBoer et al., 2015). The adsorption/desorption equilibrium and the competition effects of water vapor are likely to influence the atmosphere–soil exchange of other trace gases as well.

5 Data availability

The underlying research data can be accessed upon contact with Yafang Cheng (yafang.cheng@mpic.de) or Guo Li (guo.li@mpic.de).

Appendix A: Development and evaluation of the CKD-B method

The differential equation describing the analyte (HCHO for our experimental case) concentration C as a function of axial and radial position (z, r) in a flow tube, and a new boundary condition proposed in CKD are given as follows:

$$u\frac{\partial C}{\partial z} = D\frac{1}{r}\frac{\partial}{\partial r}\left(r\frac{\partial C}{\partial r}\right) \tag{A1}$$

$$-D\frac{\partial C}{\partial r}\bigg|_{\text{wall}} = C\frac{\bar{v}}{4}\frac{\gamma}{1-\left(\frac{\gamma}{2}\right)} \tag{A2}$$

$$-\frac{\partial C}{\partial r^*}\bigg|_{r^*=1} = N_{\text{Shw}}C \text{ with } r^* = \frac{r}{R}, \tag{A3}$$

in which u is the axial flow velocity and D is the gas diffusion coefficient under experimental conditions. $\bar{v}$ is the mean molecular speed and γ is the uptake coefficient. N_{Shw} is the Sherwood number and R is the radius of the flow tube.

Equation (A2) shows that C_{wall} (the concentration at the wall) is required to determine γ. However, the radial diffusion needs time and may result in a concentration gradient in the radial direction. Since we can only measure the averaged concentration instead of C_{wall}, the determination of γ cannot be achieved unless the C profile is determined first (Behnke et al., 1997; Monge et al., 2010; Sassine et al., 2010; Kebede et al., 2013) (for details see reference Murphy et al., 1987). Therefore the factor of $\gamma/(1-\gamma/2)$ rather than simply γ is used by Murphy et al. (1987) for a correction to the wall collision rate in the presence of a concentration gradient near the wall. Equation (A3) is taken as a dimensionless form of Eq. (A2).

For each given γ, a differential equation provided in CKD method (Eq. A1) can be solved for a C profile and the functional relationship between transmittance of the analyte in the flow tube ($C_{\text{out}}/C_{\text{in}}$, C_{out}, and C_{in} correspond to the concentrations of analyte at the outlet and the inlet of the flow tube, respectively) and γ (strictly the Sherwood number N_{Shw} as detailed in reference Murphy and Fahey, 1987) can be established. Then by measuring the transmittance, we can determine the desired uptake coefficients. It can be conceived that the γ – transmittance relation also depends on flow rate and the flow tube dimensions. Therefore, Murphy and Fahey (1987) provided a table of coefficients for a range of these parameters. When conditions were not available from the table, interpolation was often used in previous studies.

Here we directly solve the differential equation with numerical methods (code provided in the Supplement) rather than using interpolated values. As this operation is based on the CKD method, it can be specified as a CKD-based method (CKD-B), and this nomenclature is adopted above. More recently, another new analytical method has been derived by Knopf, Pöschl and Shiraiwa (KPS), based on a recently developed kinetic flux model framework and models discribing interactions of gas species with aerosol particles (Knopf et al., 2015) (for details see references therein). As the KPS method provides efficient and robust analyses and predictions of gas and particle uptake in flow tube experiments encountering diffusion limitation, here, we make a comparison between CKD-B and KPS. Figure S3 shows that both methods agree very well for deriving the dependence of transmittance $C_{\text{out}}/C_{\text{in}}$ on γ, under the specific flow rate and flow tube dimensions in our experimental case. To further test the accuracy of CKD-B method, the dependence of transmittance $C_{\text{out}}/C_{\text{in}}$ on the Sherword number (N_{Shw}) is compared between CKD-B and CKD as well. Figure S4 shows a good agreement between results from CKD (red dots) and CKD-B (black line).

The Supplement related to this article is available online at doi:10.5194/acp-16-10299-2016-supplement.

Acknowledgements. This study was supported by the Max Planck Society (MPG) and National Natural Science Foundation of China (41330635). Guo Li acknowledges the financial support from the China Scholarship Council (CSC). We are grateful to Sorowka Antje for her help with the SEM and EDX analysis of the soil sample.

The article processing charges for this open-access publication were covered by the Max Planck Society.

Edited by: F. Keutsch
Reviewed by: two anonymous referees

References

Andreae, M. O. and Merlet, P.: Emission of trace gases and aerosols from biomass burning, Global Biogeochem. Cy., 15, 955–966, 2001.

Ayers, G. P., Gillett, R. W., Granek, H., deServes, C., and Cox, R. A.: Formaldehyde production in clean marine air, Geophys. Res. Lett., 24, 401–404, 1997.

Batterman, S., Padmanabham, I., and Milne, P.: Effective gas-phase diffusion coefficients in soils at varying water content measured using a one-flow sorbent based technique, Environ. Sci. Technol., 30, 770–778, 1996.

Behnke, W., George, C., Scheer, V., and Zetzsch, C.: Production and decay of $ClNO_2$, from the reaction of gaseous N_2O_5 with NaCl solution: Bulk and aerosol experiments, J. Geophys. Res.-Atmos., 102, 3795–3804, 1997.

Brunauer, S., Emmett, P. H., and Teller, E.: Adsorption of Gases in Multimolecular Layers, J. Am. Chem. Soc., 60, 309–319, doi:10.1021/ja01269a023, 1938.

Carlier, P., Hannachi, H., and Mouvier, G.: The Chemistry of Carbonyl-Compounds in the Atmosphere – a Review, Atmos. Environ., 20, 2079–2099, 1986.

Carlos-Cuellar, S., Li, P., Christensen, A. P., Krueger, B. J., Burrichter, C., and Grassian, V. H.: Heterogeneous uptake kinetics of volatile organic compounds on oxide surfaces using a Knudsen cell reactor: Adsorption of acetic acid, formaldehyde, and methanol on alpha-Fe_2O_3, alpha-Al_2O_3, and SiO_2, J. Phys. Chem. A, 107, 4250–4261, 2003.

Chiou, C. T. and Shoup, T. D.: Soil Sorption of Organic Vapors and Effects of Humidity on Sorptive Mechanism and Capacity, Environ. Sci. Technol., 19, 1196–1200, 1985.

Dasgupta, P. K., Dong, S., Hwang, H., Yang, H. C., and Genfa, Z.: Continuous Liquid-Phase Fluorometry Coupled to a Diffusion Scrubber for the Real-Time Determination of Atmospheric Formaldehyde, Hydrogen-Peroxide and Sulfur-Dioxide, Atmos. Environ., 22, 949–963, 1988.

DeGomez, T., Kolb, P., and Kleinman, S.: Basic Soil Components, available at: http://articles.extension.org/pages/54401/basic-soil-components (accessed 10 July 2016), 2015.

DiGangi, J. P., Boyle, E. S., Karl, T., Harley, P., Turnipseed, A., Kim, S., Cantrell, C., Maudlin III, R. L., Zheng, W., Flocke, F., Hall, S. R., Ullmann, K., Nakashima, Y., Paul, J. B., Wolfe, G. M., Desai, A. R., Kajii, Y., Guenther, A., and Keutsch, F. N.: First direct measurements of formaldehyde flux via eddy covariance: implications for missing in-canopy formaldehyde sources, Atmos. Chem. Phys., 11, 10565–10578, doi:10.5194/acp-11-10565-2011, 2011.

Donaldson, M. A., Berke, A. E., and Raff, J. D.: Uptake of Gas Phase Nitrous Acid onto Boundary Layer Soil Surfaces, Environ. Sci. Technol., 48, 375–383, 2014a.

Donaldson, M. A., Bish, D. L., and Raff, J. D.: Soil surface acidity plays a determining role in the atmospheric-terrestrial exchange of nitrous acid, P. Natl. Acad. Sci. USA, 111, 18472–18477, doi:10.1073/pnas.1418545112, 2014b.

Fried, A., McKeen, S., Sewell, S., Harder, J., Henry, B., Goldan, P., Kuster, W., Williams, E., Baumann, K., Shetter, R., and Cantrell, C.: Photochemistry of formaldehyde during the 1993 Tropospheric OH Photochemistry Experiment, J. Geophys. Res.-Atmos., 102, 6283–6296, 1997.

Fried, A., Crawford, J., Olson, J., Walega, J., Potter, W., Wert, B., Jordan, C., Anderson, B., Shetter, R., Lefer, B., Blake, D., Blake, N., Meinardi, S., Heikes, B., O'Sullivan, D., Snow, J., Fuelberg, H., Kiley, C. M., Sandholm, S., Tan, D., Sachse, G., Singh, H., Faloona, I., Harward, C. N., and Carmichael, G. R.: Airborne tunable diode laser measurements of formaldehyde during TRACE-P: Distributions and box model comparisons, J. Geophys. Res.-Atmos., 108, 8798, doi:10.1029/2003JD003451, 2003.

Goss, K. U.: Effects of Temperature and Relative-Humidity on the Sorption of Organic Vapors on Quartz Sand, Environ. Sci. Technol., 26, 2287–2294, 1992.

Goss, K. U.: Effects of Temperature and Relative-Humidity on the Sorption of Organic Vapors on Clay-Minerals, Environ. Sci. Technol., 27, 2127–2132, 1993.

Goss, K. U., Buschmann, J., and Schwarzenbach, R. P.: Adsorption of organic vapors to air-dry soils: Model predictions and experimental validation, Environ. Sci. Technol., 38, 3667-3673, 2004.

Gray, C. M., Monson, R. K., and Fierer, N.: Biotic and abiotic controls on biogenic volatile organic compound fluxes from a subalpine forest floor, J. Geophys. Res.-Biogeo., 119, 547–556, 2014.

Hak, C., Pundt, I., Trick, S., Kern, C., Platt, U., Dommen, J., Ordóñez, C., Prévôt, A. S. H., Junkermann, W., Astorga-Lloréns, C., Larsen, B. R., Mellqvist, J., Strandberg, A., Yu, Y., Galle, B., Kleffmann, J., Lörzer, J. C., Braathen, G. O., and Volkamer, R.: Intercomparison of four different in-situ techniques for ambient formaldehyde measurements in urban air, Atmos. Chem. Phys., 5, 2881–2900, doi:10.5194/acp-5-2881-2005, 2005.

Heikes, B., Lee, M. H., Jacob, D., Talbot, R., Bradshaw, J., Singh, H., Blake, D., Anderson, B., Fuelberg, H., and Thompson, A. M.: Ozone, hydroperoxides, oxides of nitrogen, and hydrocarbon budgets in the marine boundary layer over the South Atlantic, J. Geophys. Res.-Atmos., 101, 24221–24234, 1996.

Jacob, D. J.: Heterogeneous chemistry and tropospheric ozone, Atmos. Environ., 34, 2131–2159, 2000.

Jacob, D. J., Heikes, B. G., Fan, S. M., Logan, J. A., Mauzerall, D. L., Bradshaw, J. D., Singh, H. B., Gregory, G. L., Talbot, R. W., Blake, D. R., and Sachse, G. W.: Origin of ozone and NO_x in the tropical troposphere: A photochemical analysis of aircraft obser-

vations over the South Atlantic basin, J. Geophys. Res.-Atmos., 101, 24235–24250, 1996.

Jaegle, L., Jacob, D. J., Brune, W. H., Faloona, I., Tan, D., Heikes, B. G., Kondo, Y., Sachse, G. W., Anderson, B., Gregory, G. L., Singh, H. B., Pueschel, R., Ferry, G., Blake, D. R., and Shetter, R. E.: Photochemistry of HO_x in the upper troposphere at northern midlatitudes, J. Geophys. Res.-Atmos., 105, 3877–3892, 2000.

Junkermann, W. and Burger, J. M.: A new portable instrument for continuous measurement of formaldehyde in ambient air, J. Atmos. Ocean. Tech., 23, 38–45, 2006.

Kahle, M., Kleber, M., and Jahn, R.: Carbon storage in loess derived surface soils from Central Germany: Influence of mineral phase variables, J. Plant Nutr. Soil Sc., 165, 141–149, 2002.

Kaiser, J., Li, X., Tillmann, R., Acir, I., Holland, F., Rohrer, F., Wegener, R., and Keutsch, F. N.: Intercomparison of Hantzsch and fiber-laser-induced-fluorescence formaldehyde measurements, Atmos. Meas. Tech., 7, 1571–1580, doi:10.5194/amt-7-1571-2014, 2014.

Kalberer, M., Ammann, M., Arens, F., Gaggeler, H. W., and Baltensperger, U.: Heterogeneous formation of nitrous acid (HONO) on soot aerosol particles, J. Geophys. Res.-Atmos., 104, 13825–13832, 1999.

Kebede, M. A., Varner, M. E., Scharko, N. K., Gerber, R. B., and Raff, J. D.: Photooxidation of Ammonia on TiO_2 as a Source of NO and NO_2 under Atmospheric Conditions, J. Am. Chem. Soc., 135, 8606–8615, 2013.

Knopf, D. A., Pöschl, U., and Shiraiwa, M.: Radial Diffusion and Penetration of Gas Molecules and Aerosol Particles through Laminar Flow Reactors, Denuders, and Sampling Tubes, Anal. Chem., 87, 3746–3754, 2015.

Kormann, R., Fischer, H., de Reus, M., Lawrence, M., Brühl, Ch., von Kuhlmann, R., Holzinger, R., Williams, J., Lelieveld, J., Warneke, C., de Gouw, J., Heland, J., Ziereis, H., and Schlager, H.: Formaldehyde over the eastern Mediterranean during MINOS: Comparison of airborne in-situ measurements with 3D-model results, Atmos. Chem. Phys., 3, 851–861, doi:10.5194/acp-3-851-2003, 2003.

Kulmala, M. and Petaja, T.: Soil Nitrites Influence Atmospheric Chemistry, Science, 333, 1586–1587, 2011.

Lammel, G.: Formation of Nitrous Acid: Parameterisation and Comparison with Observations, Max-Planck-Institut für Meteorologie, Publisher location: Hamburg, Germany, 286, 1999.

Lee, Y. N., Zhou, X., Kleinman, L. I., Nunnermacker, L. J., Springston, S. R., Daum, P. H., Newman, L., Keigley, W. G., Holdren, M. W., Spicer, C. W., Young, V., Fu, B., Parrish, D. D., Holloway, J., Williams, J., Roberts, J. M., Ryerson, T. B., and Fehsenfeld, F. C.: Atmospheric chemistry and distribution of formaldehyde and several multioxygenated carbonyl compounds during the 1995 Nashville Middle Tennessee Ozone Study, J. Geophys. Res.-Atmos., 103, 22449–22462, 1998.

Li, X., Rohrer, F., Brauers, T., Hofzumahaus, A., Lu, K., Shao, M., Zhang, Y. H., and Wahner, A.: Modeling of HCHO and CHOCHO at a semi-rural site in southern China during the PRIDE-PRD2006 campaign, Atmos. Chem. Phys., 14, 12291–12305, doi:10.5194/acp-14-12291-2014, 2014.

Liu, S. C., Trainer, M., Carroll, M. A., Hubler, G., Montzka, D. D., Norton, R. B., Ridley, B. A., Walega, J. G., Atlas, E. L., Heikes, B. G., Huebert, B. J., and Warren, W.: A Study of the Photochemistry and Ozone Budget during the Mauna-Loa-Observatory Photochemistry Experiment, J. Geophys. Res.-Atmos., 97, 10463–10471, 1992.

Lowe, D. C. and Schmidt, U.: Formaldehyde (HCHO) measurements in the nonurban atmosphere, J. Geophys. Res., 88, 10844–10858, 1983.

Monge, M. E., D'Anna, B., Mazri, L., Giroir-Fendler, A., Ammann, M., Donaldson, D. J., and George, C.: Light changes the atmospheric reactivity of soot, P. Natl. Acad. Sci. USA, 107, 6605–6609, 2010.

Morrissey, F. A. and Grismer, M. E.: Kinetics of volatile organic compound sorption/desorption on clay minerals, J. Contam. Hydrol., 36, 291–312, 1999.

Murphy, D. M. and Fahey, D. W.: Mathematical Treatment of the Wall Loss of a Trace Species in Denuder and Catalytic-Converter Tubes, Anal. Chem., 59, 2753–2759, 1987.

Ong, S. K. and Lion, L. W.: Mechanisms for Trichloroethylene Vapor Sorption onto Soil Minerals, J. Environ. Qual., 20, 180–188, 1991a.

Ong, S. K. and Lion, L. W.: Effects of Soil Properties and Moisture on the Sorption of Trichloroethylene Vapor, Water Res., 25, 29–36, 1991b.

Oswald, R., Behrendt, T., Ermel, M., Wu, D., Su, H., Cheng, Y., Breuninger, C., Moravek, A., Mougin, E., Delon, C., Loubet, B., Pommerening-Roser, A., Sorgel, M., Poschl, U., Hoffmann, T., Andreae, M. O., Meixner, F. X., and Trebs, I.: HONO Emissions from Soil Bacteria as a Major Source of Atmospheric Reactive Nitrogen, Science, 341, 1233–1235, 2013.

Parrish, D. D., Ryerson, T. B., Mellqvist, J., Johansson, J., Fried, A., Richter, D., Walega, J. G., Washenfelder, R. A., de Gouw, J. A., Peischl, J., Aikin, K. C., McKeen, S. A., Frost, G. J., Fehsenfeld, F. C., and Herndon, S. C.: Primary and secondary sources of formaldehyde in urban atmospheres: Houston Texas region, Atmos. Chem. Phys., 12, 3273–3288, doi:10.5194/acp-12-3273-2012, 2012.

Pei, J. J. and Zhang, J. S. S.: On the performance and mechanisms of formaldehyde removal by chemi-sorbents, Chem. Eng. J., 167, 59–66, 2011.

Pennell, K. D., Rhue, R. D., Rao, P. S. C., and Johnston, C. T.: Vapor-Phase Sorption of Para-Xylene and Water on Soils and Clay-Minerals, Environ. Sci. Technol., 26, 756–763, 1992.

Preunkert, S., Legrand, M., Pepy, G., Gallee, H., Jones, A., and Jourdain, B.: The atmospheric HCHO budget at Dumont d'Urville (East Antarctica): Contribution of photochemical gas-phase production versus snow emissions, J Geophys. Res.-Atmos., 118, 13319–13337, 2013.

Preunkert, S., Legrand, M., Frey, M. M., Kukui, A., Savarino, J., Gallée, H., King, M., Jourdain, B., Vicars, W., and Helmig, D.: Formaldehyde (HCHO) in air, snow, and interstitial air at Concordia (East Antarctic Plateau) in summer, Atmos. Chem. Phys., 15, 6689–6705, doi:10.5194/acp-15-6689-2015, 2015.

Price, H., Jaegle, L., Rice, A., Quay, P., Novelli, P. C., and Gammon, R.: Global budget of molecular hydrogen and its deuterium content: Constraints from ground station, cruise, and aircraft observations, J. Geophys. Res.-Atmos., 112, D22108, doi:10.1029/2006JD008152, 2007.

Punrattanasin, P. and Sariem, P.: Adsorption of Copper, Zinc, and Nickel Using Loess as Adsorbents, Pol. J. Environ. Stud., 24, 1259–1266, doi:10.15244/pjoes/30264, 2015.

Rodier, D. R. and Birks, J. W.: Evaluation of Isoprene Oxidation as an Interference in the Cartridge Sampling and Derivatization of Atmospheric Carbonyl-Compounds, Environ. Sci. Technol., 28, 2211–2215, 1994.

Ruiz, J., Bilbao, R., and Murillo, M. B.: Adsorption of different VOC onto soil minerals from gas phase: Influence of mineral, type of VOC, and air humidity, Environ. Sci. Technol., 32, 1079–1084, 1998.

Sassine, M., Burel, L., D'Anna, B., and George, C.: Kinetics of the tropospheric formaldehyde loss onto mineral dust and urban surfaces, Atmos. Environ., 44, 5468–5475, 2010.

Seinfeld, J. H. and Pandis, S. N.: Atmospheric Chemistry and Physics: From Air Pollution to Climate Change, 2nd Edn., Wiley, New York, 2006.

Smith, J. A., Chiou, C. T., Kammer, J. A., and Kile, D. E.: Effect of Soil Moisture on the Sorption of Trichloroethene Vapor to Vadose-Zone Soil at Pictinny Arsenal, New Jersey, Environ. Sci. Technol., 24, 676–683, 1990.

Su, H., Cheng, Y. F., Oswald, R., Behrendt, T., Trebs, I., Meixner, F. X., Andreae, M. O., Cheng, P., Zhang, Y., and Pöschl, U.: Soil Nitrite as a Source of Atmospheric HONO and OH Radicals, Science, 333, 1616–1618, 2011.

Tie, X., Brasseur, G., Emmons, L., Horowitz, L., and Kinnison, D.: Effects of aerosols on tropospheric oxidants: A global model study, J. Geophys. Res.-Atmos., 106, 22931–22964, 2001.

Toda, K., Yunoki, S., Yanaga, A., Takeuchi, M., Ohira, S. I., and Dasgupta, P. K.: Formaldehyde Content of Atmospheric Aerosol, Environ. Sci. Technol., 48, 6636–6643, 2014.

Unger, D. R., Lam, T. T., Schaefer, C. E., and Kosson, D. S.: Predicting the effect of moisture on vapor-phase sorption of volatile organic compounds to soils, Environ. Sci. Technol., 30, 1081–1091, 1996.

Usher, C. R., Michel, A. E., and Grassian, V. H.: Reactions on mineral dust, Chem. Rev., 103, 4883–4939, 2003.

VandenBoer, T. C., Young, C. J., Talukdar, R. K., Markovic, M. Z., Brown, S. S., Roberts, J. M., and Murphy, J. G.: Nocturnal loss and daytime source of nitrous acid through reactive uptake and displacement, Nat. Geosci., 8, 55–60, doi:10.1038/ngeo2298, 2015.

Wagner, V., von Glasow, R., Fischer, H., and Crutzen, P. J.: Are CH_2O measurements in the marine boundary layer suitable for testing the current understanding of CH_4 photooxidation?: A model study, J. Geophys. Res.-Atmos., 107, 4029, doi:10.1029/2001JD000722, 2002.

Wang, L., Wang, W. G., and Ge, M. F.: Heterogeneous uptake of NO_2 on soils under variable temperature and relative humidity conditions, J. Environ. Sci.-China, 24, 1759–1766, doi:10.1016/S1001-0742(11)61015-2, 2012.

Weller, R., Schrems, O., Boddenberg, A., Gab, S., and Gautrois, M.: Meridional distribution of hydroperoxides and formaldehyde in the marine boundary layer of the Atlantic (48° N–35° S) measured during the Albatross campaign, J. Geophys. Res.-Atmos., 105, 14401–14412, 2000.

Xu, B. Y., Shang, J., Zhu, T., and Tang, X. Y.: Heterogeneous reaction of formaldehyde on the surface of gamma-Al_2O_3 particles, Atmos. Environ., 45, 3569–3575, 2011.

Zhou, X. L., Lee, Y. N., Newman, L., Chen, X. H., and Mopper, K.: Tropospheric formaldehyde concentration at the Mauna Loa observatory during the Mauna Loa observatory photochemistry experiment 2, J. Geophys. Res.-Atmos., 101, 14711–14719, 1996.

Supplement of Atmos. Chem. Phys., 16, 10299–10311, 2016
http://www.atmos-chem-phys.net/16/10299/2016/
doi:10.5194/acp-16-10299-2016-supplement

Atmospheric Chemistry and Physics Open Access EGU

Supplement of

Uptake of gaseous formaldehyde by soil surfaces: a combination of adsorption/desorption equilibrium and chemical reactions

Guo Li et al.

Correspondence to: Yafang Cheng (yafang.cheng@mpic.de) and Min Shao (mshao@pku.edu.cn)

Initial HCHO con. C_{in} (ppb)	RH (%)	$\gamma^a \times 10^{-5}$	$\gamma^b \times 10^{-5}$	$\gamma^c \times 10^{-5}$	$\gamma^d \times 10^{-5}$	$\gamma^e \times 10^{-5}$	$\gamma^f \times 10^{-5}$
10	0	17.9 ± 0.7	17.2 ± 1.7	17.0 ± 1.6	17.4 ± 0.8	17.1 ± 0.8	16.7 ± 1.3
10	40	7.4 ± 1.2	6.3 ± 0.9	4.9 ± 0.6	4.3 ± 0.8	3.8 ± 0.9	3.5 ± 0.8
20	0	16.7 ± 0.3	16.3 ± 0.6	15.8 ± 0.7	15.5 ± 0.8	15.3 ± 0.8	15.4 ± 0.4
20	40	7.2 ± 1.0	6.6 ± 0.4	5.1 ± 0.3	4.1 ± 0.1	3.5 ± 0.1	3.2 ± 0.1
30	0	16.0 ± 0.8	15.5 ± 1.2	14.8 ± 1.2	14.8 ± 0.9	14.6 ± 1.2	14.2 ± 0.9
30	10	11.6 ± 0.3	9.4 ± 0.3	7.5 ± 0.2	6.3 ± 0.2	5.5 ± 0.1	4.8 ± 0.1
30	20	10.4 ± 0.5	7.8 ± 0.5	5.8 ± 0.3	4.7 ± 0.2	3.9 ± 0.2	3.3 ± 0.1
30	30	9.4 ± 0.3	6.5 ± 0.3	4.7 ± 0.3	3.8 ± 0.3	3.1 ± 0.3	2.7 ± 0.2
30	40	7.1 ± 0.6	6.3 ± 0.5	4.5 ± 0.4	3.4 ± 0.4	2.9 ± 0.2	2.5 ± 0.2
30	50	7.6 ± 0.3	6.0 ± 0.2	4.2 ± 0.2	3.3 ± 0.1	2.7 ± 0.1	2.3 ± 0.1
30	60	7.8 ± 0.1	6.1 ± 0.2	4.4 ± 0.2	3.6 ± 0.2	3.0 ± 0.2	2.6 ± 0.2
30	70	7.7 ± 0.4	6.0 ± 0.3	4.3 ± 0.2	3.4 ± 0.2	2.9 ± 0.2	2.5 ± 0.2
40	0	13.5 ± 0.7	13.3 ± 0.5	13.1 ± 0.5	12.8 ± 0.5	12.7 ± 0.4	12.7 ± 0.3
40	40	6.9 ± 0.1	6.1 ± 0.2	4.5 ± 0.2	3.5 ± 0.2	2.9 ± 0.1	2.5 ± 0.1

[a]Uptake coefficients at uptake time period of 5 min. [b]10 min. [c]20min. [d]30min.[e]40min.[f]50min.

The error bars represent one standard deviation of three replicates.

Table S.1. Calculated HCHO uptake coefficients as a function of initial HCHO concentration, relative humidity and uptake time period.

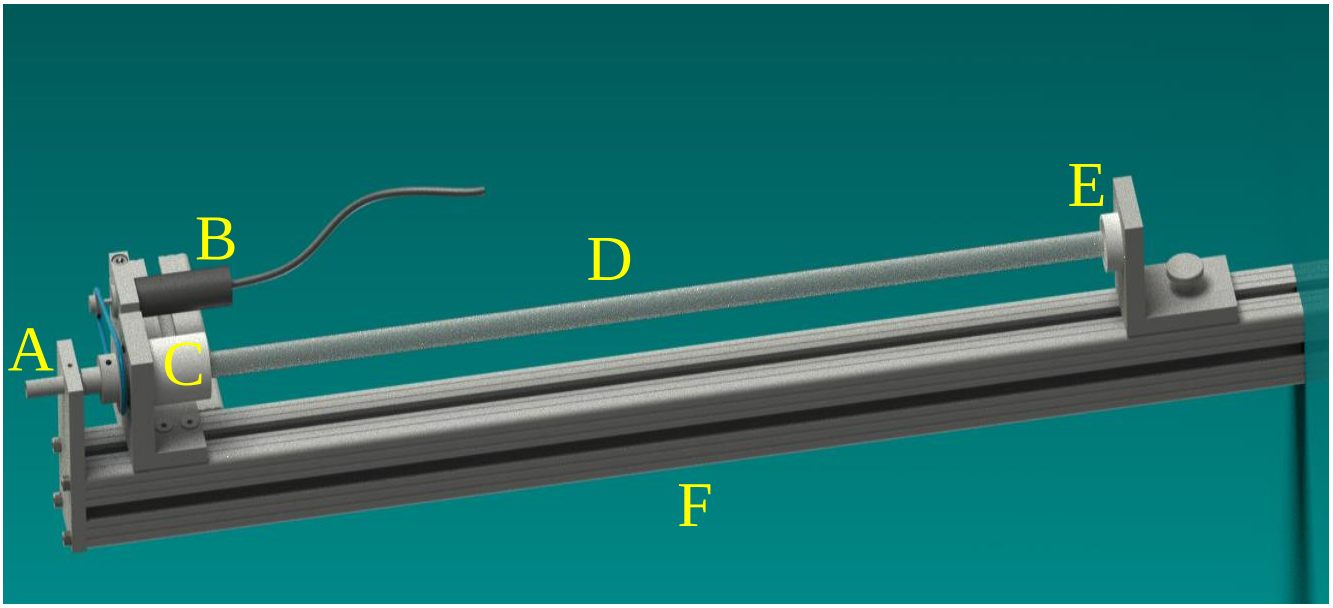

Figure S.1. Air-dried continuous rotating coating tool (ACRO). (A) flushing gas inlet; (B) motor with a driving belt; (C) fastened tubing holder; (D) coated flow tube; (E) loosened tubing holder; (F) foothold.

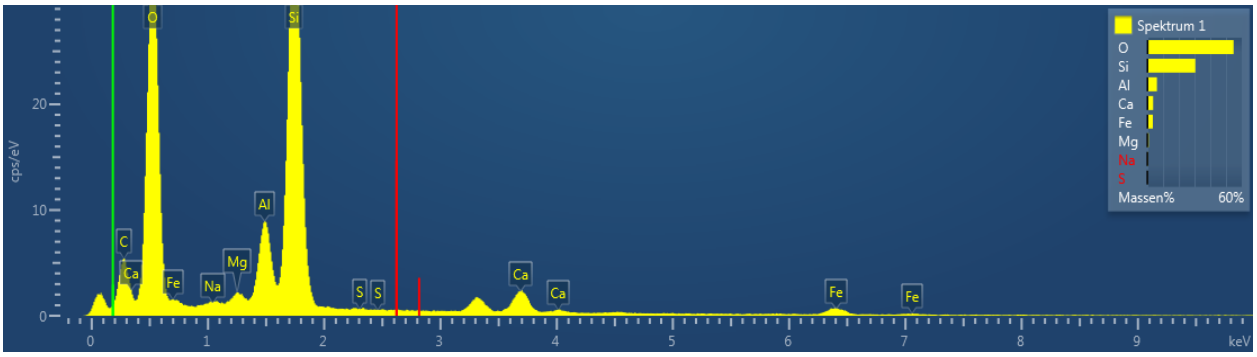

Figure S.2. Energy Dispersive X-ray (EDX) analysis of the soil sample.

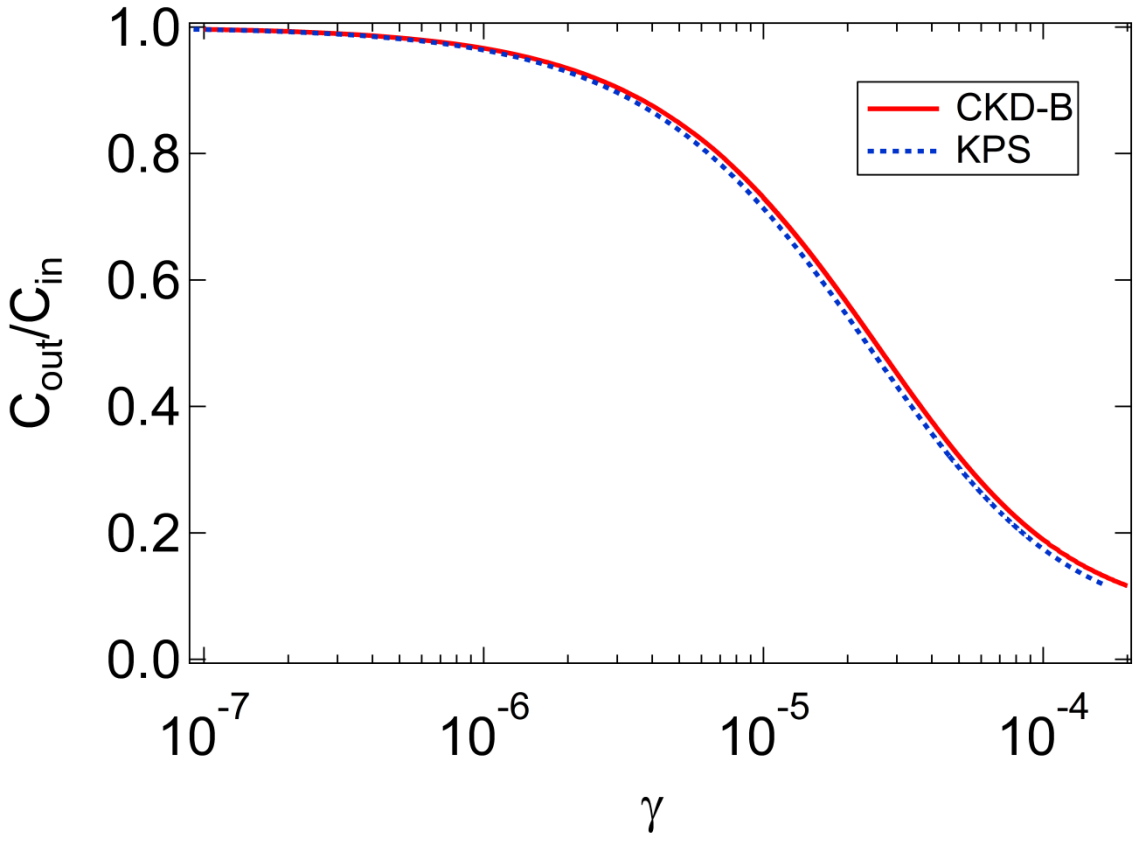

Figure S.3. Transmittance C_{out}/C_{in} versus uptake coefficients derived from both CKD-B and KPS methods, for specified dimensionless length $z^* = 0.385$ under our experimental conditions.

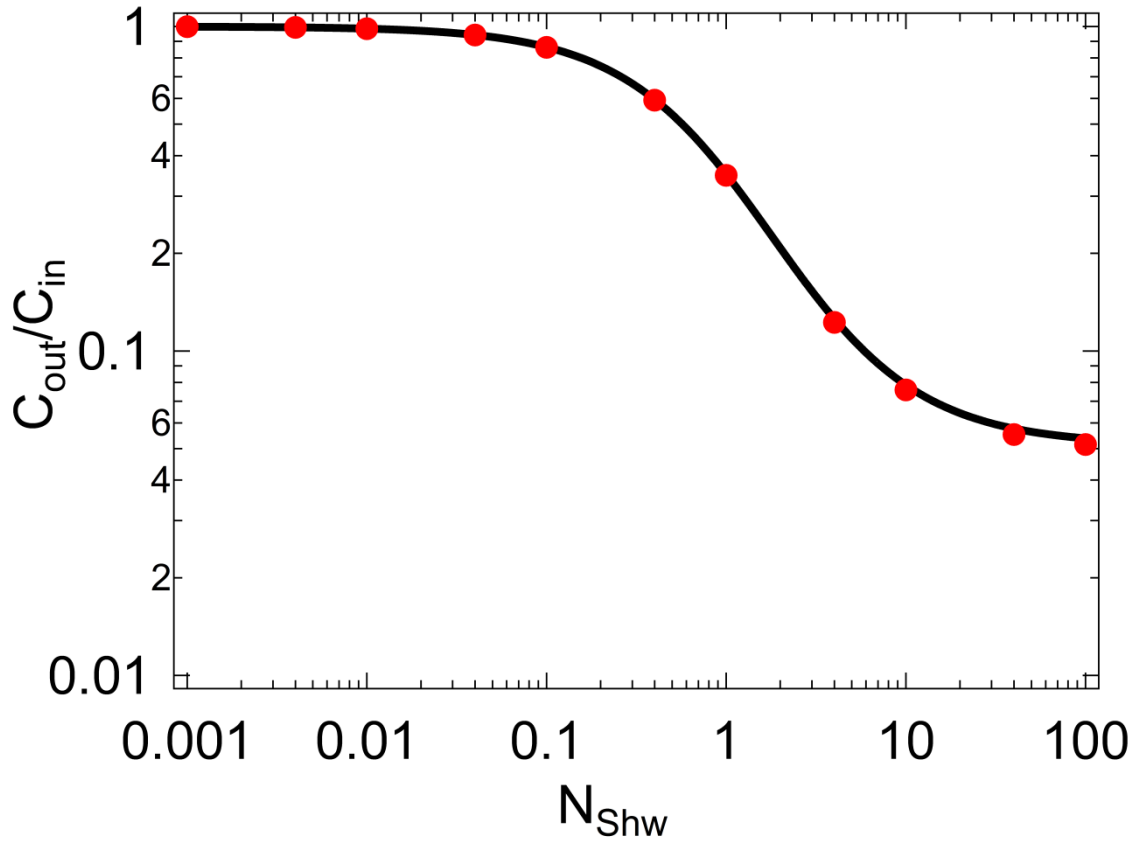

Figure S.4. Transmittance C_{out}/C_{in} versus Sherwood number N_{Shw}, for specified dimensionless length $z^* = 0.385$ under our experimental conditions. The red dots represent the values from Table I in the reference of Murphy et al., (1987); the black line denotes values from our calculations.

Matlab code mannul

(1) Parameters definition

The parameters adopted in the provided code are defined as follows:

L: flow tube length; *R*: flow tube radius; *z*: axial position; *r*: radial position; *F*: volume flow rate of carrier gas in flow tube; *D*: diffusion coefficient of analyte in the carrier gas under experimental conditions; T_0: standard temperature, 273K; P_0: standard pressure, 101kPa; *T*: temperature at experimental conditions; *P*: pressure at experimental conditions; *g*: the uptake coefficient; *g*_min: the minimum value of the uptake coefficient; *g*_max: the maximum value of the uptake coefficient; *g_n*: the number of values of *g* from *g*_min to *g*_max; *x*: the dimensionless form of radius position *r*, $x = r/R$, ranging from 0 to 1; *t*: the dimensionless form of axial position *z*, $t = z\times\pi\times D/(2\times F)\times(T_0/T)\times(P/P_0)$, ranging from 0 to t_0; t_0: $t_0 = L\times\pi\times D/(2\times F)\times(T_0/T)\times(P/P_0)$; *u*: analyte concentration at the axial and radial position (dimensionless) of (*t* , *x*); *v*: analyte mean molecular speed; *N*: Sherwood number.

For the axial and radial position (*z*, *r*) in a flow tube, see Fig. S.5.

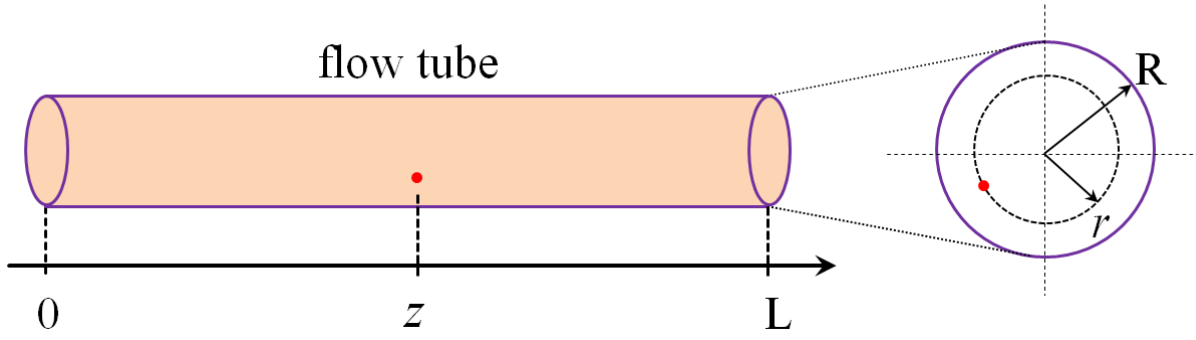

Figure S.5. Schematic of the axial and radial position (*z*, *r*) in a flow tube with length of *L* and radius of *R*.

(2) Parameters input

Open all the *.m files and input the following parameters: *L*, *R*, *F*, *D*, *T*, *P* and *v* according to the specific experimental conditions applied. Note that *g*_min, *g*_max and *g*_n should be specified in advance and also for the numbers (*n*) of *t* and *x* within their effective ranges. In principle, the larger the *n* input, the more precise the results are.

(3) Results output

After input/change of the parameters, please SAVE the parameters setting. Then RUN the Main.m file. A red process bar will show as the code is running. Please wait until the calculation ends. The output results include two tables and two plots:

`table_g = [g', end_mean_u']` = table [γ, C_{out}/C_{in}]

`table_N = [N', end_mean_u']` = table [N_{Shw}, C_{out}/C_{in}]

`plot(g, end_mean_u)` = plot (γ, C_{out}/C_{in})

`plot(N, end_mean_u)` = plot (N_{Shw}, C_{out}/C_{in})

The tables and plots will be saved automatically into the folder in which the *.m files are located.

Matlab code

Main.m

```
function Main()
L = 0.25;
% the length of the flow tube, 0.25 m
F = 1*10^(-3)/60;
% the sample volume flow rate, 1.6667e-005 m^3/s
D = 0.0000177;
% HCHO diffusion coefficient in N2 at 296k and 101kPa, 0.0000177 m^2/s
T0 = 273;
% temperature at standard conditions, 273 K
P0 = 101;
% pressure at standard conditions, 101 kPa
T = 296;
% temperature at experimental conditions, 296 K
P = 101;
% pressure at experimental conditions, 101 kPa
t0=L*pi*D/(2*F)*(T0/T)*(P/P0);
g_min= 1e-7;
g_max = 1e-4;
g_n = 100;
% g is uptake coefficient, g_n is the number of g between g_min and g_max
pdex1(t0,g_min,g_max,g_n)
```

pdex1.m

```
function pdex1(t0,g_min,g_max,g_n)
m = 1;
x = linspace(0,1,100);
% x = r* = r/R, x ranging from 0 to 1, r is radial position, R is the
% radius of the flow tube
t = linspace(0,t0,100);
% t = z* = z×pi×D/(2×F)×(T0/T)×(P/P0), z is axial position, z ranging from
% 0 to L, t ranging from 0 to t0, t0 corresponding to the whole length of
```

```
% the flow tube (dimensionless)
g = linspace(g_min,g_max,g_n);
% g is uptake coefficient,g_n is number of g between g_min and g_max
global g_i
h = waitbar(0,'Please wait...');
steps = length(g);
for i=1:length(g)
    g_i = g(i);
    sol = pdepe(m,@pdex1pde,@pdex1ic,@pdex1bc,x,t);

    u = sol(:,:,1);
    N_f(g(i))
    end_mean_u(i) = mean(u(end,:));
    waitbar(i / steps)
end
close(h)
table_g = [g',end_mean_u'];
xlswrite(['results,g',num2str(t0),'-',num2str(g_min),'.xls'], table_g)
figure
plot(g,end_mean_u)
xlabel('Uptake coefficient')
ylabel('Cout/Cin')
title ('Cout/Cin vs Uptake coefficient')
saveas(gcf,['results,g',num2str(t0),'-',num2str(g_min),'.fig'],'fig')
close gcf
N = N_f(g);
table_N = [N',end_mean_u'];
xlswrite(['results,N',num2str(t0),'-',num2str(g_min),'.xls'], table_N)
figure
plot(N,end_mean_u)
xlabel('Sherwood Number')
ylabel('Cout/Cin')
title('Cout/Cin vs Sherwood Number')
saveas(gcf,['results,N',num2str(t0),'-',num2str(g_min),'.fig'],'fig')
close gcf
```

pdex1pde.m

```
function [c,f,s] = pdex1pde(x,t,u,DuDx)
c = 1-x^2;
f = DuDx;
s = 0;
```

pdex1ic.m

```
function u0 = pdex1ic(x)
u0 = 1;
```

pdex1bc.m

```
function [pl,ql,pr,qr] = pdex1bc(xl,ul,xr,u,t)
global g_i;
pl = 0;
ql = 0;
pr = N_f(g_i)*u;
qr = 1;
```

N_f.m

```
function N = N_f(g)
v = 457.16;
% mean molecular velocity of HCHO, 457.16 m/s
R = 0.0035;
% flow tube radius, 0.0035 m
D = 0.0000177;
% HCHO diffusion coefficient in N2 at 296k and 101kPa, 0.0000177 m^2/s
N = 0.5*(v*R/D).*g./(2-g);
% Sherwood number
```

B.2 Li *et al.*, Atmos. Chem. Phys. Discussion, 2018

Physicochemical uptake and release of volatile organic compounds by soil in coated-wall flow tube experiments with ambient air

Guo Li[1,3], Yafang Cheng[1,2], Uwe Kuhn[1], Rongjuan Xu[3], Yudong Yang[3], Hannah Meusel[1], Nan Ma[2], Yusheng Wu[4], Meng Li[1], Jonathan Williams[1], Thorsten Hoffmann[5], Markus Ammann[6], Ulrich Pöschl[1], Min Shao[2,*], Hang Su[2, 1,*]

[1]Multiphase Chemistry Department, Max Planck Institute for Chemistry, Mainz, Germany

[2]Institute for Environmental and Climate Research, Jinan University, Guangzhou, China

[3]College of Environmental Sciences and Engineering, Peking University, Beijing, China

[4]State Key Joint Laboratory of Environmental Simulation and Pollution Control, College of Environmental Sciences and Engineering, Peking University, Beijing, China

[5]Institute of Inorganic Chemistry and Analytical Chemistry, Johannes Gutenberg University Mainz, Mainz, Germany

[6]Laboratory of Environmental Chemistry, Paul Scherrer Institute, 5232 Villigen, Switzerland

Correspondence to: H. Su (h.su@mpic.de) or M. Shao (mshao@pku.edu.cn)

Atmospheric Chemistry and Physics Discussion, 2018

DOI: 10.5194/acp-2018-683

Author contributions:

HS, YC and GL designed the research.

GL, RX, YY performed the experimental study.

YW provided supplementary measurement data.

GL, YC, HS, UK, HM, NM, ML, JW, TH, MA, UP, MS discussed the results.

GL wrote the paper with inputs from all coauthors.

Atmos. Chem. Phys. Discuss., https://doi.org/10.5194/acp-2018-683
Manuscript under review for journal Atmos. Chem. Phys.
Discussion started: 25 July 2018

Atmospheric Chemistry and Physics Discussions

Physicochemical uptake and release of volatile organic compounds by soil in coated-wall flow tube experiments with ambient air

Guo Li[1,3], Yafang Cheng[1,2], Uwe Kuhn[1], Rongjuan Xu[3], Yudong Yang[3], Hannah Meusel[1], Nan Ma[2], Yusheng Wu[4], Meng Li[1], Jonathan Williams[1], Thorsten Hoffmann[5], Markus Ammann[6], Ulrich Pöschl[1], Min Shao[2,*], Hang Su[2,1,*]

[1]Multiphase Chemistry Department, Max Planck Institute for Chemistry, Mainz, Germany

[2]Institute for Environmental and Climate Research, Jinan University, Guangzhou, China

[3]College of Environmental Sciences and Engineering, Peking University, Beijing, China

[4]State Key Joint Laboratory of Environmental Simulation and Pollution Control, College of Environmental Sciences and Engineering, Peking University, Beijing, China

[5]Institute of Inorganic Chemistry and Analytical Chemistry, Johannes Gutenberg University Mainz, Mainz, Germany

[6]Laboratory of Environmental Chemistry, Paul Scherrer Institute, 5232 Villigen, Switzerland

[*]*Correspondence to*: H. Su (h.su@mpic.de) or M. Shao (mshao@pku.edu.cn)

Atmos. Chem. Phys. Discuss., https://doi.org/10.5194/acp-2018-683
Manuscript under review for journal Atmos. Chem. Phys.
Discussion started: 25 July 2018

Atmospheric Chemistry and Physics Discussions

Abstract

Volatile organic compounds (VOCs) play a key role in atmospheric chemistry. Emission and deposition on soil have been suggested as important sources and sinks of atmospheric trace gases. The exchange characteristics and heterogeneous chemistry of VOCs on soil, however, are not well understood. We used a newly designed differential coated-wall flow tube system to investigate the long-term variability of bidirectional air-soil exchange of 13 VOCs at ambient air conditions of an urban background site in Beijing. Sterilized soil was investigated to address physicochemical processes and heterogeneous/multiphase reactions independently from biological activity. Most VOCs revealed net deposition with average uptake coefficients (γ) in the range of 10^{-7} – 10^{-6} (referring to the geometric soil surface area), corresponding to deposition velocities (V_d) of 0.0013 – 0.01 cm s^{-1} and soil surface resistances (R_c) of 98 – 745 s cm^{-1}, respectively. Formic acid, however, was emitted at a long-term average rate of ~ 6×10^{-3} nmol m^{-2} s^{-1}, suggesting that it was formed and released upon heterogeneous oxidation of other VOCs. The soil-atmosphere exchange of one individual VOC species can be affected by both its surface degradation/depletion caused by surface reactions and by competitive uptake or heterogeneous formation/accommodation of other VOC species. Overall, the results show that physicochemical processing and heterogeneous oxidation on soil and soil-derived dust can act as a sink or as a source of atmospheric VOCs, depending on molecular properties and environmental conditions.

Atmos. Chem. Phys. Discuss., https://doi.org/10.5194/acp-2018-683
Manuscript under review for journal Atmos. Chem. Phys.
Discussion started: 25 July 2018

Atmospheric Chemistry and Physics Discussions

1 Introduction

Volatile organic compounds (VOCs) are widely recognized to play a critical role in atmospheric chemistry and climate, because of their important impact on the atmospheric oxidation capacity and contribution to the formation of secondary organic aerosols (SOAs) (Andreae and Crutzen, 1997;Atkinson, 2000;Fuentes et al., 2000;Williams, 2004;Tunved et al., 2006;Lelieveld et al., 2008;Zhang et al., 2008;Pöschl et al., 2010), and VOCs adsorbed on aerosol particles can have severe health implications (Glikson et al., 1995;Pöschl, 2005). The main sources of VOCs include the biosphere, biomass burning and anthropogenic activities, with emissions from the biosphere accounting for ~ 90% of global total atmospheric VOCs (Guenther et al., 1995). Once VOCs are emitted, they can be removed from the atmosphere by either direct wet or dry deposition to various surfaces including vegetation and soil (130 – 270 Tg C yr^{-1}), or be transformed into SOAs (510 – 910 Tg C yr^{-1}), or be oxidized ultimately leading to the formation of CO_2 and H_2O (310 – 720 Tg C yr^{-1}) (Goldstein and Galbally, 2007). The reported discrepancies between field observations and model calculations, however, indicate many potential sources and sinks still need to be identified and quantified (Di Carlo et al., 2004;Heald et al., 2005;Volkamer et al., 2006;Goldstein and Galbally, 2007;Warneck and Williams, 2012).

Biogenic VOC emission from vegetation has long been the major focus of VOC exchange studies (e.g., Guenther et al., 1994;Gershenzon, 1994;Fuentes et al., 1996;Fall et al., 1999;Schade and Goldstein, 2002). Early studies presumed that vegetation only emitted VOCs to the air. However, more recent studies have demonstrated that VOC exchange is bidirectional, and uptake of VOCs and their oxidation products are the rule rather than the exception in many cases (Kesselmeier, 2001;Fares et al., 2015;Guenther, 2015;Cappellin et al., 2017;Karl et al., 2005;Seco et al., 2007;Karl et al., 2010;Park et al., 2013;Gordon et al., 2014b;Niinemets et al., 2014), similar to other trace gases such as NH_3 or HONO (Su et al., 2011;Su et al., 2013). In fact, Park et al. (2013) expanded the number of measured VOC species to an extremely large range covering 555 ions (with mass to charge ratios between 31 to 1263) using high–mass resolution proton-transfer-reaction mass spectrometry over an orange plantation, and found that 494 of VOC species showed bidirectional fluxes and 186 even exhibited net deposition.

Compared to the research effort dedicated to atmosphere-vegetation interactions involving VOCs, the exchange between the atmosphere and soils has received relatively little attention (Lamb et al., 1987;Guenther et al., 1995;Asensio et al., 2008). Soils have been characterized as both a source and a sink for VOCs. Soil emissions of short-chain oxygenated VOCs (e.g., methanol, acetaldehyde and acetone) and terpenes have been observed in previous studies (Warneke et al., 1999;Schade and Goldstein, 2001;Hayward et al., 2001;Schade and Custer, 2004;Lin et al., 2007;Gray et al., 2014;Bourtsoukidis et al., 2018). In contrast, some species including alcohols, aldehydes, ketones, aromatic hydrocarbons, isoprene, monoterpenes and hexenal, etc. have been reported to be deposited on various types of soil in other studies (Asensio et al., 2007a;Asensio et al., 2007b;Asensio et al., 2008;Aaltonen et al., 2013;Gray et al., 2014). Previous laboratory measurements have also indicated

that soil could serve as a temporary reservoir for formaldehyde, i.e., a large fraction (~ 70%) of formaldehyde adsorbed by soil at high mixing ratios could be re-emitted into the atmosphere at low ambient conditions, hence formaldehyde could cycle between the atmosphere and soil (Li et al., 2016). VOC emission from ground level can originate from the overlying soil litter (Gray et al., 2010;Warneke et al., 1999;Hayward et al., 2001;Schade and Goldstein, 2001), roots (Janson, 1993;Chen et al., 2004;Lin et al., 2007) and soil dwelling microorganisms (Scholler et al., 2002), for which the relative contributions depend on the soil type and various environmental parameters such as ambient relative humidity (RH), soil water content, temperature (T), and VOC mixing ratio, etc.. Therefore, VOC formation from soils involves both biotic and abiotic mechanisms. The biotic processes include root exudation, degradation of soil organic matter and leaf litter by soil microorganisms. The abiotic mechanisms involve purely physicochemical reactions (e.g., heterogeneous and multiphase transformation, evaporation, desorption) and UV-light-enhanced emission from soil vegetation or decomposition of leaf litter (Riikka et al., 2002;Rinnan et al., 2003;Zepp et al., 2007;Derendorp et al., 2011). The main mechanisms contributing to the uptake of VOCs were reported to include adsorption and degradation by roots (Simonich and Hites, 1995;Newman et al., 1997;Cho et al., 2005), biodegradation by microorganisms (van Roon et al., 2005) as well as physical/chemical adsorption by soil particles (Pignatello and Xing, 1996;Li et al., 2016).

Thus, both biotic and abiotic mechanisms can contribute to the exchange of VOCs on soils. Under real world conditions, the biotic and abiotic processes in soil are highly coupled and the net flux is the result of many complex multiphase interactions that are difficult to resolve. Furthermore, emissions from the soil may be uptaken or transformed in overlying leaf litter. Resolving the key processes requires the system to be examined in separate components. Here by applying a new reactor system we examine the physicochemical effects of soil on VOC exchange in isolation, but under real world conditions. From the perspective of soil physicochemistry, VOCs can undergo reversible adsorption and irreversible surface reactions on soils and aerosol particles, coupling gas-surface transport (adsorption), surface-bulk transport (absorption/solvation), and chemical reactions in the bulk (Pöschl et al., 2007); and VOC oxidation/decomposition products can desorb immediately or further interfere with other reactants (Ammann and Pöschl, 2007). Heterogeneous processes at the gas–surface interface can be highly complex, and the individual steps controlling the reaction rates of heterogeneous processes are rarely known (Crowley et al., 2010;Chapleski et al., 2016). Parameterizations of heterogeneous processes still tend to be empirical and most are untested in natural outdoor settings, where surfaces are prone to interferences of competitively co-adsorbing trace gas species and radicals, which is specifically crucial in the case of reactive trace gases like VOCs. While laboratory-based trace gas uptake studies normally apply individual VOC species separately, only little attention is given to interfering effects. However, laboratory studies on binary organic compound mixtures in the ppm level has shown that the photo-catalytic oxidation on catalytic surfaces (TiO_2) of one VOC species may promote or inhibit the oxidation rate of another (Lichtin et al., 1996). In contrast to laboratory conditions, ambient air is a complex composite of a vast variety of gases, aerosols and radicals, and some components may exert synergistic effects on the heterogeneous chemistry of individual or categories of

VOC species. Neglecting these synergistic effects may cause misleading results when extrapolating laboratory work to real world conditions.

This study aims to investigate the uptake, potential heterogeneous conversion and emission of VOCs on soil under real world ambient conditions. A flow tube system coated with pre-treated sterilized soil was used to investigate the physicochemical background of VOC exchange on soil independently from biological activity. Recently, the flow tube technique has been adopted to study the kinetics and mechanisms of reactive trace gas uptake onto soils (Wang et al., 2012;Donaldson et al., 2014a;Donaldson et al., 2014b;VandenBoer et al., 2015;Li et al., 2016). These investigations, however, have focused on laboratory experiments under controlled environmental conditions, where the dependence on single relevant parameters was investigated while all others were kept constant. Here, the coated-wall flow tube system was deployed at an urban field site, which allowed ambient air to pass through the flow tube and the coated soil sample to interact directly with ambient VOC species. VOC uptake coefficients (γ), which indicate the fraction of trace gas kinetic collisions with a reactive surface that lead to uptake by the surface (Ammann et al., 2013) are determined, and their dependencies on various environmental parameters are discussed. To the best of our knowledge, this is the first trial to deploy the flow tube technique for field observations to investigate uptake/emission kinetics of VOCs on soil under ambient conditions.

2 Methods

2.1 Soil sample preparation

Soil samples were collected from a scrubland site near Weiminghu lake in Peking University, Beijing, China (39°59´N, 116°18´E). Before collection, leaf litters were removed from the ground surface and only soil particles were obtained at a depth of 0-5 cm. The collected samples were air-dried in a shade place prior to grinding and sieving with a 120 mesh soil sieve. The soil pH was ~ 6.8 (1:2 soil/water (v/v), Thermo Scientific, OrionStar A211 pH meter). The soil texture comprised of 49% sand, 35% silt and 16% clay (wet sieving method) and the soil humus content was 8.8% (loss on ignition method) as analyzed by Guangdong Institute of Eco-Environmental and Soil Sciences (Guangzhou, China). Since the purpose of this study was to investigate the physicochemical interactions between VOCs and soil, the sieved soil was autoclaved for 20 min at 394 K (repeated twice with an incubation time of one day) right before the flow tube coating procedure as in the work of Li et al. (2016). Autoclaving has been reported as the most effective sterilization method for eliminating soil microorganisms compared with other methods such as fumigation, UV and microwave irradiation (Razavi darbar and Lakzian, 2007). The sterilization procedure and the autoclave time eliminated primary microbial impact on VOC exchange at the atmosphere-soil interface and minimized potential influence on soil physicochemical properties caused by the sterilization method itself (Berns et al., 2008). Moreover, a PTFE membrane filter installed upstream of the flow tube system could prevent the bacteria in the ambient air from inhabiting on the soil sample during the field measurement (see Sect. 2.2).

Soil slurry was prepared by mixing dry soil with sterilized deionized water (18.2 MΩ·cm, Millipore Corporation, Darmstadt, Germany). The slurry was uniformly injected into a glass tube with sandblasted inner surface (100 mm length, 17 mm ID), which was then installed into an air-dried continuously rotating coating tool (ACRO). The design and performance of ACRO for soil coating had been described in the work of Li et al. (2016). The coated tube was rotated with a speed of 14 rpm and flushed overnight with pure N_2 at a flow rate of ~ 0.5 L min^{-1} (purity ≥ 99.999%, RH = 0%). Note that the drying process with N_2, to some extent, purges VOCs off the soil sample. The coating mass has been shown to affect the gas uptake (Donaldson et al., 2014a;Li et al., 2016). A relatively large coating mass of ~ 95 mg cm^{-2} (corresponding to a geometric coating thickness ~ 500 μm) was chosen for our experiments. The coating procedure and mass has been experimentally shown to guarantee fair homogeneity and reproducibility of the coating in our previous study (Li et al., 2016).

Prior to the VOC exchange experiment under ambient conditions, the freshly coated tube was flushed with N_2 (purity ≥ 99.999%, RH= 0%) for 40 min to scrub potential VOC impurities from the soil which were either adsorbed/absorbed onto the soil during the coating preparation procedure or from the soil coating itself. Note that during flushing with VOCs-free N_2, many VOC species were indeed emitted (Fig. S.1). These emitted VOC species might originate from the soil surface and/or the soil bulk (including soil particles and residues of the autoclaved microorganisms) through pore diffusion. To quantify the soil layer depth contributing to these observed emissions, the desorption curves (in Fig. S.1) were fitted using the function derived in our previous study (the first function in Table 1 in Li et al., 2016) assuming that the emissions were a first order decay process. The determined desorption rate coefficient and desorption lifetime of the detected VOCs are listed in Table S.1. The longest desorption lifetime is found for formaldehyde as ~ 22 min. Moreover, we estimated the time scale t for a VOC molecule diffusing through the entire soil coating thickness δ_g (~ 500 μm) using equation $t = \delta_g^2/D_a$, where D_a is the macroscopic diffusion coefficient of VOCs within soil pores. Adopting the lower limit of a macroscopic diffusion coefficient which typically range 10^{-4} – 10^{-2} cm^2 min^{-1} for clay minerals reported by Morrissey and Grismer (1999), a VOC diffusion time of ~ 25 min was obtained. This time scale is less than or comparable to our flushing time of 40 min, suggesting that the entire soil layer could contribute to the VOC emissions by means of soil surface desorption/reaction and soil bulk pore diffusion. In addition, the amount of soil-emitted VOCs was estimated by integration of the desorption curve of methanol (which shows the highest emission signals, an order of magnitude higher than the others in Fig. S.1) using the fitting functions derived by Li et al. (2016). The emitted methanol mass is ~ 1.71 μg, which is far from being able to account for a monolayer coverage on the soil layer specific surface (see Sect. 2.3) when assuming an effective diameter of the methanol molecule of 4.2 Å according to Perera et al. (2007). Thus, the flushing procedure could provide adsorption-sites devoid of reversibly absorbed VOCs on the soil surface as well as within the soil pores, and therefore allow focus on uptake kinetics from the initial phase (VOCs-free soil) of the exchange experiment.

Atmos. Chem. Phys. Discuss., https://doi.org/10.5194/acp-2018-683
Manuscript under review for journal Atmos. Chem. Phys.
Discussion started: 25 July 2018

2.2 Measurement site, experimental setup and operation

VOC exchange measurements were conducted within the campus of Tsinghua University, Beijing, China (40.00°N, 116.20°E), from 25 August 2015 to 26 September 2015. This urban background site was 200 m east of a four-lane highway and 100 m west of a garbage station. There was a small mound nearby which was covered by grass land mixed with trees (mainly white poplars) on its northern side.

The aim of this study was to investigate VOC exchange at the atmosphere-soil interface under ambient conditions, where air temperature (T), relative humidity (RH) and VOC mixing ratio, etc. all change in concert. A flow tube system was installed in a self-built sampling box, which was located on the roof of a 2.35 m high storage container. Two openings on the sampling box allowed for direct access of ambient air into the flow tube system. The sampling box was covered with a thin non-transparent PTFE film that functioned as both a reflector for sunlight and a shelter from rainwater. The flow tube system consisted of a sample channel and a reference channel. The sample channel was equipped with a soil-coated tube in front of which a pre-tube or entrance region (with the same dimensions as the soil-coated tube, i.e., 100 mm length, 17 mm ID, but without soil coating) was installed to ensure well-developed laminar flow in the soil-coated part (Li et al., 2018). The reference channel used a ¼ inch (i.e., 6.35 mm O.D.) PFA Teflon tube (200 mm length) without coated soil. As shown in Fig. 1, ambient air was introduced into the flow tube system prior to being analyzed by a proton-transfer-reaction mass spectrometer (PTR-MS). By using solenoid valves, VOCs from the sample and reference channels were alternately analyzed by the PTR-MS (with 60 min for each channel). While one channel was connected with the PTR-MS, the other was simultaneously flushed by ambient air with the same flow rate as of the PTR-MS (~ 0.1 L/min) to prevent potential accumulation/depletion of VOCs under otherwise static conditions. PTR-MS analysis was paused on the 4 - 8th of September 2015, but the flow tube was continuously flushed with ambient air to ensure uninterrupted exposure of the soil sample to dynamic ambient conditions.

When the reference channel was connected to the PTR-MS, the detected VOC signals represented their mixing ratios in ambient air (VOC depletion within the PFA Teflon tube was negligible), denoted as C_r, which was also equal to the VOC mixing ratios at the sample tube inlet. When the sample channel was connected, the detected signals represented the VOC mixing ratios subject to interactions with the coated soil, designated as C_s. Considering the short residence time (~ 24 s) within the sample tube volume, gas-phase-reactions-induced depletion of VOCs only accounted for a small faction (~ 3% for very reactive species like isoprene and much less for the others, estimated basing on the measured gas oxidants mixing ratios (see Sect. 3.1) and assuming a background mixing ratio level of 1 ppt for OH radicals). Thus, the VOC mixing ratio difference between the reference channel and the sample channel, $C_r - C_s$, can be assumed to be mainly due to exchange of VOCs on soil. Note that the PTR-MS couldn't detect C_r and C_s simultaneously, when one channel was connected to the PTR-MS the corresponding VOC mixing ratios of the other were determined afterwards by interpolating the adjacent

measured values. Before the start of field measurements, a PTFE membrane filter (Φ: 50 mm, pore size: 0.2 μm, Millipore Corporation, USA) was installed at the air inlet of the VOC exchange system to filter bacteria as well as other particles in the ambient air. Filters were replaced every three or four days.

A commercial high sensitivity PTR-MS (Ionicon Analytik, Innsbruck, Austria), located in the aforementioned container, was used for the detection of a broad range of VOCs including isoprene, oxygenated VOCs, acetonitrile, and C6 – C7 aromatics with a time resolution of ~ 30 s (Table 1). PTR-MS is an analytical mass spectrometry technique that uses gas phase hydronium ions (H_3O^+) as ion source reagents (Lindinger et al., 1998;Yuan et al., 2017). Inside the PTR-MS drift tube, VOC species with greater proton affinity than that of water are soft-ionized by reactions with H_3O^+ and then detected by a quadruple mass spectrometer (Lindinger et al., 1998). This PTR-MS has been validated and utilized in previous field campaigns (Yuan et al., 2012;Chen et al., 2014;Yuan et al., 2013). During the field measurement, the system was running in multiple ion mode. Most of the masses were recorded for 1 s in every cycle, except for m/z 21 (0.2 s). Background signals were measured for 30 minutes every 4 hours by diverting the ambient air into a platinum catalytic converter at 370 °C (Shimadzu Inc., Japan). Aromatics, oxygenated VOCs, isoprene and acetonitrile were calibrated by a pressurized gas standard (Spectra Gases Inc., USA). Formaldehyde (m/z = 31), formic acid (m/z = 47) and acetic acid (m/z = 61) were calibrated by permeation tubes (VICI Inc., USA). Calibrations were conducted before and after the measurement period, and a single-spot calibration was conducted every three or four days with response factors varying within 15%. Uncertainties of measured species except for formaldehyde, formic acid and acetic acid were about 5% - 15%. Limits of detection (LOD) for the measured species were in the sub-ppb level listed in Table 1.

Formaldehyde detection is found to be significantly influenced by RH (Vlasenko et al., 2010;Warneke et al., 2011;Baasandorj et al., 2015). Calibrations were conducted within a range of RH (0 - 30 mmol/mol) to fit the response curve, which was then applied in ambient measurement calculations and this procedure resulted in a measurement uncertainty within ± 20%. Measurements of formic acid by PTR-MS can potentially suffer interference from ethanol and dimethyl ether when they are present in significantly higher abundance than formic acid (Baasandorj et al., 2015). At the background urban site, however, the atmospheric abundance of ethanol and dimethyl ether is supposed to be low (Good et al., 1998;Monod et al., 2003;Jia et al., 2012), giving rise to a measurement uncertainty within ± 30%. Influences from ethyl acetate on acetic acid have been found in field campaigns (Fortner et al., 2009;Baasandorj et al., 2015;Derstroff et al., 2017). The influences were corrected by introducing the m/z = 89 in the calculations (Yuan et al., 2013). However, this introduced a measurement uncertainty up to > 40 %.

2.3 Uptake coefficient and deposition velocity

The uptake coefficients (γ) of measured VOC species under ambient conditions were determined using a CKD method (CKD-B in Li et al., 2016). This CKD-B method is based on the commonly used CKD solution for correction of radial

diffusion effect (Murphy and Fahey, 1987), and has been shown to have a much better accuracy than CKD interpolation method, as CKD-B directly solves a governing differential equation with numerical methods. The CKD-B can establish the relation between the sample tube penetration (i.e., C_s/C_r) and γ of the measured VOC species, which is shown in Fig. 2 derived at an average ambient temperature of 25 °C as an example. For details of the CKD-B method, see our previous study (Li et al., 2016). Note that the uncertainty of the determined γ depends on the uncertainty of C_s/C_r as well as the relation between C_s/C_r and γ (as in Fig.2), here with the derived γ range of 10^{-7}- 10^{-6} (see Sect 3.3 and 3.4) the estimated uncertainty of γ for each VOC species was within one order of magnitude. The Reynolds number (Re) in our experiment was ~10, which ensured laminar flow conditions requiring Re < ~2000 (Murphy and Fahey, 1987;Knopf et al., 2015;Li et al., 2018). The pre-tube/entrance region length was 10 cm, and full development of laminar flow was achieved within the first ~ 1 cm for our setup. When a geometric coating thickness δ_g is larger than a critical height δ_c, the coating surface roughness may potentially distort the well-developed laminar flow and introduce uncertainties in the calculated uptake coefficients corrected for molecular diffusion effects using conventional diffusion correction methods (Li et al., 2018). According to this δ_c criterion, the geometric coating thickness of our soil sample (~ 500 μm) was much smaller than the calculated δ_c (~ 2400 μm) based on our experimental configuration, ensuring that the soil coating surface roughness effect was negligible. The uptake coefficients reported here are based on the geometric surface area of the soil sample, considering that in atmospheric models soil microstructure is likewise not taken into account (Donaldson et al., 2014a). The specific surface area of the soil, however, was also measured using a water vapor adsorption method based on the Brunauer-Emmett-Teller (BET) adsorption theory (Brunauer et al., 1938) being 15 ± 1.5 m^2 g^{-1}. To calculate the BET surface area, the mass of the adsorbed water on soil sample after equilibrium with pre-defined RH levels was determined by a non-dispersive infrared (NDIR) gas analyzer (type: Li-6262, LI-COR Biosciences Inc.) operated in differential mode. This BET surface area is comparable to that in other reports on similar soil types, e.g., 12-15 m^2 g^{-1} (Kahle et al., 2002) and 8 - 19 m^2 g^{-1} (Punrattanasin and Sariem, 2015). Accounting for the BET results, the specific surface area would reduce γ by a factor of 10^4 in our case.

The primary controlling factors of VOC exchange at the soil-atmosphere interface include gas transport and the concentration gradient between the soil surface and the atmosphere. As depicted in Fig. 3, the transport of a gas species to soil surfaces is governed by three resistances in series: the aerodynamic resistance R_a, the quasi-laminar layer resistance R_b, and the soil surface resistance R_c (Seinfeld and Pandis, 2016). The deposition or transfer velocity V_d is the inverse of the sum of these three resistances (Seinfeld and Pandis, 2016). With the coated-wall flow tube technique employed in this study, the derived γ reflects the reaction kinetics on soil and thus relates to R_c rather than R_a and R_b. Based on the calculated γ, R_c can be further derived according to equation $R_c = 4/(\omega \times \gamma)$ (Donaldson et al., 2014b;Dentener et al., 1996), where ω denotes the mean molecular speed of the VOC species. Approximations of R_a and R_b can be achieved using the methodology developed by Seinfeld and Pandis (2016), i.e., R_a and R_b can be derived based on Eqs. (19.14) and (19.17), respectively. For the basic assumptions and utilized parameters during derivations of R_a and R_b, see Sect. 3.2. Finally, v_d can be estimated as $V_d = 1/(R_a + R_b + R_c)$.

3 Results and discussion

3.1 Site specific characteristics of selected air quality indicators

Figure 4 shows the time series of site specific ambient air pollutant mixing ratios observed during the whole measurement period (A) and respective mean diel courses (B). The range of mixing ratios of selected air quality indicators like ozone (O_3), carbon monoxide (CO), nitrogen oxide (NO), nitrogen dioxide (NO_2) and sulfur dioxide (SO_2) are representative of polluted urban conditions (Bigi and Harrison, 2010). O_3 reveals peak mixing ratios in the afternoon (13:00 – 17:00 local time), which corresponds to high sunlight intensities and temperatures at this time of the day. Coincident with this maximum in O_3, reactive nitrogen species (NO_2 and NO) show decreasing trends, which may be due to decreased local NO_x emissions, and/or rapid photochemical oxidation or strong dilution in the boundary layer in the afternoon. Even though most of the selected air quality indicators reveal a significant diel cycle, CO, NO and NO_2 do not show a typical urban rush-hour pattern with traffic-associated peaks during morning and late afternoon. Rather, the site represents an urban background site without direct influences of strong nearby point sources. The relatively weak diel course of SO_2 mixing ratios with maxima during daytime can also be assumed to stem from long-range advection or midday entrainment of high concentration air masses from aloft, instead of nearby presence of ground-level emission sources (Bigi and Harrison, 2010).

3.2 Site specific characteristics and exchange of VOCs

Figure 5 displays the time series of site specific ambient air mixing ratios of VOCs, temperature (T), relative humidity (RH) during the whole measurement period (A), and respective mean diel courses (B). Among the measured VOC species, methanol has the highest mixing ratios (Fig. 5A). Methanol is ubiquitous in the lower atmosphere with mixing ratios in remote regions reported to be ~ 1 ppb (Galbally and Kirstine, 2002;Jordan et al., 2009). The high mean daytime mixing ratios of 10 - 20 ppb at this urban background site suggest strong impact of anthropogenic emissions on the local methanol budget. High mixing ratios are also found for its oxidation products formaldehyde (~ 10 ppb) and formic acid (~ 5 ppb), respectively. Formaldehyde is a key reaction intermediate of the atmospheric oxidation cycle (Li et al., 2016), and hence an indicator of the total amount of OVOCs. Its increasing trend during daytime (Fig. 5B) is indicative of strong photochemical formation. In contrast, formic acid, which can be formed from ozonization of all terminal double-bonded molecules (Osamu et al., 1994), shows lower mixing ratios during daytime than during nighttime, and similar diel trends are also found for other species including toluene, methanol, acetonitrile and benzene. The daytime decrease of the latter may be due to dilution effects by increased daytime boundary layer mixing height and/or lower atmospheric photochemical formation rates during daytime, even though some of them (e.g., formic acid) have smaller photolysis and oxidation loss rates than those of formaldehyde. On the other hand, the most significant diel profile is observed for isoprene, with mixing ratios peaking at midafternoon (around 15:00, local time) followed by a decline at late afternoon stabilizing at ~ 0.5 ppb during night. Isoprene can have an important impact on the atmospheric oxidation capacity due to its high OH reactivity both in pristine and in polluted urban regions (Williams et al., 2016). Besides anthropogenic sources like gasoline and diesel traffic exhaust

(Borbon et al., 2001;Wang et al., 2013;Wagner and Kuttler, 2014), the major summertime source of isoprene can be assumed to be biogenic, i.e., being emitted from vegetation in a light and temperature dependent manner (Guenther et al., 1993). Thus, during daytime, high mixing ratios of biogenic isoprene are anticipated at our measurement site, which was surrounded by different types of vegetation cover (see Sect. 2.2). Following the diel trend of isoprene, the two primary photochemical oxidation products of isoprene, methyl vinyl ketone (MVK) and methacrolein (MACR), also exhibit higher mixing ratios during daytime than during night.

Besides primary or secondary surface sources and sinks, the near-ground nighttime increase (or decrease) of atmospheric trace gas mixing ratios is favored by the development of a stable and shallow nocturnal boundary layer (NBL). Any nighttime emission (or deposition) of trace constituents is confined to the relatively small volume of the NBL where they accumulate (or get depleted). The growth of the atmospheric boundary layer (ABL) in the morning hours due to the influx of sensible and latent heat, and resulting upcoming convection, and the respective re-entrainment of air from the residual boundary layer aloft, being enriched with (or depleted of) atmospheric trace constituents, may confer a reasonable explanation for any increased (or reduced) daytime mixing ratios (Kuhn et al., 2002).

The exchange properties of VOCs on soil can be reflected by comparing C_r (solid lines in Fig. 5A) and C_s (dotted lines in Fig. 5 A). As shown in Fig. 5A, during the whole measurement period most of the VOC species are taken up by the soil, especially for styrene, formaldehyde, toluene and acetic acid, indicated by the discernable differences between their C_r and C_s. Only formic acid shows a slightly higher C_s than C_r, suggesting this compound is likely emitted by the soil. The time series of the mixing ratio difference $C_r - C_s$ of measured VOCs are further displayed in Fig. S.2. The integrated total amount and average surface flux of each absorbed or emitted VOC species on soil for the whole measurement period is listed in Table S.1.

3.3 Time series and mean diel courses of VOC exchange

Based on the measured C_r and C_s, the uptake coefficients of examined VOC species can be derived (see Sect. 2.3). To minimize potential impacts of measurement uncertainties (e.g., random noise of the instrument) on small $C_r - C_s$ (or large C_s/C_r) and further on the derived uptake coefficients, the calculated hourly based uptake coefficients (basing on the measured hourly mixing ratio data) were averaged to a daily basis (i.e., daily mean uptake coefficients). Figure 6A shows the time series of daily mean VOC uptake coefficients, together with those of ambient temperature (T) and relative humidity (RH). Eight species (i.e., styrene, toluene, isoprene, MVK+MACR, acetaldehyde, MEK, acetone and acetonitrile) exhibit a relatively high initial uptake coefficient, followed by a significant decrease in the first few days, indicative of progressive saturation of absorption sites on the pre-treated soil sample. For styrene and acetonitrile, this decrease prevails for the whole one-month measurement period. Occasionally, some species show short-term swaps between deposition and emission (see Fig. S.3 for the complete time series of hourly averaged data). This bidirectional exchange can be caused by fast dynamics in

ambient air conditions like temperature, relative humidity and trace gas mixing ratio, and respective status of soil saturation. Interestingly, formaldehyde only rarely shows emission from soil, suggesting strong capacity of the soil sample for absorption under ambient conditions. This result to some extent challenges our previous laboratory-based observation that soil could also act as a source for formaldehyde, when it had been saturated with formaldehyde prior to back-flushing with pure N_2, i.e., the uptake of formaldehyde by soil was shown to be reversible (Li et al., 2016). Indeed, the range of formaldehyde mixing ratios observed in Beijing was rather high for most of the time, and extremely rapid changes of mixing ratio to below a compensation point, as applied in the laboratory study, hardly occurred in the field. On the other hand, the anticipated high levels of oxidants for heterogeneous reactions on the soil under field conditions may foster the chemical conversion/oxidation of formaldehyde, that could prevent its accumulation, saturation and subsequent release (see below). Given the poor understanding of formaldehyde's budget (Jacob, 2000;Wagner et al., 2002), more research is needed to elucidate the exchange behavior of formaldehyde on various types of soils under ambient conditions. In addition, the variability of uptake coefficients of some species (e.g., isoprene, MVK+MACR, acetaldehyde, and formic acid) closely follow the trend of ambient relative humidity and temperature, suggesting that these environmental parameters influence the exchange of respective VOC species.

Mean diel variations of VOC uptake coefficients as well as those of ambient relative humidity (RH) and temperature (T) are presented in Fig. 6B. In general, uptake coefficients are quite stable over the whole day.

From a perspective of kinetic gas theory, the derived uptake coefficients can be further used to determine VOC surface reaction rates on soil which are only caused by reactions on soil surface instead of diffusion into soil pores under steady state conditions (i.e., after significant absorption saturation of the soil sample in the first few measurement days in Fig. 6A). The soil surface reaction rate is described as: $(\gamma \times \omega)/4 \times [\mathrm{VOC(g)}]$. γ and ω are the daily average uptake coefficients and mean molecular speed (at an average temperature of 298 K) of each VOC species, respectively. [VOC(g)] is the VOC mixing ratio in ambient air (i.e., C_r). Accordingly, the corresponding surface reaction (or wall loss) rate coefficient k_w is $(\gamma \times \omega)/4$, equivalent to the inverse of R_c. Note that only formic acid shows negative uptake coefficients for most of the measurement time period, and its emission rate cannot be described by the above reaction rate expression accounting for surface uptake processes. Instead, the soil surface emission rate of formic acid is calculated from a flux point of view, which equates to $F \times (C_r - C_s)/S$. F is the volumetric flow rate in the sample tube and S is the geometric surface area of the soil sample. The time series of surface reaction rates are shown in Fig. S.4. k_w is shown in Table S.3 and further discussed in the following section.

3.4 Exchange of VOCs interpreted in terms of long-term mean uptake coefficients and deposition velocities

Figure 7 shows the averaged uptake coefficients for days with continuous instrumental operation (16 days within the one-month field measurement) for each VOC species. The vast majority of VOC species reveal positive uptake coefficients, indicating that these species tend to be absorbed and retained or converted into other products in the soil (net soil influx).

Highest uptake coefficients are found for styrene and formaldehyde, with mean values in the order of 10^{-6}. The uptake coefficient of formaldehyde is in the same range as reported earlier for laboratory experiments, where sterilized agricultural soil was flushed by pure N_2 containing different mixing ratio levels of formaldehyde under varying RH conditions (Li et al., 2016).

In Fig. 7, only formic acid reveals a negative mean uptake coefficient, which is indicative of emissions from soil (Li et al., 2018). This short-chain organic acid is regarded as one of the terminal products in the oxidation processes of many VOC species present in the atmosphere (Charbouillot et al., 2012). Therefore, the heterogeneous formation from previously adsorbed/absorbed VOCs may confer a reasonable explanation for its accumulation and subsequent release, as further discussed in following sections.

As mentioned previously, the long-term mean uptake coefficients can be used to derive the soil surface reaction (or wall loss) rate coefficient k_w of each VOC species, which reflects the soil surface exchange properties. Here k_w has a unit of cm s^{-1} and can be interpreted as a deposition velocity without gas transport resistance (i.e., $R_a + R_b$) effects (Pöschl et al., 1998). As the initial soil sterilization procedure eliminates potential impacts from soil bacteria, the observed exchange of these VOC species is primarily influenced by physicochemical factors. To have a general understanding of how different physicochemical factors may affect k_w, the calculated k_w of each VOC species are listed in Table S.3, together with the basic physicochemical parameters possibly related to the trace gas exchange (i.e., gas phase reaction rate coefficients with OH radicals and O_3, Henry's law constant, vapor pressure and octanol-water partition coefficient). In general, differences of k_w found among these species cannot be explained by any of the physicochemical factors alone, which suggests that VOC exchange at the atmosphere-soil interface is a complex multifunctional process.

Deposition velocity V_d is a key parameter used in models to describe trace gas uptake by soils and is the inverse of the sum of three resistances in series: the aerodynamic resistance R_a, the quasi-laminar layer resistance R_b, and the soil surface resistance R_c (Fig. 3). As described in Sect. 2.4, only R_c can directly be derived from the calculated uptake coefficients. R_a and R_b are calculated adopting the approach proposed by Seinfeld and Pandis (2016): In Table 2, the case of neutral stable temperature profiles is adopted for R_a calculation (Eq. 19.14 in Seinfeld and Pandis 2016). The season is set to autumn (cropland before harvest). To assess the impact of R_a and R_b on derived V_d, three types of land use categories including shrubs (category 1 in Table 2), urban (category 2) and barren land (category 3) are selected mimicking our field environmental conditions and soil type characteristics. The detailed parameters adopted for R_a and R_b derivation and the calculated R_a, R_b, R_c and V_d are shown in Table 2. As $R_c >> R_a + R_b$, the VOC uptake is not limited by atmospheric gas phase transport (R_a+R_b) or by land use type. Rather the uptake on the soil surface (R_c) is the primary rate-limiting step for dry deposition of these VOC species, even for the largest γ observed in our study. Note that V_d of formic acid intrinsically reveals negative values, as this organic acid is released from the soil.

Previous VOC exchange studies on various soil types such as agricultural soil, tropical soil, plantation floor and forest understory, etc., have spanned a huge range of V_d with three orders of magnitude (0.01 – 1 cm s^{-1}) for the VOC species investigated here (Hartmann et al., 1991;Karl et al., 2005;Sanhueza et al., 2004;Schade and Custer, 2004;Stickler et al., 2007;Jordan et al., 2009;Schade et al., 2011;Gordon et al., 2014a;Cleveland and Yavitt, 1997). Our calculated V_d (0.001 – 0.01 cm s^{-1}) is at the very low end of previous studies. This can be due to a variety of reasons: on the one hand, our soil sample is bare soil without any vegetation cover while previous flux studies included different types of vegetation covers (grass, leaf litter, agricultural crops, etc.), which might significantly alter the measured deposition velocity. On the other hand, our soil sample is sterilized aiming to investigate the physiochemical processes on soil, yet the soil bacteria can significantly modify the VOC exchange as can be expected in the previous studies. In fact, several studies have demonstrated that soil bacteria can consume atmospheric VOCs (Misra et al., 1996;Cleveland and Yavitt, 1998;Stacheter et al., 2013;Lynch et al., 2014). From the physicochemical point of view, low V_d may also arise from competitions among different VOC species for surface absorption sites, as has been observed in controlled laboratory studies by Lichtin et al. (1996) for photo-catalytic reactions of binary VOC mixtures on TiO_2 surfaces. Likewise, interfering effects of O_3, OH and NO_3 radicals on VOC photo-catalytic TiO_2 surface reactions could be demonstrated (Ao et al., 2004). We assume that this phenomenon is universal for catalytic surfaces and also applies for soil.

To further validate the plausibility of our calculated γ and derived V_d, we calculate the surface resistance, R_c, using a regional-scale numerical model developed by Wesely (Seinfeld and Pandis, 2016;Wesely, 1989), which considered only physicochemical factors affecting gas deposition on ground surface for formaldehyde, acetic acid and acetaldehyde as typical VOC representatives. As a proxy for bare soil properties in the present study, the land use type is set to barren land (mostly desert), and the seasonal category is chosen as autumn (cropland before harvest). All other input parameters are the same as used in the original literature (Wesely, 1989). The model outputs a R_c for formaldehyde of 167 s cm^{-1}, which is in fair agreement with our results (98 s cm^{-1}). Due to a very small effective Henry's law constant adopted in the model (15 M atm^{-1} for water with near-neutral pH) the derived R_c for acetaldehyde is even much higher than based on our measurements (66667 s cm^{-1} versus 291 s cm^{-1}), corroborating our relatively low range of observed VOC uptake. In contrast, acetic acid bears a much higher effective Henry's law constant (4×10^6 M atm^{-1}), revealing a much smaller R_c than based on our measurements (0.3 versus 214 s cm^{-1}), underpinning the intense impact of VOC physicochemical characteristics on modelled uptake resistances.

3.5 VOC exchange dependence on environmental parameters

In order to explore potential effects of environmental factors on the exchange of these VOC species at the atmosphere-soil interface, the relation between uptake coefficients and ambient relative humidity (RH), temperature (T) and mixing ratio (C) is further examined, and those VOC species showing significant dependencies are shown in Fig 8. RH affects the amount of

surface-adsorbed water and can accelerate or slow down trace gas uptake rates (Crowley et al., 2010). On the one hand, high-RH induced condensed water may attract water-soluble or hydrophilic gas species and hence enhance their uptake (Pei and Zhang, 2011), or decrease their net emission. This mechanism applies, e.g., to hydrophilic formaldehyde and formic acid (see Table S.3 for respective Henry's law constants). On the other hand, more water molecules on soil surfaces tend to repel the hydrophobic species more strongly or reduce gas uptake by means of competitive adsorption effects between water molecules and gas species (Ruiz et al., 1998;Goss et al., 2004;Donaldson et al., 2014a;Li et al., 2016). This can provide a reasonable explanation for the negative RH dependence of hydrophobic acetaldehyde in Fig. 8. However, the uptake coefficients of hydrophobic isoprene and its primary degradation products (i.e., MVK+MACR) also increase at high RH.

From the physical perspective of vapor pressure, increased temperature leads to decreased trace gas uptake and increased emission. This is in line with the decreased uptake of isoprene, MVK+MACR and formaldehyde, and enhanced emission of formic acid at higher temperatures shown in Fig. 8. Note that in the natural environment all environmental variables change in concert, and the diel courses of RH and T are intrinsically anti-correlated. As a result, the dependencies of VOC exchange on RH and T in Fig. 8 show opposite trends. Consequently, the governing parameter among each other cannot individually be inferred from field measurements, and both dependencies can further be masked by the dependence on gas mixing ratio changing simultaneously in the ambient air.

Even though the calculation of uptake coefficients intrinsically accounts for the gas phase mixing ratios, higher mixing ratios have been shown to reduce uptake coefficients (Sassine et al., 2010;Wang et al., 2012). A negative effect of increased mixing ratios on uptake coefficients is also observed for isoprene and MVK+MACR in Fig. 8. Our previous laboratory experiments on formaldehyde (Li et al., 2016) showed that this trend was more pronounced under dry conditions (RH = 0%) than under humid conditions (RH = 40%), in agreement with the formaldehyde pattern shown here. On the contrary, increased mixing ratios lead to enhanced uptake coefficients for acetaldehyde. The negative effect of mixing ratios on uptake coefficients (as for isoprene and MVK+MACR) can be understood as competition among the individual VOC molecules for reactive uptake sites, or with other VOCs whose mixing ratios show a simultaneous increase (Li et al., 2016). However, the observed positive effect of mixing ratios on uptake coefficients of acetaldehyde remains unexplained. Other processes like acetaldehyde heterogeneous degradation/depletion may be involved, as high acetaldehyde uptake coefficients are observed preferentially during daytime (Fig. 6B) when the atmospheric oxidation capacity is high (see ozone mixing ratios in Fig. 4B).

3.6 VOC exchange correlation analysis

As discussed above, the uptake dynamics of one individual VOC species may be biased, either (i) by competitive co-absorption of other VOCs or trace gases from ambient air (Lichtin et al., 1996;Ao et al., 2004), or (ii) by formation on the soil through heterogeneous conversion of precursor compounds that have been absorbed earlier (Ammann and Pöschl, 2007;Pöschl et al., 2007), or (iii) by depletion of the individual VOC species due to heterogeneous degradation. To explore

potential interactions/interferences of VOC species among each other, correlation analyses of the exchange rates (i.e., the concentration difference between the reference channel and the sample channel $C_r - C_s$ times the volumetric flow rate F) of measured VOC species are conducted for each pair of species. The results are presented in Fig. 9 in terms of Pearson correlation coefficients, together with the molecular structure of each investigated species. The interplay of sorption, heterogeneous reactions and desorption kinetics of VOCs is complex, and heterogeneous reactions may require time periods from milliseconds to weeks or even months to reach equilibrium (Xing and Pignatello, 1996;Ammann and Pöschl, 2007). Hence, to also account for slow kinetics, the correlation analysis in Fig. 9 is based on daily integrals. VOC exchange rates instead of uptake coefficients are used to allow for a budget approach. Positive correlations are indicated in red colors, and some pairs of VOC species show high positive correlation (deep red color code in Fig. 9), suggesting they have similar exchange characteristics. For example, MVK and MACR are the first generation oxidation products of isoprene (Jordan et al., 2009). Thus, the observed high correlation coefficient between MVK+MACR and isoprene can be explained by their similar molecular structures shown in Fig. 9. The same holds for the strong correlation between methanol and formaldehyde, methanol and acetone, as well as for MEK and acetone: similar molecular structures and functional groups result in analogous exchange and reaction mechanisms on soil.

Negative correlations in Fig. 9 are indicated in blue colors. As aforementioned, formic acid is at the very end of the VOC oxidation chain, and is exclusively emitted from the soil sample while all other VOCs tend to be taken up. Thus, correlations of formic acid with other VOCs are negative as such (blue in Fig. 9). High negative correlation coefficients are obtained between formic acid and some species (i.e., acetone, isoprene, formaldehyde, styrene and methanol), indicative of possible generation and emission of formic acid due to heterogeneous transformation of these deposited compounds. In the atmosphere, photo-oxidation of acetone contributes to the abundance of formic acid, and the dominant pathway for formic acid formation via acetone photo-oxidation is the reaction of OH radical with acetone-derived formaldehyde (Chattopadhyay et al., 2015). Formic acid production through photo-oxidation of isoprene has been found under high NO_x circumstances (Paulot et al., 2009). Under ambient conditions, gas phase reactions of styrene with OH radical and O_3 can occur respectively, with formaldehyde and benzaldehyde as major products and formic acid as the minor (Tuazon et al., 1993). Methanol has been reported to play an important role in upper tropospheric photo-oxidation chemistry via its contribution to the HO_x budget after its oxidation to formaldehyde (Tie et al., 2003;Singh et al., 1995;Singh et al., 2000;Singh et al., 2004;Colomb et al., 2006). Notably, formaldehyde is an important intermediate of VOC oxidation and a direct precursor of formic acid (e.g, Adewuyi et al., 1984;Chameides, 1984). All these studies suggest the existence of one or several pathways for formic acid formation through heterogeneous reactions of these VOC precursors.

Atmos. Chem. Phys. Discuss., https://doi.org/10.5194/acp-2018-683
Manuscript under review for journal Atmos. Chem. Phys.
Discussion started: 25 July 2018

4. Implications for atmospheric chemistry

4.1 Formic acid formation through heterogeneous transformation of formaldehyde

We know from the above discussions that: (1) formaldehyde uptake reveal a relatively high correlation with formic acid emission; (2) formaldehyde is an important intermediate of VOC oxidation and a direct precursor of formic acid; (3) formaldehyde shows continuous and even increasing uptake during the whole field measurement (see Fig. 6A). All these results evidence formaldehyde may act as the best candidate for heterogeneous formation of formic acid on soil.

In terms of physicochemistry, formaldehyde is much less stable than formic acid (~ 1 day versus ~ 25 days of mean atmospheric chemical lifetime, see Millet et al., 2015), which indicates its faster turnover rates also on soil surfaces. Moreover, the mean retention coefficient of formaldehyde has been shown to be considerably higher than for formic acid in cloud/ice water (Jost et al., 2017), inferring a reasonable explanation for the preferential release of the organic acid from the soil. Furthermore, aldehydes in general undergo accretion reactions (i.e., aldol condensation type reactions) in acidic media and similar chemistry has been shown to occur on mineral oxides (Li et al., 2001), therefore mineral-rich bare soils can serve as a sink for these compounds. We know from controlled laboratory experiments on individual trace gas mixtures that the presence of nitric oxide (NO) promotes the conversion of formaldehyde on photocatalytic surfaces, and also the yield of formic acid was found higher under the presence of NO (Ao et al., 2004). In contrast, sulfate ions formed from the presence of SO_2 competed with formaldehyde for adsorption sites on the catalytic surfaces, and the conversion of formaldehyde and the yield of formic acid were lower under the presence of SO_2; and also other VOC species were shown to inhibit heterogeneous conversion of formaldehyde (Ao et al., 2004). According to our results, formaldehyde is a relatively reactive short-term intermediate for formic acid production, rather than being directly released to the atmosphere under authentic ambient air oxidizing conditions in Beijing city. In general, a catalytic effect of soil can be anticipated by its composition of a variety of mineral oxides (silicon oxide, iron oxide and titanium oxide, etc.). Therefore, our soil sample may serve as a catalytic surface for degradation of the deposited precursors with formaldehyde as the most important intermediate, which can be further oxidized to build up formic acid by heterogeneous reactions on the soil, followed by formic acid emission. This catalytic effect may be further enhanced by the co-existence of other deposited oxidants (O_3, OH radical, NO_2 and peroxides, etc.) on the soil surfaces.

4.2 Physicochemical reactions on bare soil and soil-derived dust may act as a potential source of formic acid

The only VOC that have been observed to be released from the soil sample investigated here is formic aid, which represents a final organic product of the VOC oxidation cascade. Formic acid is one of the most abundant organic acids in the atmosphere, existing in gas phase, cloud and rain water as well as snow and even polar ice (Chebbi and Carlier, 1996;Sanhueza and Andreae, 1991;Maupetit and Delmas, 1994;Sempére and Kawamura, 1994;Löflund et al., 2002;van Pinxteren et al., 2005;Mungall et al., 2018). In remote regions like the Amazon forest, short-chain organic acids have been

shown to be responsible for 60 - 80% of rainwater acidity (Galloway et al., 1982;Stavrakou et al., 2012), and also over boreal forests and in urban areas they contribute significantly to the free acidity in precipitation (Khare et al., 1999;Stavrakou et al., 2012), and hence can regulate pH-dependence of aqueous reactions in clouds (Vet et al., 2014) and can contribute to acidification of soil.

Gas phase photochemical oxidation of biogenic VOCs is considered to be the dominant global atmospheric source of formic acid. Modelled budget analyses implicate the existence of one or more large missing sources for formic acid, i.e., the annually produced formic acid (100 - 120 Tg yr^{-1}) is two to three times larger than can be explained based on the current understanding of primary and secondary (gas phase) atmospheric processes and aqueous-phase cloud/rain chemistry (Barth et al., 2007;Paulot et al., 2011;Veres et al., 2011;Le Breton et al., 2012;Stavrakou et al., 2012;Cady-Pereira et al., 2014;Schobesberger et al., 2016;Millet et al., 2015), even when using a Master Chemical Mechanism (MCM) that was updated with recently proposed additional photochemical formation pathways for formic acid, like OH oxidation of isoprene and aromatics (Yuan et al., 2015). This suggests the existence of either a key gap in current understanding of hydrocarbon oxidation or large and widespread, yet unidentified sources for formic acid (Millet et al., 2015).

Previous model estimations of soil emissions of formic acid were based on a few available field measurements (Paulot et al., 2011;Millet et al., 2015). These ambient studies found formic acid emissions from dry savanna soil (Sanhueza and Andreae, 1991) and coniferous forest soil (Enders et al., 1992), respectively, to be an important source of the local formic acid budget. The former study reported daily average emission rate of 1.4×10^{-1} nmol m^{-2} s^{-1}, which is much larger than the estimated long-term mean emission rate of 6×10^{-3} nmol m^{-2} s^{-1} (see Table S.2) in the present study. This large discrepancy can be due to different emission/formation mechanisms of formic acid. For the dry savanna soil, emissions of formic acid may be caused by soil bacteria or physicochemical partitioning between the soil reservoir and the atmosphere. In our case, emissions are rather attributed to physicochemical processes on soil (more specifically, heterogeneous oxidation processes) instead of microbial activities and reservoir of the soil itself, due to the applied sterilization and flushing procedures on the soil sample prior to field experiment. To the best of our knowledge, this study is the first trial to evaluate the potential contribution of physicochemical processes on soil under real ambient conditions to the atmospheric budget of formic acid. Assuming the heterogeneous formation of formic acid also applies to other bare soil types around the globe, a global formic acid source strength of ~ 0.24 Tg yr^{-1} can be estimated using the average emission rate obtained here and a global barren land (i.e., bare soil and land with very sparse vegetation) surface area of ~ 2.8×10^{7} km^2 (Roser and Ritchie, 2018). This source strength due to heterogeneous reactions on bare soils is comparable to that from anthropogenic and biofuel emissions (0.4 Tg yr^{-1} by Millet et al., 2015) but still much less than the missing source strength. Note that the magnitude of the emission rate here used for calculation also depends on the mixing ratio levels of ambient VOC precursors and other environmental parameters such as temperature and relative humidity. As our measurement site is an urban background site with high VOC mixing ratios, the estimated source strength can be considered as an upper limit. Considering the still poorly understood budget of

formic acid (Millet, 2012;Paulot et al., 2011), more investigations are needed to quantify the contributions of different types of soil as a potential source of formic acid.

Wind erosion of soil is an important pathway to generate mineral dust aerosols (Zender et al., 2011). Thus, our soil-based formic acid formation mechanism may also apply to soil-derived dust. Indeed, field measurements have identified formic acid to be among the most abundant carboxylic acids in collected mineral dust (Falkovich et al., 2004;Khare et al., 1998). However, dust was treated as a sink of gaseous formic acid in recent model simulations (with a simulated dust uptake of 1.2 Tg yr^{-1} in Millet et al., 2015;Paulot et al., 2011) based on laboratory-observed uptake of formic acid on clay minerals followed by fast surface saturation (Hatch et al., 2007). Here, we may predict heterogeneous transformations of other co-adsorbed VOCs in the ambient air (e.g., formaldehyde) followed by emission of formic acid on dust, preferentially under low relative humidity conditions (Fig. 8). Based on our observed emission rate, a global emission strength can be roughly estimated by assuming that dust particles have a mean diameter of 2 μm and a density of 2.2 g cm^{-3} as adopted by Hatch et al. (2007). Using an average atmospheric dust loading of 18 Tg (Kok et al., 2017) would result in a formic acid source of ~ 2.4×10^{-5} Tg yr^{-1}. Note that estimating the emission of dust aerosol particles, a 10000 times lower emission rate for formic acid should be applied to account for the real available surface (versus the geometric surface used here for soil, to reflect common model input needs). Clearly, this additional formic acid source on dust is much smaller and can be considered negligible. However, our observed formic acid emission to some extent challenges model applications of high initial uptake coefficients on clay minerals derived from laboratory experiments; and previous model simulation may need to be re-constrained.

Aging of organic aerosols by heterogeneous reactions with OH radicals has been proposed as an important secondary source of formic acid (Molina et al., 2004;Paulot et al., 2011), and formic acid heterogeneous production was indeed observed during organic aerosol aging in the laboratory (Eliason et al., 2003;Molina et al., 2004;Walser et al., 2007;Vlasenko et al., 2008;Malecha and Nizkorodov, 2016). Stavrakou et al. (2012) modelled the heterogeneous oxidation of organic aerosols as a source of formic acid assuming that one molecule of formic acid is formed per molecule of OH lost. They calculated an extra global annual formic acid flux of 27 Tg, which is still less that the missing source invoked to explain their remote sensing total column observations (see also Millet et al., 2015). However, based on high concentrations of reactive oxygen species (ROS) prevailing in atmospheric aerosol particles (Chung et al., 2006;Verma et al., 2015;Tong et al., 2016), we may consider more VOC precursors being oxidizing to formic acid than has been adopted in the model.

5 Conclusions

VOC heterogeneous chemistry at the gas-surface interface of soils play a central role in regulating atmospheric trace gas mixing ratios. In the present study, a coated-wall flow tube system coupled with a PTR-MS analysis was adopted to

investigate the exchange of common VOC species at the atmosphere-soil interface at real-world ambient air conditions of an urban background site in Beijing. Almost all VOCs show an average net deposition on the pre-treated sterilized soil, examined over an extended exposure of one month. The derived deposition velocities are found to be at the lower end of ranges reported for natural soil habitats, but were in fair agreement with models based on pure physicochemistry. Only formic acid displays a long-term emission. The emission of formic acid is solely due to physicochemical processes (i.e., heterogeneous transformations of absorbed VOC precursors) on soil, which represents an additional ground-based source of this organic acid.

At ambient atmospheric conditions, both the relatively low uptake coefficients derived for the majority of VOC species and the emission of formic acid from the soil to some extent challenge the applicability of models using uptake coefficients derived from laboratory-based uptake measurements, where single VOC species or simple mixtures are supplied using purging air devoid of oxidizing agents. Field measurements as presented here, with all relevant parameters changing in concert, may call attention for the existence of yet unknown interferences or synergetic effects. Considering the potential relevance of biotic processes in natural soils, follow-up studies are needed to explore its contribution to VOC exchange at the soil-atmosphere interface.

Acknowledgments

This study was supported by the National Natural Science Foundation of China (grant nos. 91644218 and 41330635), the "Pearl River Talents Program" of Guangdong Province, China (grant no. 2016ZT06N263), the National Key Research and Development Program of China (grant no. 2017YFC0210104) and the Max Planck Society (MPG). Guo Li acknowledges the financial support from the China Scholarship Council (CSC).

References

Aaltonen, H., Aalto, J., Kolari, P., Pihlatie, M., Pumpanen, J., Kulmala, M., Nikinmaa, E., Vesala, T., and Bäck, J.: Continuous VOC flux measurements on boreal forest floor, Plant and Soil, 369, 241-256, 10.1007/s11104-012-1553-4, 2013.

Adewuyi, Y. G., Cho, S.-Y., Tsay, R.-P., and Carmichael, G. R.: Importance of formaldehyde in cloud chemistry, Atmospheric Environment (1967), 18, 2413-2420, https://doi.org/10.1016/0004-6981(84)90011-8, 1984.

Ammann, M., and Pöschl, U.: Kinetic model framework for aerosol and cloud surface chemistry and gas-particle interactions – Part 2: Exemplary practical applications and numerical simulations, Atmos. Chem. Phys., 7, 6025-6045, 10.5194/acp-7-6025-2007, 2007.

Ammann, M., Cox, R. A., Crowley, J. N., Jenkin, M. E., Mellouki, A., Rossi, M. J., Troe, J., and Wallington, T. J.: Evaluated kinetic and photochemical data for atmospheric chemistry: Volume VI – heterogeneous reactions with liquid substrates, Atmos. Chem. Phys., 13, 8045-8228, 10.5194/acp-13-8045-2013, 2013.

Andreae, M. O., and Crutzen, P. J.: Atmospheric aerosols: Biogeochemical sources and role in atmospheric chemistry, Science, 276, 1052-1058, 1997.

Ao, C. H., Lee, S. C., Zou, S. C., and Mak, C. L.: Inhibition effect of SO2 on NOx and VOCs during the photodegradation of synchronous indoor air pollutants at parts per billion (ppb) level by TiO2, Applied Catalysis B: Environmental, 49, 187-193, https://doi.org/10.1016/j.apcatb.2003.12.011, 2004.

Asensio, D., Penuelas, J., Filella, I., and Llusia, J.: On-line screening of soil VOCs exchange responses to moisture, temperature and root presence, Plant and Soil, 291, 249-261, 2007a.

Asensio, D., Peñuelas, J., Llusià, J., Ogaya, R., and Filella, I.: Interannual and interseasonal soil CO2 efflux and VOC exchange rates in a Mediterranean holm oak forest in response to experimental drought, Soil Biology and Biochemistry, 39, 2471-2484, https://doi.org/10.1016/j.soilbio.2007.04.019, 2007b.

Asensio, D., Penuelas, J., Prieto, P., Estiarte, M., Filella, I., and Llusia, J.: Interannual and seasonal changes in the soil exchange rates of monoterpenes and other VOCs in a Mediterranean shrubland, European Journal of Soil Science, 59, 878-891, 2008.

Atkinson, R.: Atmospheric chemistry of VOCs and NOx, Atmospheric Environment, 34, 2063-2101, 2000.

Baasandorj, M., Millet, D. B., Hu, L., Mitroo, D., and Williams, B. J.: Measuring acetic and formic acid by proton-transfer-reaction mass spectrometry: sensitivity, humidity dependence, and quantifying interferences, Atmos Meas Tech, 8, 1303-1321, 10.5194/amt-8-1303-2015, 2015.

Barth, M. C., Kim, S. W., Skamarock, W. C., Stuart, A. L., Pickering, K. E., and Ott, L. E.: Simulations of the redistribution of formaldehyde, formic acid, and peroxides in the 10 July 1996 Stratospheric-Tropospheric Experiment: Radiation, Aerosols, and Ozone deep convection storm, Journal of Geophysical Research: Atmospheres, 112, n/a-n/a, 10.1029/2006JD008046, 2007.

Berns, A. E., Philipp., H., Narres, H. D., Burauel, P., Vereecken, H., and Tappe, W.: Effect of gamma-sterilization and autoclaving on soil organic matter structure as studied by solid state NMR, UV and fluorescence spectroscopy, European Journal of Soil Science, 59, 540-550, doi:10.1111/j.1365-2389.2008.01016.x, 2008.

Bigi, A., and Harrison, R. M.: Analysis of the air pollution climate at a central urban background site, Atmospheric Environment, 44, 2004-2012, https://doi.org/10.1016/j.atmosenv.2010.02.028, 2010.

Borbon, A., Fontaine, H., Veillerot, M., Locoge, N., Galloo, J. C., and Guillermo, R.: An investigation into the traffic-related fraction of isoprene at an urban location, Atmospheric Environment, 35, 3749-3760, https://doi.org/10.1016/S1352-2310(01)00170-4, 2001.

Bourtsoukidis, E., Behrendt, T., Yañez-Serrano, A. M., Hellén, H., Diamantopoulos, E., Catão, E., Ashworth, K., Pozzer, A., Quesada, C. A., Martins, D., Sá, M., Araujo, A., Brito, J., Artaxo, P., Kesselmeier, J., Lelieveld, J., and Williams, J.: Strong sesquiterpene emissions from Amazonian soils, Nature Communications, 2018.

Brunauer, S., Emmett, P. H., and Teller, E.: Adsorption of Gases in Multimolecular Layers, J. Am. Chem. Soc., 60, 309-319, 10.1021/ja01269a023, 1938.

Cady-Pereira, K. E., Chaliyakunnel, S., Shephard, M. W., Millet, D. B., Luo, M., and Wells, K. C.: HCOOH measurements from space: TES retrieval algorithm and observed global distribution, Atmos. Meas. Tech., 7, 2297-2311, 10.5194/amt-7-2297-2014, 2014.

Cappellin, L., Algarra Alarcon, A., Herdlinger-Blatt, I., Sanchez, J., Biasioli, F., Martin, S. T., Loreto, F., and McKinney, K. A.: Field observations of volatile organic compound (VOC) exchange in red oaks, Atmos. Chem. Phys., 17, 4189-4207, 10.5194/acp-17-4189-2017, 2017.

Chameides, W. L.: The photochemistry of a remote marine stratiform cloud, Journal of Geophysical Research: Atmospheres, 89, 4739-4755, 10.1029/JD089iD03p04739, 1984.

Chapleski, R. C., Zhang, Y., Troya, D., and Morris, J. R.: Heterogeneous chemistry and reaction dynamics of the atmospheric oxidants, O_3, NO_3, and OH, on organic surfaces, Chemical Society Reviews, 45, 3731-3746, 10.1039/C5CS00375J, 2016.

Charbouillot, T., Gorini, S., Voyard, G., Parazols, M., Brigante, M., Deguillaume, L., Delort, A.-M., and Mailhot, G.: Mechanism of carboxylic acid photooxidation in atmospheric aqueous phase: Formation, fate and reactivity, Atmospheric Environment, 56, 1-8, https://doi.org/10.1016/j.atmosenv.2012.03.079, 2012.

Chattopadhyay, A., Chatterjee, P., and Chakraborty, T.: Photo-oxidation of Acetone to Formic Acid in Synthetic Air and Its Atmospheric Implication, The Journal of Physical Chemistry A, 119, 8146-8155, 10.1021/acs.jpca.5b04905, 2015.

Chebbi, A., and Carlier, P.: Carboxylic acids in the troposphere, occurrence, sources, and sinks: A review, Atmospheric Environment, 30, 4233-4249, https://doi.org/10.1016/1352-2310(96)00102-1, 1996.

Chen, F., Ro, D. K., Petri, J., Gershenzon, J., Bohlmann, J., Pichersky, E., and Tholl, D.: Characterization of a root-specific Arabidopsis terpene synthase responsible for the formation of the volatile monoterpene 1,8-cineole, Plant Physiology, 135, 1956-1966, 2004.

Chen, W. T., Shao, M., Lu, S. H., Wang, M., Zeng, L. M., Yuan, B., and Liu, Y.: Understanding primary and secondary sources of ambient carbonyl compounds in Beijing using the PMF model, Atmospheric Chemistry and Physics, 14, 3047-3062, 2014.

Cho, C. W., Sung, K., Coapcioglu, M. Y., and Drew, M.: Influence of water content and plants on the dissipation of chlorinated volatile organic compounds in soil, Water Air and Soil Pollution, 167, 259-271, 2005.

Chung, M. Y., Lazaro, R. A., Lim, D., Jackson, J., Lyon, J., Rendulic, D., and Hasson, A. S.: Aerosol-Borne Quinones and Reactive Oxygen Species Generation by Particulate Matter Extracts, Environmental Science & Technology, 40, 4880-4886, 10.1021/es0515957, 2006.

Cleveland, C. C., and Yavitt, J. B.: Consumption of atmospheric isoprene in soil, Geophysical Research Letters, 24, 2379-2382, 10.1029/97GL02451, 1997.

Cleveland, C. C., and Yavitt, J. B.: Microbial Consumption of Atmospheric Isoprene in a Temperate Forest Soil, Applied and Environmental Microbiology, 64, 172-177, 1998.

Colomb, A., Williams, J., Crowley, J., Gros, V., Hofmann, R., Salisbury, G., Klüpfel, T., Kormann, R., Stickler, A., Forster, C., and Lelieveld, J.: Airborne Measurements of Trace Organic Species in the Upper Troposphere Over Europe: the Impact of Deep Convection, Environmental Chemistry, 3, 244-259, https://doi.org/10.1071/EN06020, 2006.

Crowley, J. N., Ammann, M., Cox, R. A., Hynes, R. G., Jenkin, M. E., Mellouki, A., Rossi, M. J., Troe, J., and Wallington, T. J.: Evaluated kinetic and photochemical data for atmospheric chemistry: Volume V – heterogeneous reactions on solid substrates, Atmos. Chem. Phys., 10, 9059-9223, 10.5194/acp-10-9059-2010, 2010.

Dentener, F. J., Carmichael, G. R., Zhang, Y., Lelieveld, J., and Crutzen, P. J.: Role of mineral aerosol as a reactive surface in the global troposphere, J. Geophys. Res., 101, 22869–22889, 1996.

Derendorp, L., Holzinger, R., and Röckmann, T.: UV-induced emissions of C2–C5 hydrocarbons from leaf litter, Environmental Chemistry, 8, 602-611, https://doi.org/10.1071/EN11024, 2011.

Derstroff, B., Hüser, I., Bourtsoukidis, E., Crowley, J. N., Fischer, H., Gromov, S., Harder, H., Janssen, R. H. H., Kesselmeier, J., Lelieveld, J., Mallik, C., Martinez, M., Novelli, A., Parchatka, U., Phillips, G. J., Sander, R., Sauvage, C., Schuladen, J., Stönner, C., Tomsche, L., and Williams, J.: Volatile organic compounds (VOCs) in photochemically aged air from the eastern and western Mediterranean, Atmos. Chem. Phys., 17, 9547-9566, 10.5194/acp-17-9547-2017, 2017.

Di Carlo, P., Brune, W. H., Martinez, M., Harder, H., Lesher, R., Ren, X., Thornberry, T., Carroll, M. A., Young, V., Shepson, P. B., Riemer, D., Apel, E., and Campbell, C.: Missing OH Reactivity in a Forest: Evidence for Unknown Reactive Biogenic VOCs, Science, 304, 722-725, 10.1126/science.1094392, 2004.

Donaldson, M. A., Berke, A. E., and Raff, J. D.: Uptake of Gas Phase Nitrous Acid onto Boundary Layer Soil Surfaces, Environ Sci Technol, 48, 375-383, 2014a.

Donaldson, M. A., Bish, D. L., and Raff, J. D.: Soil surface acidity plays a determining role in the atmospheric-terrestrial exchange of nitrous acid, Proceedings of the National Academy of Sciences of the United States of America, 111, 18472-18477, 2014b.

Eliason, T. L., Aloisio, S., Donaldson, D. J., Cziczo, D. J., and Vaida, V.: Processing of unsaturated organic acid films and aerosols by ozone, Atmospheric Environment, 37, 2207-2219, https://doi.org/10.1016/S1352-2310(03)00149-3, 2003.

Enders, G., Dlugi, R., Steinbrecher, R., Clement, B., Daiber, R., Eijk, J. v., Gäb, S., Haziza, M., Helas, G., Herrmann, U., Kessel, M., Kesselmeier, J., Kotzias, D., Kourtidis, K., Kurth, H. H., McMillen, R. T., Roider, G., Schürmann, W., Teichmann, U., and Torres, L.: Biosphere/Atmosphere interactions: Integrated research in a European coniferous forest ecosystem, Atmospheric Environment. Part A. General Topics, 26, 171-189, http://dx.doi.org/10.1016/0960-1686(92)90269-Q, 1992.

Falkovich, A. H., Schkolnik, G., Ganor, E., and Rudich, Y.: Adsorption of organic compounds pertinent to urban environments onto mineral dust particles, Journal of Geophysical Research: Atmospheres, 109, n/a-n/a, 10.1029/2003JD003919, 2004.

Fall, R., Karl, T., Hansel, A., Jordan, A., and Lindinger, W.: Volatile organic compounds emitted after leaf wounding: On-line analysis by proton-transfer-reaction mass spectrometry, Journal of Geophysical Research-Atmospheres, 104, 15963-15974, 1999.

Fares, S., Paoletti, E., Loreto, F., and Brilli, F.: Bidirectional Flux of Methyl Vinyl Ketone and Methacrolein in Trees with Different Isoprenoid Emission under Realistic Ambient Concentrations, Environmental Science & Technology, 49, 7735-7742, 10.1021/acs.est.5b00673, 2015.

Fortner, E. C., Zheng, J., Zhang, R., Knighton, W. B., Volkamer, R. M., Sheehy, P., Molina, L., and Andre, M.: Measurements of Volatile Organic Compounds Using Proton Transfer Reaction - Mass Spectrometry during the MILAGRO 2006 Campaign, Atmospheric Chemistry and Physics, 9, 467-481, 2009.

Fuentes, J. D., Wang, D., Neumann, H. H., Gillespie, T. J., DenHartog, G., and Dann, T. F.: Ambient biogenic hydrocarbons and isoprene emissions from a mixed deciduous forest, Journal of Atmospheric Chemistry, 25, 67-95, 1996.

Fuentes, J. D., Lerdau, M., Atkinson, R., Baldocchi, D., Bottenheim, J. W., Ciccioli, P., Lamb, B., Geron, C., Gu, L., Guenther, A., Sharkey, T. D., and Stockwell, W.: Biogenic hydrocarbons in the atmospheric boundary layer: A review, Bulletin of the American Meteorological Society, 81, 1537-1575, 2000.

Galbally, I. E., and Kirstine, W.: The Production of Methanol by Flowering Plants and the Global Cycle of Methanol, Journal of Atmospheric Chemistry, 43, 195-229, 10.1023/a:1020684815474, 2002.

Galloway, J. N., Likens, G. E., Keene, W. C., and Miller, J. M.: The composition of precipitation in remote areas of the world, Journal of Geophysical Research: Oceans, 87, 8771-8786, 10.1029/JC087iC11p08771, 1982.

Gershenzon, J.: Metabolic Costs of Terpenoid Accumulation in Higher-Plants, Journal of Chemical Ecology, 20, 1281-1328, 1994.

Glikson, M., Rutherford, S., Simpson, R. W., Mitchell, C. A., and Yago, A.: Microscopic and submicron components of atmospheric particulate matter during high asthma periods in Brisbane, Queensland, Australia, Atmospheric Environment, 29, 549-562, https://doi.org/10.1016/1352-2310(94)00278-S, 1995.

Goldstein, A. H., and Galbally, I. E.: Known and unexplored organic constituents in the earth's atmosphere, Environmental Science & Technology, 41, 1514-1521, 2007.

Good, D. A., Francisco, J. S., Jain, A. K., and Wuebbles, D. J.: Lifetimes and global warming potentials for dimethyl ether and for fluorinated ethers: CH3OCF3 (E143a), CHF2OCHF2 (E134), CHF2OCF3 (E125), Journal of Geophysical Research: Atmospheres, 103, 28181-28186, 10.1029/98JD01880, 1998.

Gordon, M., Vlasenko, A., Staebler, R. M., Stroud, C., Makar, P. A., Liggio, J., Li, S. M., and Brown, S.: Uptake and emission of VOCs near ground level below a mixed forest at Borden, Ontario, Atmospheric Chemistry and Physics, 14, 9087-9097, 2014a.

Gordon, M., Vlasenko, A., Staebler, R. M., Stroud, C., Makar, P. A., Liggio, J., Li, S. M., and Brown, S.: Uptake and emission of VOCs near ground level below a mixed forest at Borden, Ontario, Atmos. Chem. Phys., 14, 9087-9097, 10.5194/acp-14-9087-2014, 2014b.

Goss, K. U., Buschmann, J., and Schwarzenbach, R. P.: Adsorption of organic vapors to air-dry soils: Model predictions and experimental validation, Environmental Science & Technology, 38, 3667-3673, 2004.

Gray, C. M., Monson, R. K., and Fierer, N.: Emissions of volatile organic compounds during the decomposition of plant litter, Journal of Geophysical Research-Biogeosciences, 115, 2010.

Gray, C. M., Monson, R. K., and Fierer, N.: Biotic and abiotic controls on biogenic volatile organic compound fluxes from a subalpine forest floor, Journal of Geophysical Research-Biogeosciences, 119, 547-556, 2014.

Guenther, A., Zimmerman, P., and Wildermuth, M.: Natural Volatile Organic-Compound Emission Rate Estimates for United-States Woodland Landscapes, Atmospheric Environment, 28, 1197-1210, 1994.

Guenther, A., Hewitt, C. N., Erickson, D., Fall, R., Geron, C., Graedel, T., Harley, P., Klinger, L., Lerdau, M., Mckay, W. A., Pierce, T., Scholes, B., Steinbrecher, R., Tallamraju, R., Taylor, J., and Zimmerman, P.: A Global-Model of Natural Volatile Organic-Compound Emissions, Journal of Geophysical Research-Atmospheres, 100, 8873-8892, 1995.

Guenther, A. B., Zimmerman, P. R., Harley, P. C., Monson, R. K., and Fall, R.: Isoprene and monoterpene emission rate variability: Model evaluations and sensitivity analyses, Journal of Geophysical Research: Atmospheres, 98, 12609-12617, 10.1029/93JD00527, 1993.

Hartmann, W. R., Santana, M., Hermoso, M., Andreae, M. O., and Sanhueza, E.: Diurnal cycles of formic and acetic acids in the northern part of the Guayana shield, Venezuela, Journal of Atmospheric Chemistry, 13, 63-72, 10.1007/bf00048100, 1991.

Hatch, C. D., Gough, R. V., and Tolbert, M. A.: Heterogeneous uptake of the C₁ to C₄ organic acids on a swelling clay mineral, Atmos. Chem. Phys., 7, 4445-4458, 10.5194/acp-7-4445-2007, 2007.

Hayward, S., Muncey, R. J., James, A. E., Halsall, C. J., and Hewitt, C. N.: Monoterpene emissions from soil in a Sitka spruce forest, Atmospheric Environment, 35, 4081-4087, 2001.

Heald, C. L., Jacob, D. J., Park, R. J., Russell, L. M., Huebert, B. J., Seinfeld, J. H., Liao, H., and Weber, R. J.: A large organic aerosol source in the free troposphere missing from current models, Geophysical Research Letters, 32, n/a-n/a, 10.1029/2005GL023831, 2005.

Jacob, D. J.: Heterogeneous chemistry and tropospheric ozone, Atmospheric Environment, 34, 2131-2159, http://dx.doi.org/10.1016/S1352-2310(99)00462-8, 2000.

Janson, R. W.: Monoterpene Emissions from Scots Pine and Norwegian Spruce, Journal of Geophysical Research-Atmospheres, 98, 2839-2850, 1993.

Jia, L., Xu, Y., and Shi, Y.: Investigation of the ozone formation potential for ethanol using a smog chamber, Chinese Science Bulletin, 57, 4472-4481, 10.1007/s11434-012-5375-9, 2012.

Jordan, C., Fitz, E., Hagan, T., Sive, B., Frinak, E., Haase, K., Cottrell, L., Buckley, S., and Talbot, R.: Long-term study of VOCs measured with PTR-MS at a rural site in New Hampshire with urban influences, Atmospheric Chemistry and Physics, 9, 4677-4697, 2009.

Jost, A., Szakáll, M., Diehl, K., Mitra, S. K., and Borrmann, S.: Chemistry of riming: the retention of organic and inorganic atmospheric trace constituents, Atmos. Chem. Phys., 17, 9717-9732, 10.5194/acp-17-9717-2017, 2017.

Kahle, M., Kleber, M., and Jahn, R.: Carbon storage in loess derived surface soils from Central Germany: Influence of mineral phase variables, Journal of Plant Nutrition and Soil Science, 165, 141-149, 2002.

Karl, T., Harley, P., Guenther, A., Rasmussen, R., Baker, B., Jardine, K., and Nemitz, E.: The bi-directional exchange of oxygenated VOCs between a loblolly pine (Pinus taeda) plantation and the atmosphere, Atmospheric Chemistry and Physics, 5, 3015-3031, 2005.

Karl, T., Harley, P., Emmons, L., Thornton, B., Guenther, A., Basu, C., Turnipseed, A., and Jardine, K.: Efficient Atmospheric Cleansing of Oxidized Organic Trace Gases by Vegetation, Science, 330, 816-819, 2010.

Kesselmeier, J.: Exchange of short-chain oxygenated volatile organic compounds (VOCs) between plants and the atmosphere: A compilation of field and laboratory studies, Journal of Atmospheric Chemistry, 39, 219-233, 2001.

Khare, P., Kumar, N., Satsangi, G. S., Kumari, K. M., and Srivastava, S. S.: Formate and acetate in particulate matter and dust fall at Dayalbagh, Agra (India), Chemosphere, 36, 2993-3002, https://doi.org/10.1016/S0045-6535(97)10096-0, 1998.

Khare, P., Kumar, N., Kumari, K. M., and Srivastava, S. S.: Atmospheric formic and acetic acids: An overview, Reviews of Geophysics, 37, 227-248, 10.1029/1998RG900005, 1999.

Knopf, D. A., Poschl, U., and Shiraiwa, M.: Radial Diffusion and Penetration of Gas Molecules and Aerosol Particles through Laminar Flow Reactors, Denuders, and Sampling Tubes, Anal Chem, 87, 3746-3754, 2015.

Kok, J. F., Ridley, D. A., Zhou, Q., Miller, R. L., Zhao, C., Heald, C. L., Ward, D. S., Albani, S., and Haustein, K.: Smaller desert dust cooling effect estimated from analysis of dust size and abundance, Nature Geoscience, 10, 274, 10.1038/ngeo2912
https://www.nature.com/articles/ngeo2912#supplementary-information, 2017.

Kuhn, U., Rottenberger, S., Biesenthal, T., Ammann, C., Wolf, A., Schebeske, G., Oliva, S. T., Tavares, T. M., and Kesselmeier, J.: Exchange of short-chain monocarboxylic acids by vegetation at a remote tropical forest site in Amazonia, Journal of Geophysical Research: Atmospheres, 107, LBA 36-31-LBA 36-18, 10.1029/2000JD000303, 2002.

Lamb, B., Guenther, A., Gay, D., and Westberg, H.: A National Inventory of Biogenic Hydrocarbon Emissions, Atmospheric Environment, 21, 1695-1705, 1987.

Le Breton, M., McGillen, M. R., Muller, J. B. A., Bacak, A., Shallcross, D. E., Xiao, P., Huey, L. G., Tanner, D., Coe, H., and Percival, C. J.: Airborne observations of formic acid using a chemical ionization mass spectrometer, Atmos. Meas. Tech., 5, 3029-3039, 10.5194/amt-5-3029-2012, 2012.

Lelieveld, J., Butler, T. M., Crowley, J. N., Dillon, T. J., Fischer, H., Ganzeveld, L., Harder, H., Lawrence, M. G., Martinez, M., Taraborrelli, D., and Williams, J.: Atmospheric oxidation capacity sustained by a tropical forest, Nature, 452, 737, 10.1038/nature06870 https://www.nature.com/articles/nature06870#supplementary-information, 2008.

Li, G., Su, H., Li, X., Kuhn, U., Meusel, H., Hoffmann, T., Ammann, M., Pöschl, U., Shao, M., and Cheng, Y.: Uptake of gaseous formaldehyde by soil surfaces: a combination of adsorption/desorption equilibrium and chemical reactions, Atmos. Chem. Phys., 16, 10299-10311, 10.5194/acp-16-10299-2016, 2016.

Li, G., Su, H., Kuhn, U., Meusel, H., Ammann, M., Shao, M., Pöschl, U., and Cheng, Y.: Technical note: Influence of surface roughness and local turbulence on coated-wall flow tube experiments for gas uptake and kinetic studies, Atmos. Chem. Phys., 18, 2669-2686, 10.5194/acp-18-2669-2018, 2018.

Li, P., K. A. Perreau, E. Covington, C. H. Song, G. R. Carmichael, and Grassian, V. H.: Heterogeneous reactions of volatile organic compounds on oxide particles of the most abundant crustal elements: Surface reactions of acetaldehyde, acetone, and propionaldehyde on SiO2, Al2O3, Fe2O3, TiO2, and CaO, Journal of Geophysical Research: Atmospheres, 106, 5517-5529, doi:10.1029/2000JD900573, 2001.

Lichtin, N. N., Avudaithai, M., Berman, E., and Grayfer, A.: TiO2-photocatalyzed oxidative degradation of binary mixtures of vaporized organic compounds, Solar Energy, 56, 377-385, https://doi.org/10.1016/0038-092X(96)00014-X, 1996.

Lin, C., Owen, S. M., and Penuelas, J.: Volatile organic compounds in the roots and rhizosphere of Pinus spp., Soil Biology & Biochemistry, 39, 951-960, 2007.

Lindinger, W., Hansel, A., and Jordan, A.: Proton-transfer-reaction mass spectrometry (PTR-MS): on-line monitoring of volatile organic compounds at pptv levels, Chemical Society Reviews, 27, 347-354, 1998.

Löflund, M., Kasper-Giebl, A., Schuster, B., Giebl, H., Hitzenberger, R., and Puxbaum, H.: Formic, acetic, oxalic, malonic and succinic acid concentrations and their contribution to organic carbon in cloud water, Atmospheric Environment, 36, 1553-1558, https://doi.org/10.1016/S1352-2310(01)00573-8, 2002.

Lynch, R. C., Darcy, J. L., Kane, N. C., Nemergut, D. R., and Schmidt, S. K.: Metagenomic evidence for metabolism of trace atmospheric gases by high-elevation desert Actinobacteria, Frontiers in Microbiology, 5, 10.3389/fmicb.2014.00698, 2014.

Malecha, K. T., and Nizkorodov, S. A.: Photodegradation of Secondary Organic Aerosol Particles as a Source of Small, Oxygenated Volatile Organic Compounds, Environmental Science & Technology, 50, 9990-9997, 10.1021/acs.est.6b02313, 2016.

Maupetit, F., and Delmas, R. J.: Carboxylic acids in high-elevation Alpine glacier snow, Journal of Geophysical Research: Atmospheres, 99, 16491-16500, 10.1029/94JD03315, 1994.

Millet, D. B.: Atmospheric chemistry: Natural atmospheric acidity, Nature Geosci, 5, 8-9, 2012.

Millet, D. B., Baasandorj, M., Farmer, D. K., Thornton, J. A., Baumann, K., Brophy, P., Chaliyakunnel, S., de Gouw, J. A., Graus, M., Hu, L., Koss, A., Lee, B. H., Lopez-Hilfiker, F. D., Neuman, J. A., Paulot, F., Peischl, J., Pollack, I. B., Ryerson,

T. B., Warneke, C., Williams, B. J., and Xu, J.: A large and ubiquitous source of atmospheric formic acid, Atmos. Chem. Phys., 15, 6283-6304, 10.5194/acp-15-6283-2015, 2015.

Misra, G., Pavlostathis, S. G., Perdue, E. M., and Araujo, R.: Aerobic biodegradation of selected monoterpenes, Applied Microbiology and Biotechnology, 45, 831-838, 10.1007/s002530050770, 1996.

Molina, M. J., Ivanov, A. V., Trakhtenberg, S., and Molina, L. T.: Atmospheric evolution of organic aerosol, Geophysical Research Letters, 31, n/a-n/a, 10.1029/2004GL020910, 2004.

Monod, A., Bonnefoy, N., Kaluzny, P., Denis, I., Foster, P., and Carlier, P.: Methods for sampling and analysis of tropospheric ethanol in gaseous and aqueous phases, Chemosphere, 52, 1307-1319, https://doi.org/10.1016/S0045-6535(03)00327-8, 2003.

Morrissey, F. A., and Grismer, M. E.: Kinetics of volatile organic compound sorption/desorption on clay minerals, Journal of Contaminant Hydrology, 36, 291-312, https://doi.org/10.1016/S0169-7722(98)00150-8, 1999.

Mungall, E. L., Abbatt, J. P. D., Wentzell, J. J. B., Wentworth, G. R., Murphy, J. G., Kunkel, D., Gute, E., Tarasick, D. W., Sharma, S., Cox, C. J., Uttal, T., and Liggio, J.: High gas-phase mixing ratios of formic and acetic acid in the High Arctic, Atmos. Chem. Phys. Discuss., 2018, 1-26, 10.5194/acp-2018-60, 2018.

Murphy, D. M., and Fahey, D. W.: Mathematical Treatment of the Wall Loss of a Trace Species in Denuder and Catalytic-Converter Tubes, Anal Chem, 59, 2753-2759, 1987.

Newman, L. A., Strand, S. E., Choe, N., Duffy, J., Ekuan, G., Ruszaj, M., Shurtleff, B. B., Wilmoth, J., Heilman, P., and Gordon, M. P.: Uptake and biotransformation of trichloroethylene by hybrid poplars, Environmental Science & Technology, 31, 1062-1067, 1997.

Niinemets, Ü., Fares, S., Harley, P., and Jardine, K. J.: Bidirectional exchange of biogenic volatiles with vegetation: emission sources, reactions, breakdown and deposition, Plant, Cell & Environment, 37, 1790-1809, 10.1111/pce.12322, 2014.

Osamu, H., Peter, N., Stefan, L., and K., M. G.: Formation of formic acid and organic peroxides in the ozonolysis of ethene with added water vapour, Geophysical Research Letters, 21, 1523-1526, doi:10.1029/94GL01174, 1994.

Park, J. H., Goldstein, A. H., Timkovsky, J., Fares, S., Weber, R., Karlik, J., and Holzinger, R.: Active Atmosphere-Ecosystem Exchange of the Vast Majority of Detected Volatile Organic Compounds, Science, 341, 643-647, 2013.

Paulot, F., Crounse, J. D., Kjaergaard, H. G., Kroll, J. H., Seinfeld, J. H., and Wennberg, P. O.: Isoprene photooxidation: new insights into the production of acids and organic nitrates, Atmos. Chem. Phys., 9, 1479-1501, 10.5194/acp-9-1479-2009, 2009.

Paulot, F., Wunch, D., Crounse, J. D., Toon, G. C., Millet, D. B., DeCarlo, P. F., Vigouroux, C., Deutscher, N. M., González Abad, G., Notholt, J., Warneke, T., Hannigan, J. W., Warneke, C., de Gouw, J. A., Dunlea, E. J., De Mazière, M., Griffith, D. W. T., Bernath, P., Jimenez, J. L., and Wennberg, P. O.: Importance of secondary sources in the atmospheric budgets of formic and acetic acids, Atmos. Chem. Phys., 11, 1989-2013, 10.5194/acp-11-1989-2011, 2011.

Pei, J. J., and Zhang, J. S. S.: On the performance and mechanisms of formaldehyde removal by chemi-sorbents, Chem Eng J, 167, 59-66, 2011.

Perera, A., Sokolić, F., and Zoranić, L.: Microstructure of neat alcohols, Physical Review E, 75, 060502, 10.1103/PhysRevE.75.060502, 2007.

Pignatello, J. J., and Xing, B. S.: Mechanisms of slow sorption of organic chemicals to natural particles, Environmental Science & Technology, 30, 1-11, 1996.

Pöschl, U., Canagaratna, M., Jayne, J. T., Molina, L. T., Worsnop, D. R., Kolb, C. E., and Molina, M. J.: Mass Accommodation Coefficient of H2SO4 Vapor on Aqueous Sulfuric Acid Surfaces and Gaseous Diffusion Coefficient of H2SO4 in N2/H2O, The Journal of Physical Chemistry A, 102, 10082-10089, 10.1021/jp982809s, 1998.

Pöschl, U.: Atmospheric Aerosols: Composition, Transformation, Climate and Health Effects, Angewandte Chemie International Edition, 44, 7520-7540, 10.1002/anie.200501122, 2005.

Pöschl, U., Rudich, Y., and Ammann, M.: Kinetic model framework for aerosol and cloud surface chemistry and gas-particle interactions – Part 1: General equations, parameters, and terminology, Atmos. Chem. Phys., 7, 5989-6023, 10.5194/acp-7-5989-2007, 2007.

Pöschl, U., Martin, S. T., Sinha, B., Chen, Q., Gunthe, S. S., Huffman, J. A., Borrmann, S., Farmer, D. K., Garland, R. M., Helas, G., Jimenez, J. L., King, S. M., Manzi, A., Mikhailov, E., Pauliquevis, T., Petters, M. D., Prenni, A. J., Roldin, P., Rose, D., Schneider, J., Su, H., Zorn, S. R., Artaxo, P., and Andreae, M. O.: Rainforest Aerosols as Biogenic Nuclei of Clouds and Precipitation in the Amazon, Science, 329, 1513-1516, 10.1126/science.1191056, 2010.

Punrattanasin, P., and Sariem, P.: Adsorption of Copper, Zinc, and Nickel Using Loess as Adsorbents, Pol. J. Environ. Stud., 24, 1259-1266, 10.15244/pjoes/30264, 2015.

Razavi darbar, S., and Lakzian, A.: Evaluation of chemical and biological consequences of soil sterilization methods, Caspian Journal of Environmental Sciences, 5, 87-91, 2007.

Riikka, N., J., M. P., Jouko, S., Anu, W., Satu, T., and Toini, H.: Elevated UV-B radiation alters fluxes of methane and carbon dioxide in peatland microcosms, Global Change Biology, 8, 361-371, doi:10.1046/j.1354-1013.2002.00478.x, 2002.

Rinnan, R., Impiö, M., Silvola, J., Holopainen, T., and Martikainen, P. J.: Carbon dioxide and methane fluxes in boreal peatland microcosms with different vegetation cover—effects of ozone or ultraviolet-B exposure, Oecologia, 137, 475-483, 10.1007/s00442-003-1366-5, 2003.

Ruiz, J., Bilbao, R., and Murillo, M. B.: Adsorption of different VOC onto soil minerals from gas phase: Influence of mineral, type of VOC, and air humidity, Environmental Science & Technology, 32, 1079-1084, 1998.

Sanhueza, E., and Andreae, M. O.: Emission of Formic and Acetic-Acids from Tropical Savanna Soils, Geophysical Research Letters, 18, 1707-1710, 1991.

Sanhueza, E., Holzinger, R., Kleiss, B., Donoso, L., and Crutzen, P. J.: New insights in the global cycle of acetonitrile: release from the ocean and dry deposition in the tropical savanna of Venezuela, Atmospheric Chemistry and Physics, 4, 275-280, 2004.

Sassine, M., Burel, L., D'Anna, B., and George, C.: Kinetics of the tropospheric formaldehyde loss onto mineral dust and urban surfaces, Atmospheric Environment, 44, 5468-5475, 2010.

Schade, G. W., and Goldstein, A. H.: Fluxes of oxygenated volatile organic compounds from a ponderosa pine plantation, Journal of Geophysical Research-Atmospheres, 106, 3111-3123, 2001.

Schade, G. W., and Goldstein, A. H.: Plant physiological influences on the fluxes of oxygenated volatile organic compounds from ponderosa pine trees, Journal of Geophysical Research-Atmospheres, 107, 2002.

Schade, G. W., and Custer, T. G.: OVOC emissions from agricultural soil in northern Germany during the 2003 European heat wave, Atmospheric Environment, 38, 6105-6114, 2004.

Schade, G. W., Solomon, S. J., Dellwik, E., Pilegaard, K., and Ladstatter-Weissenmayer, A.: Methanol and other VOC fluxes from a Danish beech forest during late springtime, Biogeochemistry, 106, 337-355, 2011.

Schobesberger, S., Lopez-Hilfiker, F. D., Taipale, D., Millet, D. B., D'Ambro, E. L., Rantala, P., Mammarella, I., Zhou, P., Wolfe, G. M., Lee, B. H., Boy, M., and Thornton, J. A.: High upward fluxes of formic acid from a boreal forest canopy, Geophysical Research Letters, 43, 9342-9351, 10.1002/2016GL069599, 2016.

Scholler, C. E. G., Gurtler, H., Pedersen, R., Molin, S., and Wilkins, K.: Volatile metabolites from actinomycetes, Journal of Agricultural and Food Chemistry, 50, 2615-2621, 2002.

Seco, R., Penuelas, J., and Filella, I.: Short-chain oxygenated VOCs: Emission and uptake by plants and atmospheric sources, sinks, and concentrations, Atmospheric Environment, 41, 2477-2499, 2007.

Seinfeld, J. H., and Pandis, S. N.: Dry Deposition, in: Atmospheric Chemistry and Physics: from Air Pollution to Climate Change, 3rd ed., John Wiley & Sons, Inc., Hoboken, New Jersey, 2016.

Sempére, R., and Kawamura, K.: Comparative distributions of dicarboxylic acids and related polar compounds in snow, rain and aerosols from urban atmosphere, Atmospheric Environment, 28, 449-459, https://doi.org/10.1016/1352-2310(94)90123-6, 1994.

Simonich, S. L., and Hites, R. A.: Organic Pollutant Accumulation in Vegetation, Environmental Science & Technology, 29, 2905-2914, 1995.

Singh, H., Chen, Y., Tabazadeh, A., Fukui, Y., Bey, I., Yantosca, R., Jacob, D., Arnold, F., Wohlfrom, K., Atlas, E., Flocke, F., Blake, D., Blake, N., Heikes, B., Snow, J., Talbot, R., Gregory, G., Sachse, G., Vay, S., and Kondo, Y.: Distribution and fate of selected oxygenated organic species in the troposphere and lower stratosphere over the Atlantic, Journal of Geophysical Research: Atmospheres, 105, 3795-3805, 10.1029/1999JD900779, 2000.

Singh, H. B., Kanakidou, M., Crutzen, P. J., and Jacob, D. J.: High concentrations and photochemical fate of oxygenated hydrocarbons in the global troposphere, Nature, 378, 50, 10.1038/378050a0, 1995.

Singh, H. B., Salas, L. J., Chatfield, R. B., Czech, E., Fried, A., Walega, J., Evans, M. J., Field, B. D., Jacob, D. J., Blake, D., Heikes, B., Talbot, R., Sachse, G., Crawford, J. H., Avery, M. A., Sandholm, S., and Fuelberg, H.: Analysis of the atmospheric distribution, sources, and sinks of oxygenated volatile organic chemicals based on measurements over the Pacific during TRACE-P, Journal of Geophysical Research: Atmospheres, 109, n/a-n/a, 10.1029/2003JD003883, 2004.

Stacheter, A., Noll, M., Lee, C. K., Selzer, M., Glowik, B., Ebertsch, L., Mertel, R., Schulz, D., Lampert, N., Drake, H. L., and Kolb, S.: Methanol oxidation by temperate soils and environmental determinants of associated methylotrophs, ISME J, 7, 1051-1064, 10.1038/ismej.2012.167, 2013.

Stavrakou, T., Muller, J. F., Peeters, J., Razavi, A., Clarisse, L., Clerbaux, C., Coheur, P. F., Hurtmans, D., De Maziere, M., Vigouroux, C., Deutscher, N. M., Griffith, D. W. T., Jones, N., and Paton-Walsh, C.: Satellite evidence for a large source of formic acid from boreal and tropical forests, Nature Geosci, 5, 26-30, http://www.nature.com/ngeo/journal/v5/n1/abs/ngeo1354.html#supplementary-information, 2012.

Stickler, A., Fischer, H., Bozem, H., Gurk, C., Schiller, C., Martinez-Harder, M., Kubistin, D., Harder, H., Williams, J., Eerdekens, G., Yassaa, N., Ganzeveld, L., Sander, R., and Lelieveld, J.: Chemistry, transport and dry deposition of trace gases in the boundary layer over the tropical Atlantic Ocean and the Guyanas during the GABRIEL field campaign, Atmospheric Chemistry and Physics, 7, 3933-3956, 2007.

Su, H., Cheng, Y., Oswald, R., Behrendt, T., Trebs, I., Meixner, F. X., Andreae, M. O., Cheng, P., Zhang, Y., and Pöschl, U.: Soil Nitrite as a Source of Atmospheric HONO and OH Radicals, Science, 333, 1616-1618, 10.1126/science.1207687, 2011.

Su, H., Cheng, Y., and Pöschl, U.: The Exchange of Soil Nitrite and Atmospheric HONO: A Missing Process in the Nitrogen Cycle and Atmospheric Chemistry, in: Disposal of Dangerous Chemicals in Urban Areas and Mega Cities: Role of Oxides and Acids of Nitrogen in Atmospheric Chemistry, edited by: Barnes, I., and Rudziński, K. J., Springer Netherlands, Dordrecht, 93-99, 2013.

Tie, X., Guenther, A., and Holland, E.: Biogenic methanol and its impacts on tropospheric oxidants, Geophysical Research Letters, 30, n/a-n/a, 10.1029/2003GL017167, 2003.

Tong, H., Arangio, A. M., Lakey, P. S. J., Berkemeier, T., Liu, F., Kampf, C. J., Brune, W. H., Pöschl, U., and Shiraiwa, M.: Hydroxyl radicals from secondary organic aerosol decomposition in water, Atmos. Chem. Phys., 16, 1761-1771, 10.5194/acp-16-1761-2016, 2016.

Tuazon, E. C., Arey, J., Atkinson, R., and Aschmann, S. M.: Gas-phase reactions of 2-vinylpyridine and styrene with hydroxyl and NO3 radicals and ozone, Environmental Science & Technology, 27, 1832-1841, 10.1021/es00046a011, 1993.

Tunved, P., Hansson, H. C., Kerminen, V. M., Strom, J., Dal Maso, M., Lihavainen, H., Viisanen, Y., Aalto, P. P., Komppula, M., and Kulmala, M.: High natural aerosol loading over boreal forests, Science, 312, 261-263, 2006.

van Pinxteren, D., Plewka, A., Hofmann, D., Müller, K., Kramberger, H., Svrcina, B., Bächmann, K., Jaeschke, W., Mertes, S., Collett, J. L., and Herrmann, H.: Schmücke hill cap cloud and valley stations aerosol characterisation during FEBUKO (II): Organic compounds, Atmospheric Environment, 39, 4305-4320, https://doi.org/10.1016/j.atmosenv.2005.02.014, 2005.

van Roon, A., Parsons, J. R., Krap, L., and Govers, H. A. J.: Fate and transport of monoterpenes through soils. Part II: Calculation of the effect of soil temperature, water saturation and organic carbon content, Chemosphere, 61, 129-138, 2005.

VandenBoer, T. C., Young, C. J., Talukdar, R. K., Markovic, M. Z., Brown, S. S., Roberts, J. M., and Murphy, J. G.: Nocturnal loss and daytime source of nitrous acid through reactive uptake and displacement, Nature Geoscience, 8, 55-60, 2015.

Veres, P. R., Roberts, J. M., Cochran, A. K., Gilman, J. B., Kuster, W. C., Holloway, J. S., Graus, M., Flynn, J., Lefer, B., Warneke, C., and de Gouw, J.: Evidence of rapid production of organic acids in an urban air mass, Geophysical Research Letters, 38, n/a-n/a, 10.1029/2011GL048420, 2011.

Verma, V., Fang, T., Xu, L., Peltier, R. E., Russell, A. G., Ng, N. L., and Weber, R. J.: Organic Aerosols Associated with the Generation of Reactive Oxygen Species (ROS) by Water-Soluble PM2.5, Environmental Science & Technology, 49, 4646-4656, 10.1021/es505577w, 2015.

Vet, R., Artz, R. S., Carou, S., Shaw, M., Ro, C.-U., Aas, W., Baker, A., Bowersox, V. C., Dentener, F., Galy-Lacaux, C., Hou, A., Pienaar, J. J., Gillett, R., Forti, M. C., Gromov, S., Hara, H., Khodzher, T., Mahowald, N. M., Nickovic, S., Rao, P. S. P., and Reid, N. W.: A global assessment of precipitation chemistry and deposition of sulfur, nitrogen, sea salt, base cations, organic acids, acidity and pH, and phosphorus, Atmospheric Environment, 93, 3-100, https://doi.org/10.1016/j.atmosenv.2013.10.060, 2014.

Vlasenko, A., George, I. J., and Abbatt, J. P. D.: Formation of Volatile Organic Compounds in the Heterogeneous Oxidation of Condensed-Phase Organic Films by Gas-Phase OH, The Journal of Physical Chemistry A, 112, 1552-1560, 10.1021/jp0772979, 2008.

Vlasenko, A., Macdonald, A. M., Sjostedt, S. J., and Abbatt, J. P. D.: Formaldehyde measurements by Proton transfer reaction - Mass Spectrometry (PTR-MS): correction for humidity effects, Atmos Meas Tech, 3, 1055-1062, 2010.

Volkamer, R., Jimenez, J. L., San Martini, F., Dzepina, K., Zhang, Q., Salcedo, D., Molina, L. T., Worsnop, D. R., and Molina, M. J.: Secondary organic aerosol formation from anthropogenic air pollution: Rapid and higher than expected, Geophysical Research Letters, 33, n/a-n/a, 10.1029/2006GL026899, 2006.

Wagner, P., and Kuttler, W.: Biogenic and anthropogenic isoprene in the near-surface urban atmosphere — A case study in Essen, Germany, Science of The Total Environment, 475, 104-115, https://doi.org/10.1016/j.scitotenv.2013.12.026, 2014.

Wagner, V., von Glasow, R., Fischer, H., and Crutzen, P. J.: Are CH2O measurements in the marine boundary layer suitable for testing the current understanding of CH4 photooxidation?: A model study, Journal of Geophysical Research: Atmospheres, 107, ACH 3-1-ACH 3-14, 10.1029/2001JD000722, 2002.

Walser, M. L., Park, J., Gomez, A. L., Russell, A. R., and Nizkorodov, S. A.: Photochemical Aging of Secondary Organic Aerosol Particles Generated from the Oxidation of d-Limonene, The Journal of Physical Chemistry A, 111, 1907-1913, 10.1021/jp066293l, 2007.

Wang, J.-L., Chew, C., Chang, C.-Y., Liao, W.-C., Lung, S.-C. C., Chen, W.-N., Lee, P.-J., Lin, P.-H., and Chang, C.-C.: Biogenic isoprene in subtropical urban settings and implications for air quality, Atmospheric Environment, 79, 369-379, https://doi.org/10.1016/j.atmosenv.2013.06.055, 2013.

Wang, L., Wang, W. G., and Ge, M. F.: Heterogeneous uptake of NO2 on soils under variable temperature and relative humidity conditions, J Environ Sci-China, 24, 1759-1766, 10.1016/S1001-0742(11)61015-2, 2012.

Warneck, P., and Williams, J.: Trace Gases, in: The Atmospheric Chemist's Companion: Numerical Data for Use in the Atmospheric Sciences, Springer Netherlands, Dordrecht, 69-125, 2012.

Warneke, C., Karl, T., Judmaier, H., Hansel, A., Jordan, A., Lindinger, W., and Crutzen, P. J.: Acetone, methanol, and other partially oxidized volatile organic emissions from dead plant matter by abiological processes: Significance for atmospheric HOx chemistry, Global Biogeochemical Cycles, 13, 9-17, 1999.

Warneke, C., Veres, P., Holloway, J. S., Stutz, J., Tsai, C., Alvarez, S., Rappenglueck, B., Fehsenfeld, F. C., Graus, M., Gilman, J. B., and de Gouw, J. A.: Airborne formaldehyde measurements using PTR-MS: calibration, humidity dependence, inter-comparison and initial results, Atmos. Meas. Tech., 4, 2345-2358, 10.5194/amt-4-2345-2011, 2011.

Wesely, M. L.: Parameterization of Surface Resistances to Gaseous Dry Deposition in Regional-Scale Numerical Models, Atmospheric Environment, 23, 1293-1304, 1989.

Williams, J.: Organic Trace Gases in the Atmosphere: An Overview, Environmental Chemistry, 1, 125-136, https://doi.org/10.1071/EN04057, 2004.

Williams, J., Keßel, S. U., Nölscher, A. C., Yang, Y., Lee, Y., Yáñez-Serrano, A. M., Wolff, S., Kesselmeier, J., Klüpfel, T., Lelieveld, J., and Shao, M.: Opposite OH reactivity and ozone cycles in the Amazon rainforest and megacity Beijing: Subversion of biospheric oxidant control by anthropogenic emissions, Atmospheric Environment, 125, 112-118, https://doi.org/10.1016/j.atmosenv.2015.11.007, 2016.

Xing, B., and Pignatello, J. J.: Time-dependent isotherm shape of organic compounds in soil organic matter: Implications for sorption mechanism, Environmental Toxicology and Chemistry, 15, 1282-1288, 10.1002/etc.5620150805, 1996.

Yuan, B., Shao, M., de Gouw, J., Parrish, D. D., Lu, S. H., Wang, M., Zeng, L. M., Zhang, Q., Song, Y., Zhang, J. B., and Hu, M.: Volatile organic compounds (VOCs) in urban air: How chemistry affects the interpretation of positive matrix factorization (PMF) analysis, Journal of Geophysical Research-Atmospheres, 117, 2012.

Yuan, B., Hu, W. W., Shao, M., Wang, M., Chen, W. T., Lu, S. H., Zeng, L. M., and Hu, M.: VOC emissions, evolutions and contributions to SOA formation at a receptor site in eastern China, Atmos. Chem. Phys., 13, 8815-8832, 10.5194/acp-13-8815-2013, 2013.

Yuan, B., Veres, P. R., Warneke, C., Roberts, J. M., Gilman, J. B., Koss, A., Edwards, P. M., Graus, M., Kuster, W. C., Li, S. M., Wild, R. J., Brown, S. S., Dubé, W. P., Lerner, B. M., Williams, E. J., Johnson, J. E., Quinn, P. K., Bates, T. S., Lefer, B., Hayes, P. L., Jimenez, J. L., Weber, R. J., Zamora, R., Ervens, B., Millet, D. B., Rappenglück, B., and de Gouw, J. A.: Investigation of secondary formation of formic acid: urban environment vs. oil and gas producing region, Atmos. Chem. Phys., 15, 1975-1993, 10.5194/acp-15-1975-2015, 2015.

Yuan, B., Koss, A. R., Warneke, C., Coggon, M., Sekimoto, K., and de Gouw, J. A.: Proton-Transfer-Reaction Mass Spectrometry: Applications in Atmospheric Sciences, Chemical Reviews, 117, 13187-13229, 10.1021/acs.chemrev.7b00325, 2017.

Zender, C. S., Miller, R. L. L., and Tegen, I.: Quantifying mineral dust mass budgets:Terminology, constraints, and current estimates, Eos, Transactions American Geophysical Union, 85, 509-512, 10.1029/2004EO480002, 2011.

Zepp, R. G., Erickson Iii, D. J., Paul, N. D., and Sulzberger, B.: Interactive effects of solar UV radiation and climate change on biogeochemical cycling, Photochemical & Photobiological Sciences, 6, 286-300, 10.1039/B700021A, 2007.

Zhang, Y. H., Su, H., Zhong, L. J., Cheng, Y. F., Zeng, L. M., Wang, X. S., Xiang, Y. R., Wang, J. L., Gao, D. F., Shao, M., Fan, S. J., and Liu, S. C.: Regional ozone pollution and observation-based approach for analyzing ozone–precursor relationship during the PRIDE-PRD2004 campaign, Atmospheric Environment, 42, 6203-6218, https://doi.org/10.1016/j.atmosenv.2008.05.002, 2008.

Atmos. Chem. Phys. Discuss., https://doi.org/10.5194/acp-2018-683
Manuscript under review for journal Atmos. Chem. Phys.
Discussion started: 25 July 2018

Atmospheric Chemistry and Physics Discussions

List of Tables:

Table 1. List of reported VOC species along with their protonated m/z, and 5-minute limits of detection (LOD).

Protonated (m/z)	Species	LOD (ppt)	Protonated (m/z)	Species	LOD (ppt)
21	$H_3{}^{18}O^+$		69	isoprene	70
39	$H_3{}^{18}O^+$ (H_2O)		71	MVK+MACR	109
31	formaldehyde	101	73	MEK	198
33	methanol	355	79	benzene	78
42	acetonitrile	87	93	toluene	93
45	acetaldehyde	112	105	styrene	55
47	formic acid	277			
59	acetone	77			
61	acetic acid	243			

MVK: methyl vinyl ketone; MACR: methacrolein; MEK: methyl ethyl ketone.

Atmos. Chem. Phys. Discuss., https://doi.org/10.5194/acp-2018-683
Manuscript under review for journal Atmos. Chem. Phys.
Discussion started: 25 July 2018

Atmospheric Chemistry and Physics Discussions

Table 2. Parameters used for resistance calculations to infer the relative importance of R_c versus R_a and R_b, and the resulting deposition velocities (V_d) of measured VOC species.

VOCs species	γ ($\times 10^{-7}$)	ω (cm s^{-1})	D (cm^2 s^{-1})	u_* (cm s^{-1})			z_0 (cm)			R_c (s cm^{-1})	R_a (s cm^{-1})			R_b (s cm^{-1})			V_d (cm s^{-1})		
				1	2	3	1	2	3		1	2	3	1	2	3	1	2	3
Styrene	12.30	24636	0.08	30	45	20	10	100	4	132	0.67	0.32	1.12	0.27	0.18	0.40	0.008	0.008	0.007
Formaldehyde	8.92	45870	0.17	30	45	20	10	100	4	98	0.67	0.32	1.12	0.15	0.10	0.23	0.01	0.01	0.01
Toluene	6.74	26194	0.08	30	45	20	10	100	4	227	0.67	0.32	1.12	0.26	0.17	0.38	0.004	0.004	0.004
Isoprene	6.06	30468	0.09	30	45	20	10	100	4	217	0.67	0.32	1.12	0.24	0.16	0.36	0.005	0.005	0.005
Acetic acid	5.77	32435	0.12	30	45	20	10	100	4	214	0.67	0.32	1.12	0.20	0.13	0.30	0.005	0.005	0.005
MVK+MACR	4.80	30029	0.10	30	45	20	10	100	4	278	0.67	0.32	1.12	0.23	0.15	0.35	0.004	0.004	0.004
Acetaldehyde	3.63	37876	0.13	30	45	20	10	100	4	291	0.67	0.32	1.12	0.19	0.12	0.28	0.003	0.003	0.003
Methanol	3.43	44414	0.16	30	45	20	10	100	4	263	0.67	0.32	1.12	0.16	0.11	0.24	0.004	0.004	0.004
MEK	2.27	29609	0.09	30	45	20	10	100	4	595	0.67	0.32	1.12	0.23	0.16	0.35	0.002	0.002	0.002
Acetone	2.16	32990	0.11	30	45	20	10	100	4	561	0.67	0.32	1.12	0.21	0.14	0.32	0.002	0.002	0.002
Acetonitrile	2.12	39237	0.16	30	45	20	10	100	4	480	0.67	0.32	1.12	0.17	0.11	0.25	0.002	0.002	0.002
Benzene	1.89	28448	0.09	30	45	20	10	100	4	745	0.67	0.32	1.12	0.24	0.16	0.36	0.001	0.001	0.001
Formic acid	-2.15	37044	0.15	30	45	20	10	100	4	-502	0.67	0.32	1.12	0.17	0.12	0.26	-0.002	-0.002	-0.002

γ: uptake coefficient; ω: mean molecular speed at 25 °C; D: molecular diffusion coefficient at 25 °C; u_*: friction velocity, the listed values are averaged between the day and night cases by Zhang et al., (2003); z_0: aerodynamic surface roughness length, the listed values are referred to Zhang et al., (2002); R_c: soil surface resistance; R_a: aerodynamic resistance, calculated using the equation (19.14) in (Seinfeld and Pandis, 2016), where the reference height z is set as 300 m; R_b: quasi-laminar layer resistance, calculated using the equation (19.17) in (Seinfeld and Pandis, 2016), where the air kinematic viscosity ν is 0.16 cm^2 s^{-1}; V_d: deposition velocity; The numbers in the table header denote different land use categories adopted from Zhang et al., (2002; 2003): 1 shrubs; 2 urban; 3 barren land (mostly desert).

Atmos. Chem. Phys. Discuss., https://doi.org/10.5194/acp-2018-683
Manuscript under review for journal Atmos. Chem. Phys.
Discussion started: 25 July 2018

Atmospheric Chemistry and Physics Discussions

List of Figures:

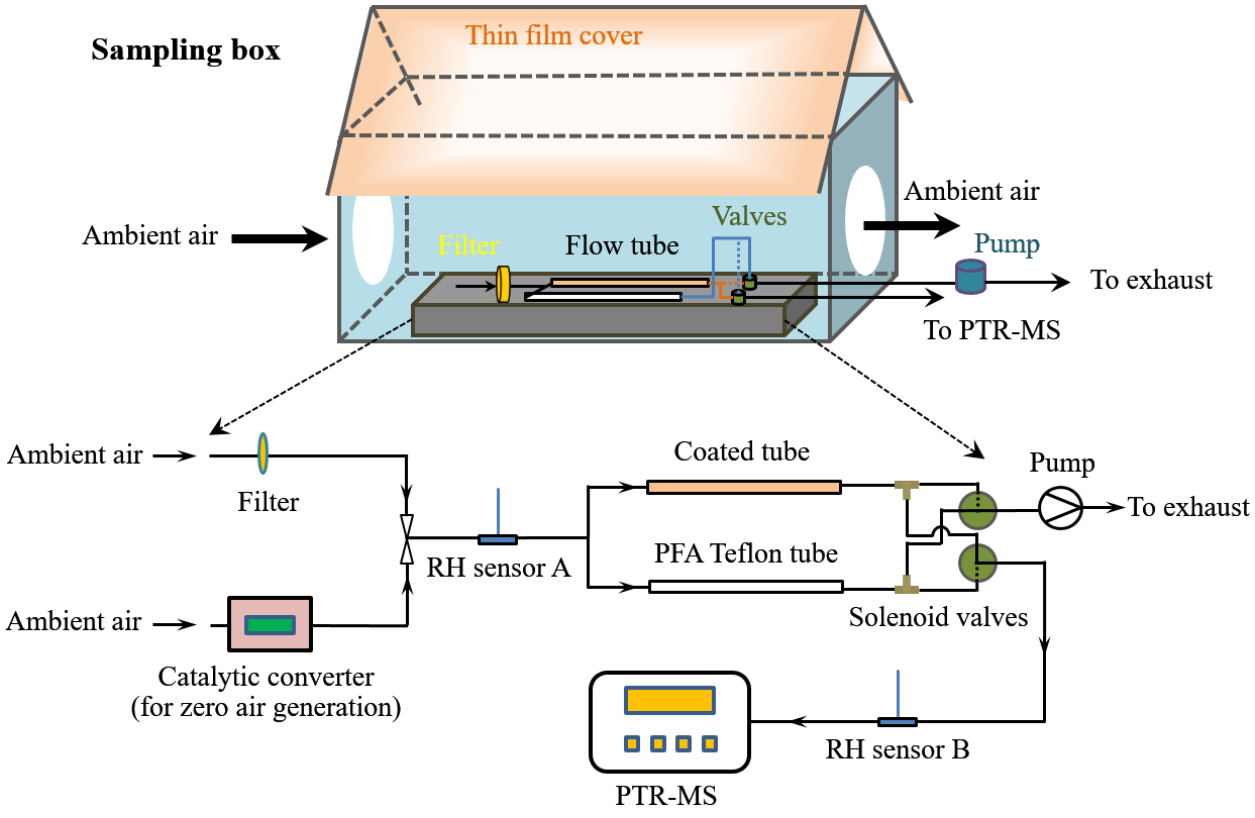

Figure 1. Schematic illustration of the experimental setup.

Atmos. Chem. Phys. Discuss., https://doi.org/10.5194/acp-2018-683
Manuscript under review for journal Atmos. Chem. Phys.
Discussion started: 25 July 2018

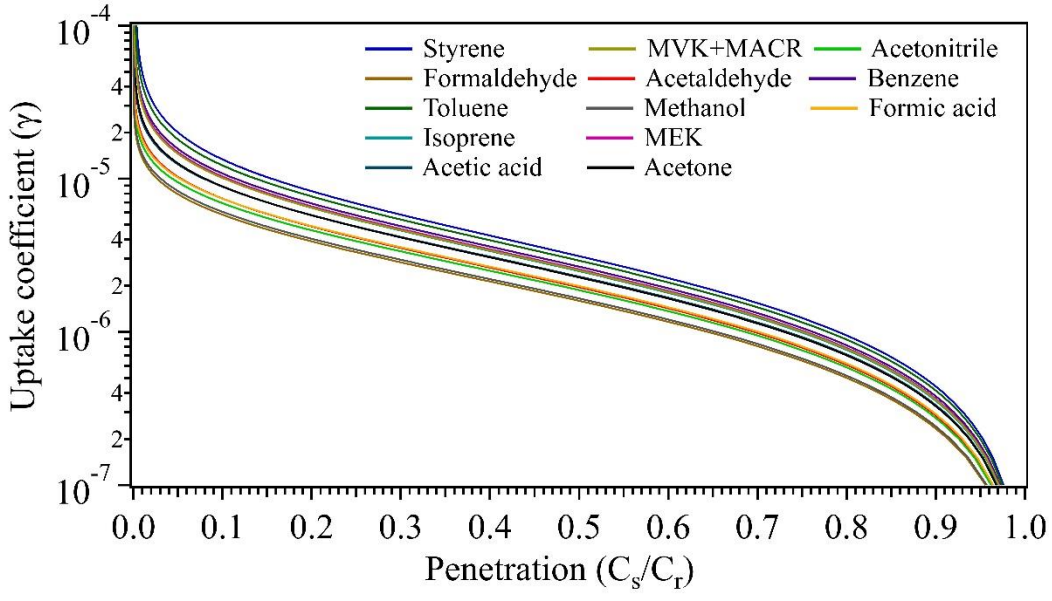

Figure 2. Schematic of the uptake coefficients versus the penetrations of measured VOC species. Derivation of the uptake coefficients are based on the experimental parameters: volumetric flow rate F = 0.1 L min^{-1} at 1 atm and 298 K; coated-wall flow tube dimension, d = 1.6 cm, L = 10 cm.

Atmos. Chem. Phys. Discuss., https://doi.org/10.5194/acp-2018-683
Manuscript under review for journal Atmos. Chem. Phys.
Discussion started: 25 July 2018

Atmospheric Chemistry and Physics Discussions

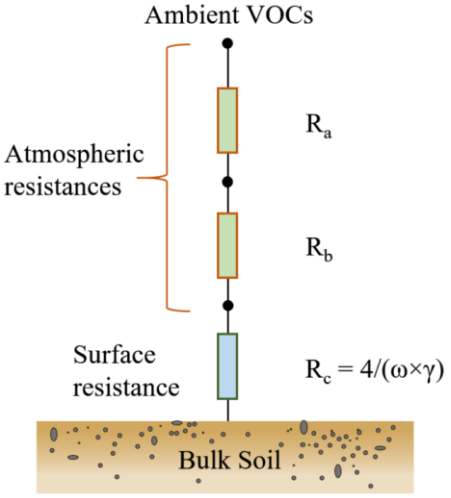

Figure 3. Schematic of the resistance model for VOC species dry deposition on soil

Atmos. Chem. Phys. Discuss., https://doi.org/10.5194/acp-2018-683
Manuscript under review for journal Atmos. Chem. Phys.
Discussion started: 25 July 2018

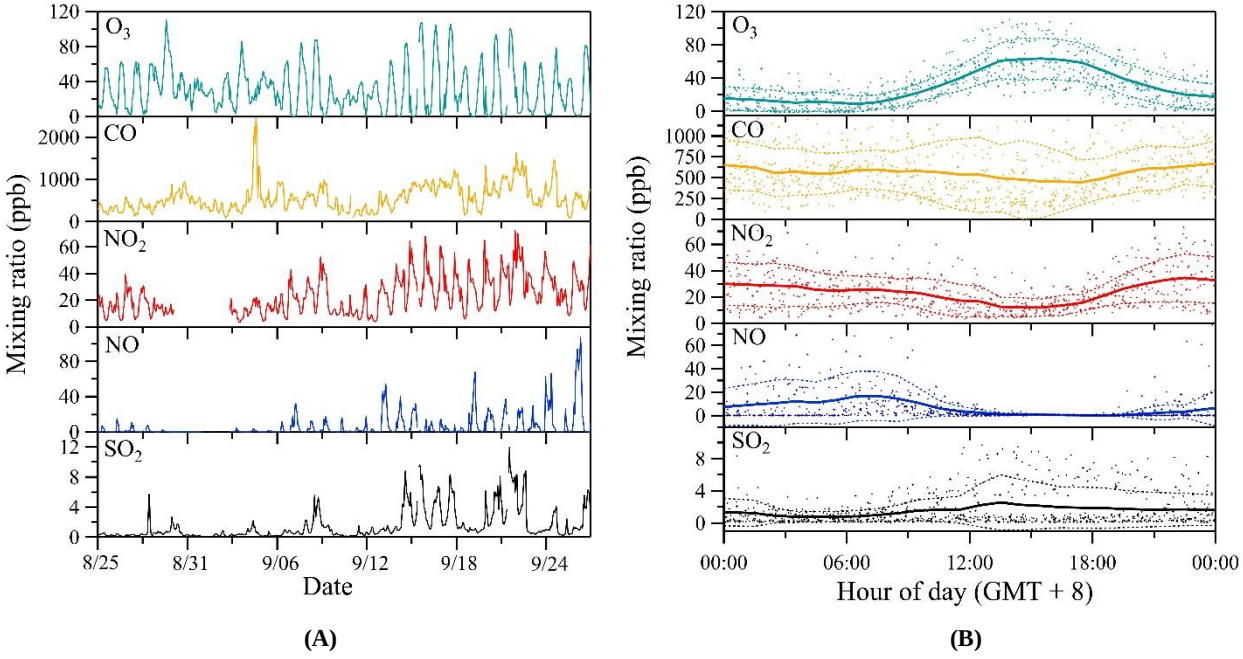

Figure 4. Time series of observed ambient air mixing ratios of prominent gas phase pollutants (A) and respective mean diel courses (B). In (B), symbols denote individual hourly averaged data, and the thick solid lines respective mean diel profile. Thin dashed lines represent one standard deviation (± 1 SD) from the mean value.

Atmos. Chem. Phys. Discuss., https://doi.org/10.5194/acp-2018-683
Manuscript under review for journal Atmos. Chem. Phys.
Discussion started: 25 July 2018

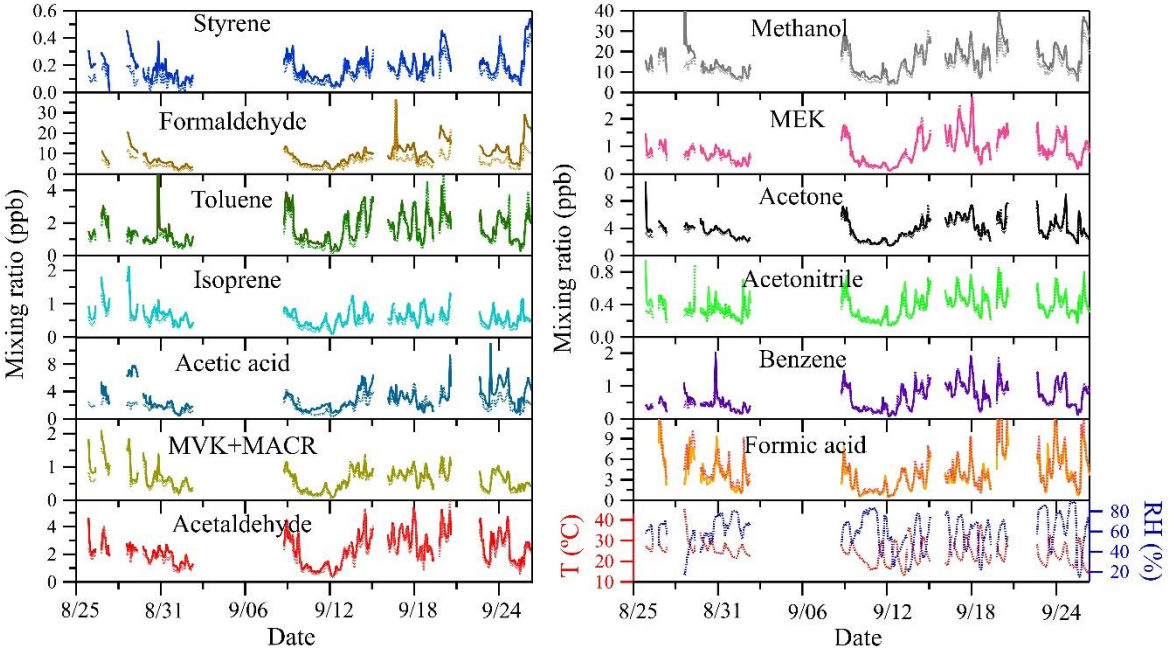

Figure 5. (A)

Atmos. Chem. Phys. Discuss., https://doi.org/10.5194/acp-2018-683
Manuscript under review for journal Atmos. Chem. Phys.
Discussion started: 25 July 2018

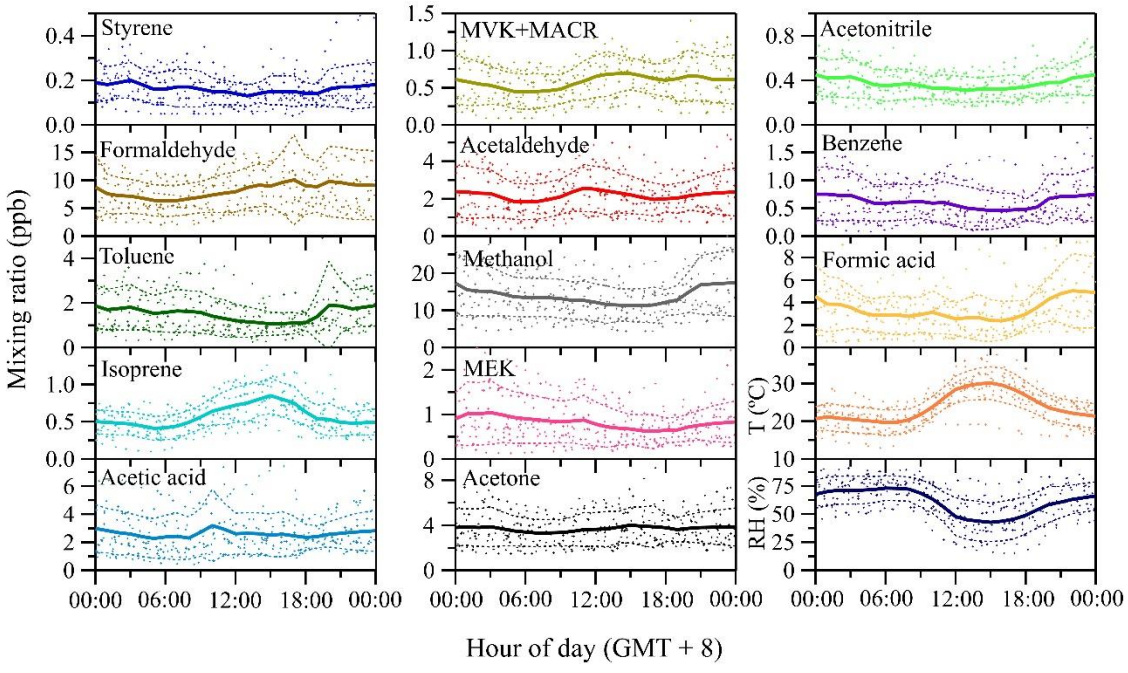

Figure 5. (B)

Figure 5. Time series of observed ambient air mixing ratios of VOCs and air temperature and relative humidity (A), and respective mean diel courses (B). Solid lines in (A) denote ambient air mixing ratios at the outlet of the reference tube, and dotted lines at the outlet of the sample tube. In (B), symbols denote individual hourly averaged data, and the thick solid lines respective mean diel profile. Thin dashed lines represent one standard deviation (± 1 SD) from the mean value.

Atmos. Chem. Phys. Discuss., https://doi.org/10.5194/acp-2018-683
Manuscript under review for journal Atmos. Chem. Phys.
Discussion started: 25 July 2018

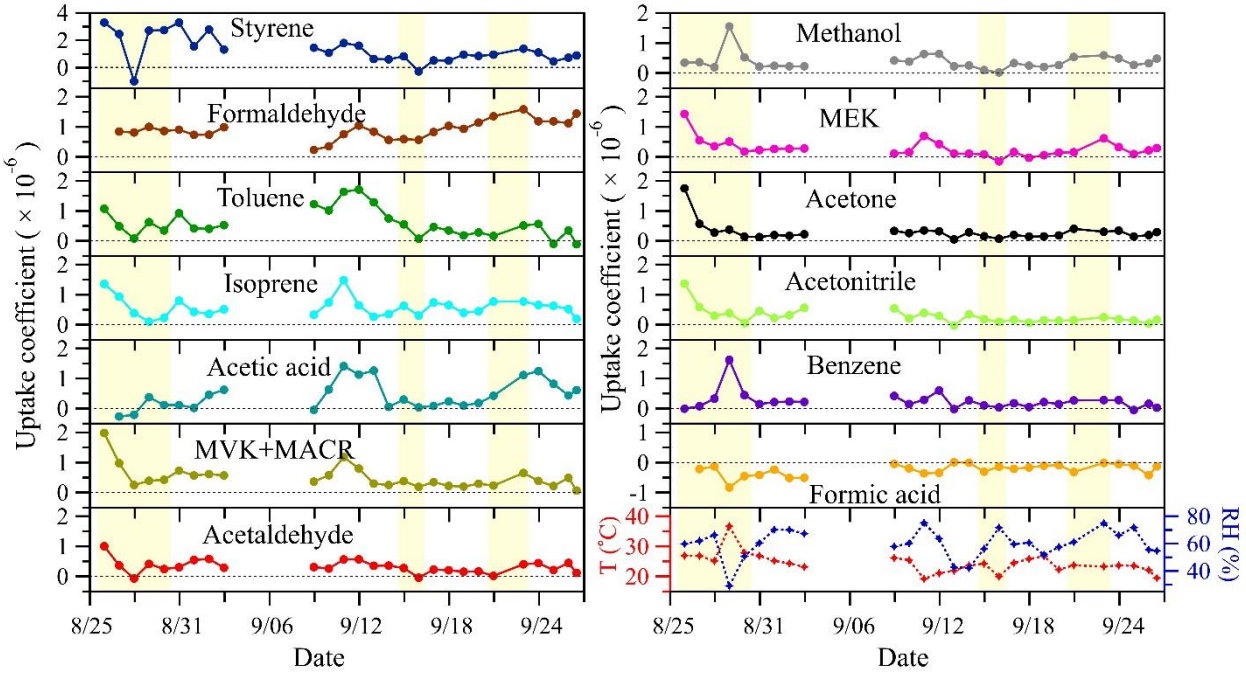

Figure 6. (A)

Atmos. Chem. Phys. Discuss., https://doi.org/10.5194/acp-2018-683
Manuscript under review for journal Atmos. Chem. Phys.
Discussion started: 25 July 2018

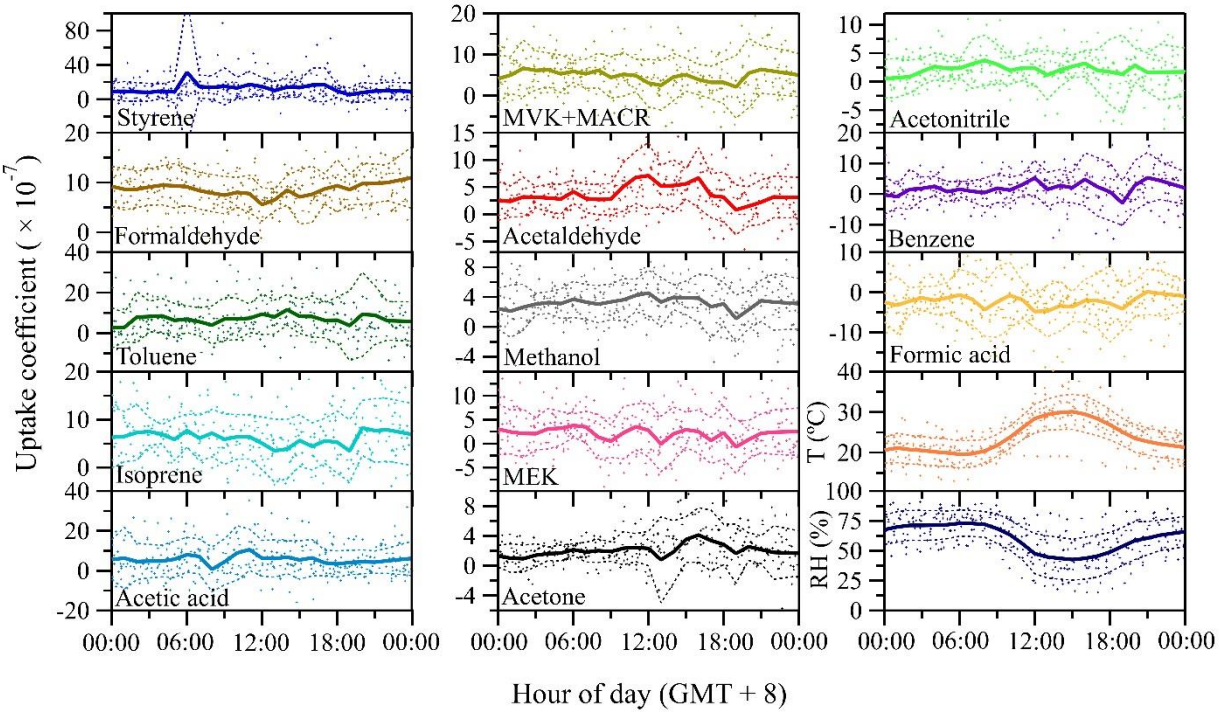

Figure 6. (B)

Figure 6. Time series of the uptake coefficients of measured VOC species and air temperature and relative humidity (A), and respective mean diel courses (B). In (A), each symbol represents daily averaged data and the yellow shaded areas indicate the days when measurements were not continuously running all day long. In (B), symbols denote individual hourly averaged data, and the thick solid lines respective mean diel profiles. Thin dashed lines represent one standard deviation (± 1 SD) from mean values.

Atmos. Chem. Phys. Discuss., https://doi.org/10.5194/acp-2018-683
Manuscript under review for journal Atmos. Chem. Phys.
Discussion started: 25 July 2018

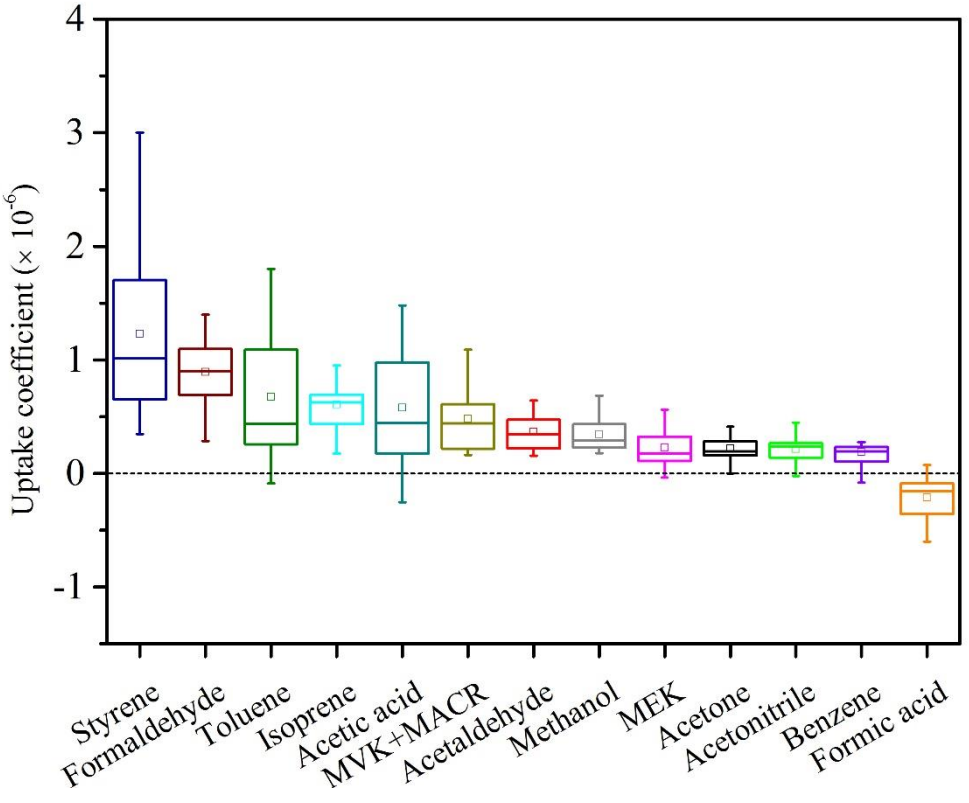

Figure 7. Box-and-whisker plots of the uptake coefficients of measured VOC species, based on daily averaged data. Minimum, 25th, 50th, 75th percentile and maximum are indicated by bars, and mean values by squares.

Atmos. Chem. Phys. Discuss., https://doi.org/10.5194/acp-2018-683
Manuscript under review for journal Atmos. Chem. Phys.
Discussion started: 25 July 2018

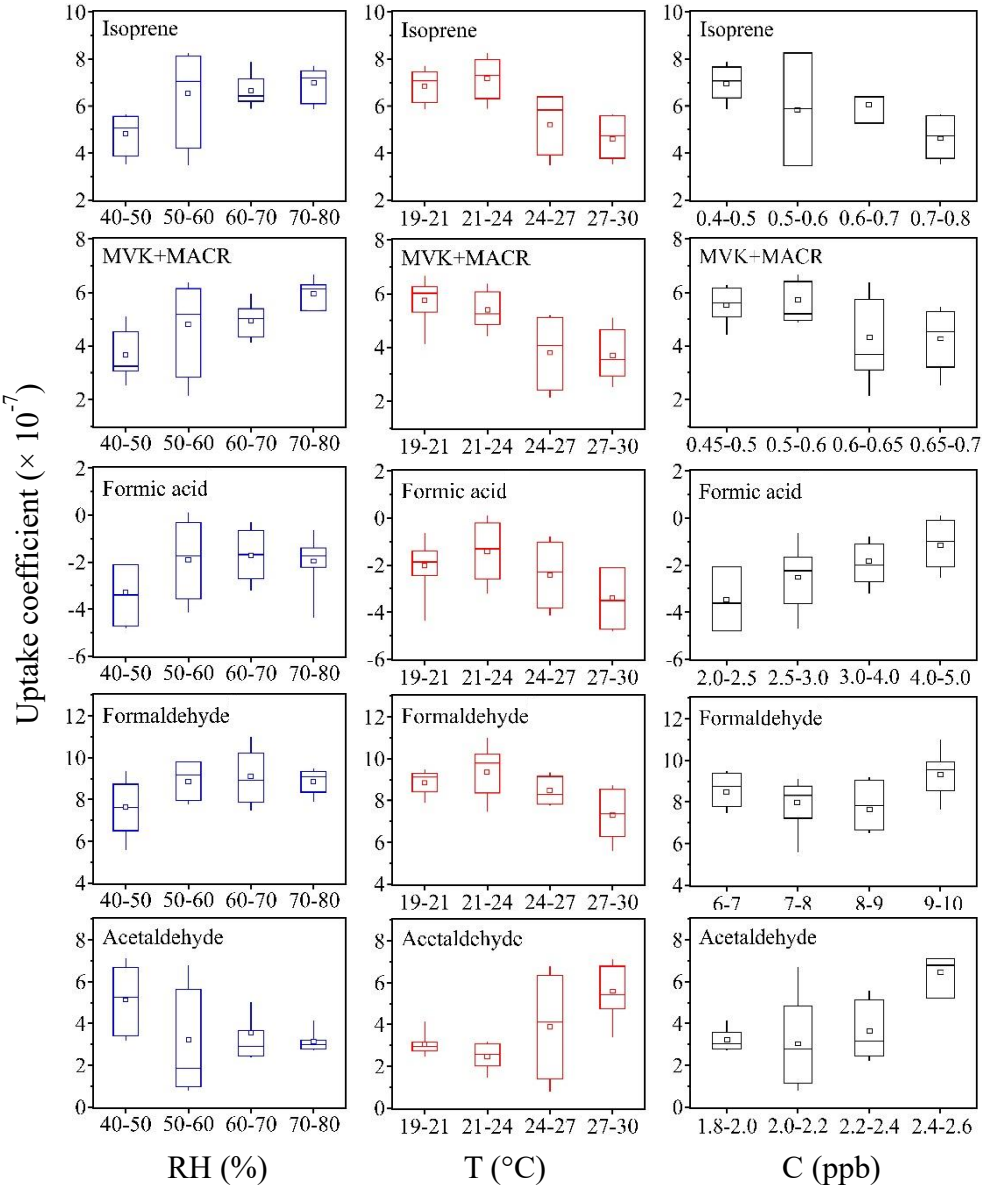

Figure 8. Dependence of daily averaged uptake coefficients on ambient relative humidity (RH), temperature (T) and mixing ratios (C). Minimum, 25th, 50th, 75th percentile and maximum of the box-and-whisker plots are indicated by bars, and mean values by squares. The uptake coefficient dependence is based on the days when measurements were continuously running all day long. Note that negative uptake coefficients (for formic acid) indicate emission.

Atmos. Chem. Phys. Discuss., https://doi.org/10.5194/acp-2018-683
Manuscript under review for journal Atmos. Chem. Phys.
Discussion started: 25 July 2018

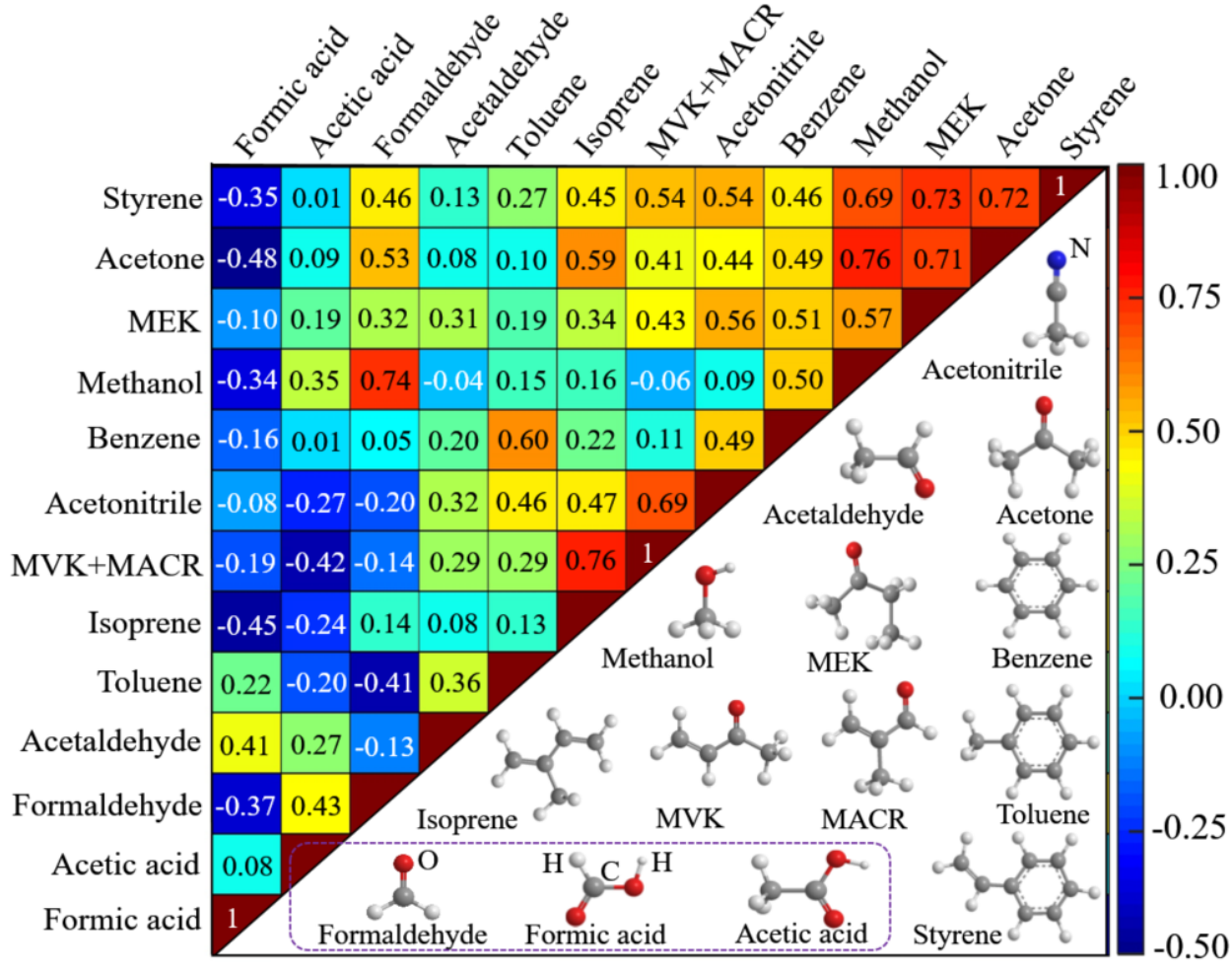

Figure 9. Correlation of the exchange of measured VOC species (upper left) and their molecular structures (lower right). Correlation between each pair of VOCs is reflected by the correlation coefficient, shown in the plot. The correlation coefficient between each individual species itself is 1, a correlation coefficient of 0 means no correlation, and -1 implies complete anti-correlation.

Supplemental Information

Table S.1. Determined VOC desorption rate coefficient and desorption lifetime on the soil sample, during flushing with VOCs-free N_2.

	VOC species												
	A	B	C	D	E	F	G	H	I	J	K	L	M
Desorption rate coefficient ($\times 10^{-3}$ s^{-1})	-	0.8	-	-	1.6	4.3	3.7	3.0	4.1	5.6	4.8	-	3.1
Desorption lifetime (min)	-	22.2	-	-	10.8	3.9	4.5	5.7	4.1	3.0	3.5	-	5.4

A: styrene, B: formaldehyde, C: toluene, D: isoprene, E: acetic acid, F: MVK+MACR, G: acetaldehyde, H: methanol, I: MEK, J: acetone, K: acetonitrile, L: benzene, M: formic acid. The symbol "-" means no detected emissions of this compound from the soil.

Table S.2. Integrated total amount and average surface flux of each adsorbed or emitted VOC species on soil for the whole measurement period.

	VOC species												
	A	B	C	D	E	F	G	H	I	J	K	L	M
Integrated total amount (μg)	0.54	11.86	2.08	0.75	2.51	0.58	1.18	9.54	0.37	1.98	0.15	0.34	-2.29
Average surface flux (nmol m^{-2} s^{-1})	0.001	0.047	0.003	0.001	0.005	0.001	0.003	0.036	0.001	0.004	0.0004	0.001	-0.006

A: styrene, B: formaldehyde, C: toluene, D: isoprene, E: acetic acid, F: MVK+MACR, G: acetaldehyde, H: methanol, I: MEK, J: acetone, K: acetonitrile, L: benzene, M: formic acid. Positive values mean soil uptake and negative values mean soil emission.

Table S.3. Basic physicochemical parameters (at 298 K) of the measured VOC species.

	VOC species													
	A	B	C	D	E	F_1	F_2	G	H	I	J	K	L	M
$k_w \times 10^3$ (cm s^{-1})	7.6	10	4.4	4.6	4.7	3.6	3.6	3.4	3.8	1.7	1.8	2.1	1.3	-2.0
$k_{OH} \times 10^{12}$ (cm^3 $molecule^{-1}$ s^{-1})	58	9.4	5.6	100	0.74[a]	20	29	15	0.94	1.2	0.17	0.049[b]	1.2	0.37[a]
$k_{O3} \times 10^{18}$ (cm^3 $molecule^{-1}$ s^{-1})	17	< 0.01	< 0.01	13	N[c]	5.2	1.2	< 0.01	< 0.01	N	< 0.01	≤ 0.15[b]	< 0.01	N[c]
$H \times 10^2$ (mol m^{-3} Pa^{-1})	0.33	3200	0.15	0.013	5000	30	6.0	15	220	18	25	50	0.18	7000
P (mm Hg)	6.4	3.89	28.4	550	15.7	152	155	902	127	90.6	231	88.8	94.8	42.6
log K_{ow}	3.05	0.35	2.73	2.42	-0.17	0.41	0.59[d]	0.45	-0.74	0.29	-0.24	-0.34	2.13	-0.54

A: styrene, B: formaldehyde, C: toluene, D: isoprene, E: acetic acid, F_1: MVK, F_2: MACR, G: acetaldehyde, H: methanol, I: MEK, J: acetone, K: acetonitrile, L: benzene, M: formic acid. k_w: surface reaction (or wall loss) rate coefficient, k_{OH}: rate coefficient of VOCs reaction with OH radicals in gas phase, k_{O3}: rate coefficient of VOCs reaction with O_3, H: Henry's law constant, P: vapor pressure, K_{ow}: octanol-water partition coefficient. Both k_{OH} and k_{O3} data refer to Atkinson and Arey (2003), H data refer to Sander (2015), P and K_{ow} data are from https://pubchem.ncbi.nlm.nih.gov/ and Sangster (1989), unless otherwise noted by a: (Dagaut et al., 1988), b: (Harris et al., 1981), c: (Chebbi and Carlier, 1996) and d: (Barratt, 1996). Positive values of k_w mean soil uptake and negative values mean soil emission. N means the values are negligible.

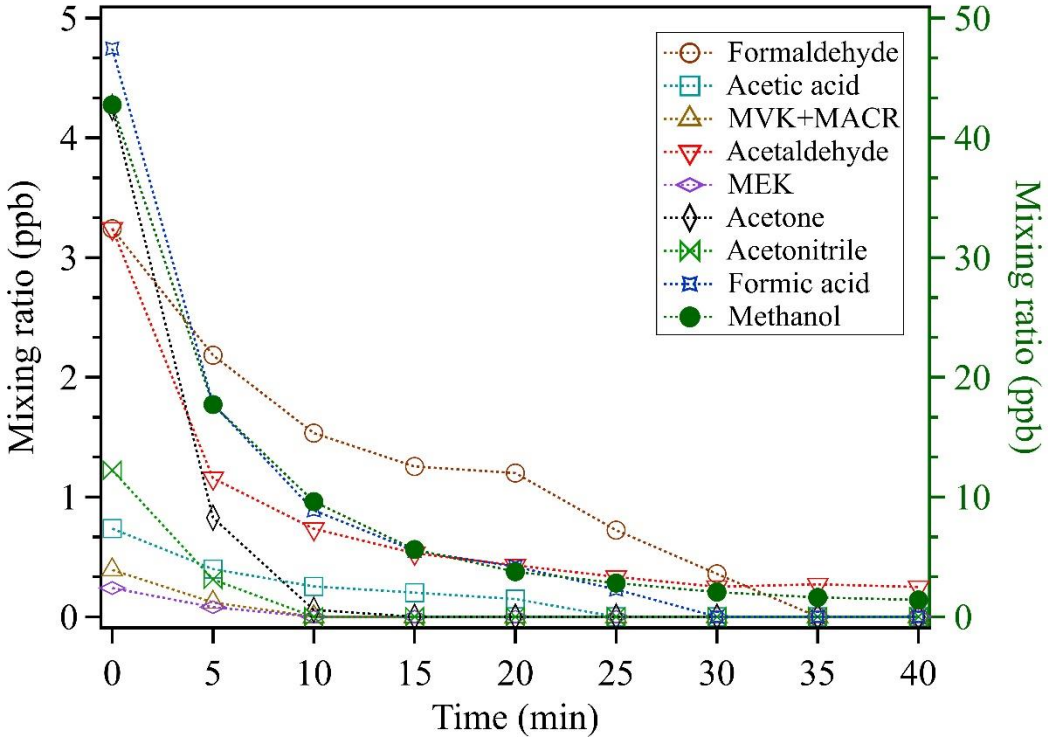

Figure S.1. Time course of VOC mixing ratios at the outlet of the freshly coated sample tube flushed with VOCs-free N_2, prior to the ambient air uptake experiment. Methanol mixing ratios are referred to the right vertical axis and the other species are referred to the left.

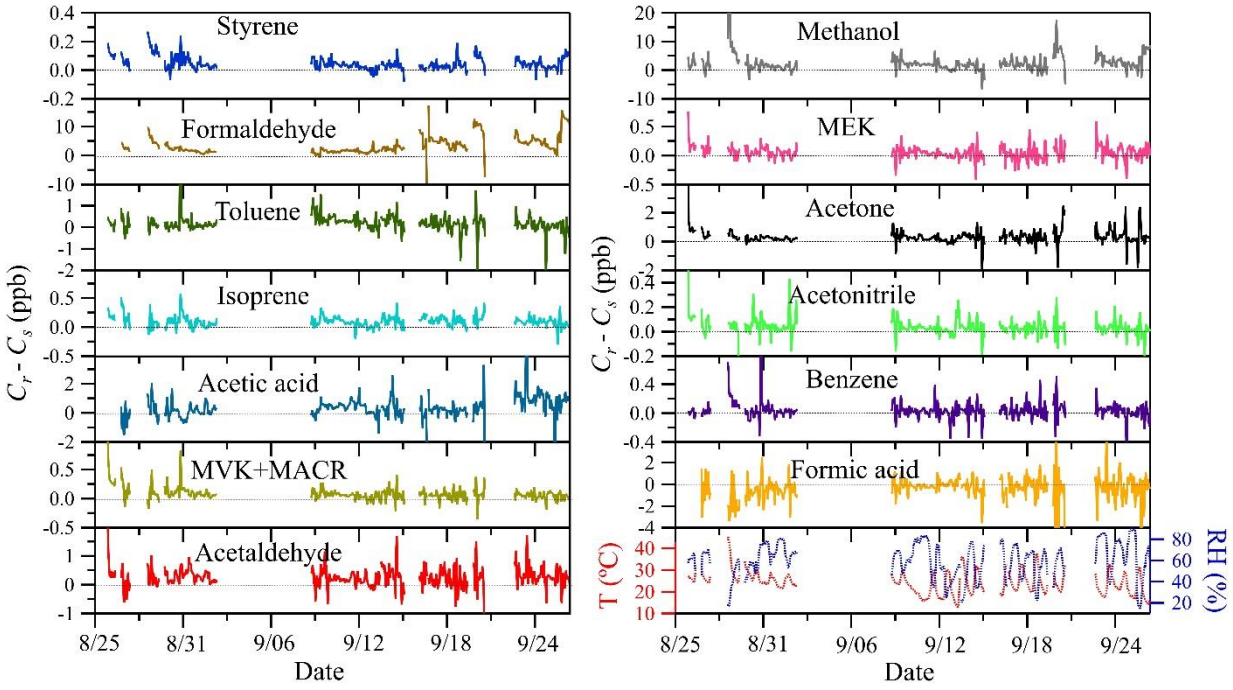

Figure S.2. Time series of the measured VOC mixing ratio differences between the reference channel and the sample channel: $C_r - C_s$. The lines are plotted using hourly averaged data.

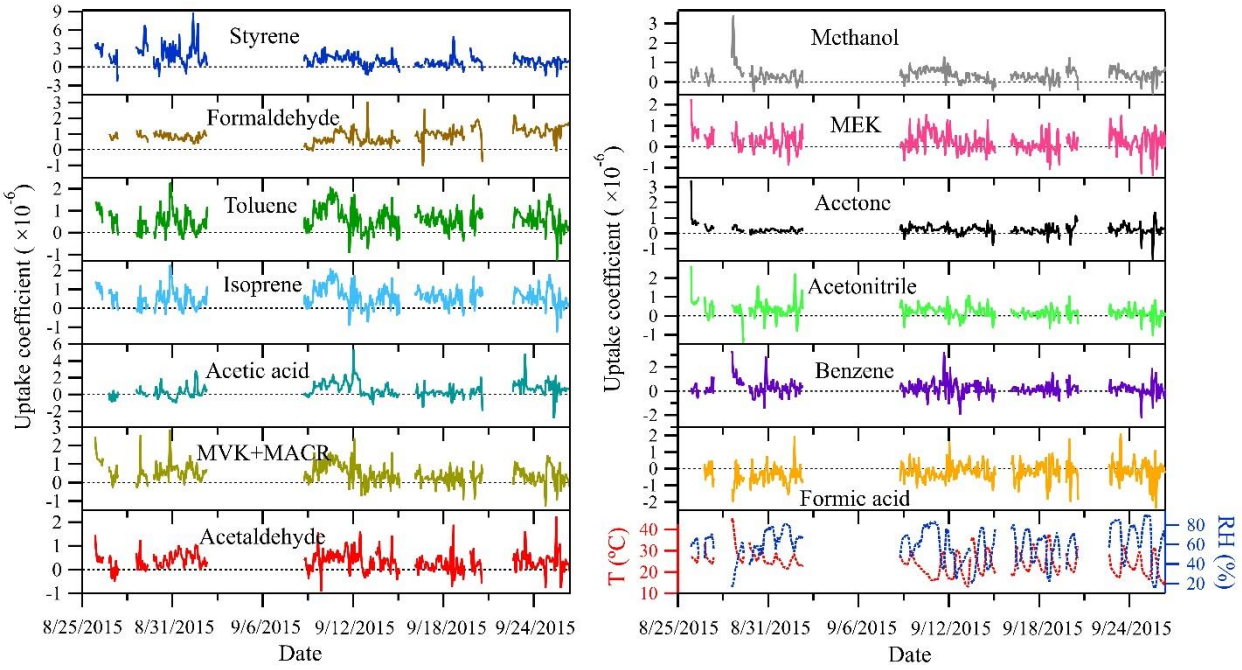

Figure S.3. Time series of the uptake coefficients of measured VOC species. The lines are plotted using hourly averaged data.

5

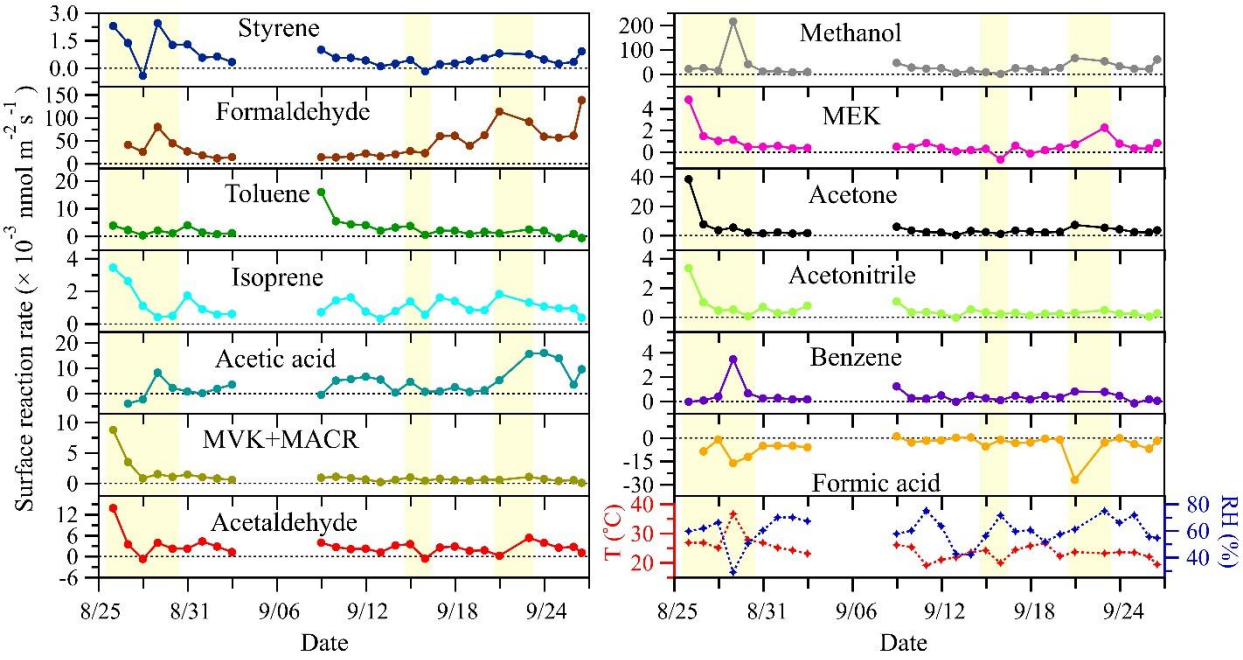

Figure S.4. Time series of the soil surface reaction rate of measured VOC species and air temperature (T) and relative humidity (RH). Each symbol represents daily averaged data and the yellow shaded areas indicate the days when measurements were not continuously running all day long. Positive values mean soil uptake and negative values mean soil emission. At the first three days of the measurement date, the significant decrease of the surface reaction rate for most of the VOC species can be rationalized by combined effect of soil surface adsorption/desorption equilibrium and bulk (soil pores) absorption saturation.

References:

Atkinson, R., and Arey, J.: Atmospheric Degradation of Volatile Organic Compounds, Chemical Reviews, 103, 4605-4638, 10.1021/cr0206420, 2003.

Barratt, M. D.: Quantitative structure-Activity relationships for skin irritation and corrosivity of neutral and electrophilic organic chemicals, Toxicol In Vitro, 10, 247-256, 1996.

Chebbi, A., and Carlier, P.: Carboxylic acids in the troposphere, occurrence, sources, and sinks: A review, Atmospheric Environment, 30, 4233-4249, https://doi.org/10.1016/1352-2310(96)00102-1, 1996.

Dagaut, P., Wallington, T. J., Liu, R., and Kurylo, M. J.: The gas phase reactions of hydroxyl radicals with a series of carboxylic acids over the temperature range 240–440 K, International Journal of Chemical Kinetics, 20, 331-338, doi:10.1002/kin.550200406, 1988.

Harris, G. W., Kleindienst, T. E., and Pitts, J. N.: Rate constants for the reaction of OH radicals with CH3CN, C2H5CN AND CH2CH-CN in the temperature range 298–424 K, Chemical Physics Letters, 80, 479-483, https://doi.org/10.1016/0009-2614(81)85061-0, 1981.

Sander, R.: Compilation of Henry's law constants (version 4.0) for water as solvent, Atmos. Chem. Phys., 15, 4399-4981, 10.5194/acp-15-4399-2015, 2015.

Sangster, J.: Octanol-Water Partition Coefficients of Simple Organic Compounds, Journal of Physical and Chemical Reference Data, 18, 1111-1229, 10.1063/1.555833, 1989.

B.3 Li *et al.*, Atmos. Chem. Phys., 2018

Technical note: Influence of surface roughness and local turbulence on coated-wall flow tube experiments for gas uptake and kinetic studies

Guo Li[1,4], Hang Su[2, 1], Uwe Kuhn[1], Hannah Meusel[1], Markus Ammann[3], Min Shao[2,4], Ulrich Pöschl[1], Yafang Cheng[1,2]

[1]Multiphase Chemistry Department, Max Planck Institute for Chemistry, Mainz, Germany

[2]Institute for Environmental and Climate Research, Jinan University, Guangzhou, China

[3]Laboratory of Environmental Chemistry, Paul Scherrer Institute, 5232 Villigen, Switzerland

[4]College of Environmental Sciences and Engineering, Peking University, Beijing, China

Correspondence to: Y. Cheng (yafang.cheng@mpic.de) and H. Su (h.su@mpic.de)

Atmospheric Chemistry and Physics, 2018

DOI: 10.5194/acp-18-2669-2018

Author contributions:

YC and HS designed the research.

GL, YC, HS, UP developed the methods.

GL, YC, HS, UP, UK, MA, MS discussed the results.

GL, YC, HS wrote the paper with inputs from all coauthors.

Atmos. Chem. Phys., 18, 2669–2686, 2018
https://doi.org/10.5194/acp-18-2669-2018

Atmospheric Chemistry and Physics
Open Access
EGU

Technical note: Influence of surface roughness and local turbulence on coated-wall flow tube experiments for gas uptake and kinetic studies

Guo Li[1,4], Hang Su[2,1], Uwe Kuhn[1], Hannah Meusel[1], Markus Ammann[3], Min Shao[2,4], Ulrich Pöschl[1], and Yafang Cheng[1,2]

[1]Multiphase Chemistry Department, Max Planck Institute for Chemistry, Mainz, Germany
[2]Institute for Environmental and Climate Research, Jinan University, Guangzhou, China
[3]Laboratory of Environmental Chemistry, Paul Scherrer Institute, Villigen, Switzerland
[4]College of Environmental Sciences and Engineering, Peking University, Beijing, China

Correspondence: Yafang Cheng (yafang.cheng@mpic.de) and Hang Su (h.su@mpic.de)

Received: 12 March 2017 – Discussion started: 28 April 2017
Revised: 21 January 2018 – Accepted: 23 January 2018 – Published: 23 February 2018

Abstract. Coated-wall flow tube reactors are frequently used to investigate gas uptake and heterogeneous or multiphase reaction kinetics under laminar flow conditions. Coating surface roughness may potentially distort the laminar flow pattern, induce turbulence and introduce uncertainties in the calculated uptake coefficient based on molecular diffusion assumptions (e.g., Brown/Cooney–Kim–Davis (CKD)/Knopf–Pöschl–Shiraiwa (KPS) methods), which has not been fully resolved in earlier studies. Here, we investigate the influence of surface roughness and local turbulence on coated-wall flow tube experiments for gas uptake and kinetic studies. According to laminar boundary theory and considering the specific flow conditions in a coated-wall flow tube, we derive and propose a critical height δ_c to evaluate turbulence effects in the design and analysis of coated-wall flow tube experiments. If a geometric coating thickness δ_g is larger than δ_c, the roughness elements of the coating may cause local turbulence and result in overestimation of the real uptake coefficient (γ). We further develop modified CKD/KPS methods (i.e., CKD-LT/KPS-LT) to account for roughness-induced local turbulence effects. By combination of the original methods and their modified versions, the maximum error range of γ_{CKD} (derived with the CKD method) or γ_{KPS} (derived with the KPS method) can be quantified and finally γ can be constrained. When turbulence is generated, γ_{CKD} or γ_{KPS} can bear large difference compared to γ. Their difference becomes smaller for gas reactants with lower uptake (i.e., smaller γ) and/or for a smaller ratio of the geometric coating thickness to the flow tube radius (δ_g / R_0). On the other hand, the critical height δ_c can also be adjusted by optimizing flow tube configurations and operating conditions (i.e., tube diameter, length, and flow velocity), to ensure not only unaffected laminar flow patterns but also other specific requirements for an individual flow tube experiment. We use coating thickness values from previous coated-wall flow tube studies to assess potential roughness effects using the δ_c criterion. In most studies, the coating thickness was sufficiently small to avoid complications, but some may have been influenced by surface roughness and local turbulence effects.

1 Motivation

Coated-wall flow tube reactors have been extensively employed for investigations of uptake and reaction kinetics of gases with reactive liquid/semisolid/solid surfaces (Howard, 1979; Kolb et al., 2010). To simulate various heterogeneous or multiphase reactions relevant to atmospheric chemistry, these coated reactive surfaces can span a broad scale including aqueous inorganic acids (Jayne et al., 1997; Pöschl et al., 1998), inorganic salts (Davies and Cox, 1998; Chu et al., 2002; Qiu et al., 2011), organic acids and sugars (Shiraiwa et al., 2012; Steimer et al., 2015), proteins (Shiraiwa et al., 2011), soot (McCabe and Abbatt, 2009; Khalizov et al., 2010; Monge et al., 2010), mineral dust (El Zein and Bed-

janian, 2012; Bedjanian et al., 2013), ice (Fernandez et al., 2005; McNeill et al., 2006; Petitjean et al., 2009; Symington et al., 2012; Hynes et al., 2001, 2002; Bartels-Rausch et al., 2005), and soils (Stemmler et al., 2006; Wang et al., 2012; Donaldson et al., 2014a, b; VandenBoer et al., 2015; Li et al., 2016). Reactive uptake kinetics to a condensed phase material are normally described in terms of the uptake coefficient, γ, which represents the net loss rate of a gas reactant at the surface normalized to its gas kinetic collision rate. Due to uptake or chemical reactions of gases at the walls, radial concentration gradients can develop in the tube and radial diffusion can limit the observed gas uptake. The most commonly utilized methods for evaluating and correcting gas diffusion effects in flow tube studies include the numerical methods of Brown (Brown, 1978) and Cooney–Kim–Davis (CKD, Cooney et al., 1974; Murphy and Fahey, 1987; Davis, 1973), and the recently developed analytical Knopf–Pöschl–Shiraiwa method (KPS, Knopf et al., 2015). All of these methods are derived based on the assumptions that loss at the walls occurs through a first-order process (characterized by γ) and that the gas flow in flow tubes is a well-developed laminar flow. The second assumption ensures that the flow velocity profile is parabolic and that the radial transport of the gas reactant is solely caused by molecular diffusion.

It is well known that the flow conditions in a tube depend on the Reynolds number, Re (Eq. 1),

$$Re = \frac{\rho \times V_{\mathrm{avg}} \times d}{\mu} = \frac{V_{\mathrm{avg}} \times d}{\nu}, \quad (1)$$

where ρ is density of the fluid passing through the tube, V_{avg} is average velocity of the fluid (i.e., the volumetric flow rate divided by the cross-sectional area of the tube), d is diameter of the tube, and μ and ν are dynamic viscosity and kinematic viscosity of the fluid, respectively. A laminar flow can be expected when Re is less than ~ 2000 (Murphy and Fahey, 1987; Knopf et al., 2015). Here, the expression of Re quantifies the nature of the fluid itself (i.e., ρ, V_{avg}, μ and ν) and the tube geometry (i.e., d), but it does not account for the effects of surface roughness. For a list of abbreviations and symbols used in the context, see Appendix A.

Surface roughness effects on flow conditions were firstly discussed by Nikuradse (1950). Based on his work, the Moody diagram has been extensively used in industry to predict the effects of surface roughness (roughness height δ_{r} or relative roughness δ_{r}/d) on flow characteristics (in terms of friction factor). According to the Moody chart, when the surface roughness is small enough (i.e., $\delta_{\mathrm{r}}/d \leq 5\,\%$), the roughness effects within the low Reynolds number regime ($Re < 2000$, characteristic of laminar flow) are negligible. Recent experimental and theoretical studies, however, have found significant effects of surface roughness on laminar flow characteristics (fraction factor, pressure drop, critical Reynolds number and heat transfer, etc.) in microchannels and pipes even under conditions of $\delta_{\mathrm{r}}/d \leq 5\,\%$ (Herwig et al., 2008; Zhang et al., 2010; Zhou and Yao, 2011; Gloss and Herwig, 2010). This is because not only the ratio of δ_{r} and d but also other factors, such as shape of roughness elements (Herwig et al., 2008; Zhang et al., 2010) and spacing between different roughness elements (Zhang et al., 2010), may determine the influence of surface roughness on the flow conditions.

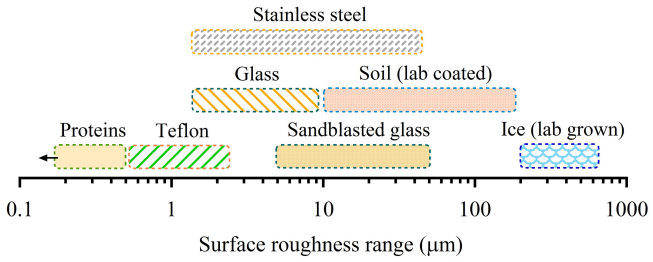

Figure 1. Typical surface roughness for materials commonly used in flow tube gas uptake and kinetic experiments. Data sources are https://neutrium.net/fluid_flow/absolute-roughness/ and http://www.edstech.com/design-tools.html. The soil roughness refers to Li et al. (2016) and the ice roughness refers to Onstott et al. (2013) and Landy et al. (2015).

Moreover, compared to the rough pipe surfaces commonly dealt with in industry (with $0 \leq \delta_{\mathrm{r}} \leq 50\,\mu\mathrm{m}$; see http://mdmetric.com/tech/surfruff.htm), the surfaces used in atmospherically relevant flow tube studies are with much larger surface roughness (e.g., inorganic salts, organic acids and proteins, soot, mineral dust, ice and soils, with $0 \leq \delta_{\mathrm{r}} \leq \sim 650\,\mu\mathrm{m}$; see Fig. 1), and the roughness of these surfaces is sometimes beyond the criterion of $\delta_{\mathrm{r}}/d \leq \sim 5\,\%$. The reported specific surface areas of these coatings span a wide range from ~ 20 to $\sim 100\,\mathrm{m^2\,g^{-1}}$ with a coated film thickness scale from tens of micrometers to several hundreds of micrometers (Davies and Cox, 1998; Chu et al., 2002; McCabe and Abbatt, 2009; Khalizov et al., 2010; El Zein and Bedjanian, 2012; Bedjanian et al., 2013; Shiraiwa et al., 2012; Wang et al., 2012; Donaldson et al., 2014a, b; VandenBoer et al., 2015). These geometrical characteristics indicate considerable porosity in the coating layer and significant roughness on their surfaces.

Although the surface roughness effects can be potentially important, there has been a long-lasting debate on whether the coating surface roughness could disturb the fully developed laminar flow in flow tube kinetic experiments (Taylor et al., 2006; Herwig et al., 2008), and its effects were usually not well quantified in most of the previous gas uptake and/or kinetic studies (Davies and Cox, 1998; Chu et al., 2002; McCabe and Abbatt, 2009; Khalizov et al., 2010; El Zein and Bedjanian, 2012; Bedjanian et al., 2013; Shiraiwa et al., 2012; Wang et al., 2012; Donaldson et al., 2014a, b; VandenBoer et al., 2015; Li et al., 2016). It is, however, conceivable that as the roughness of the coating surfaces increases it would eventually distort the steady laminar regime

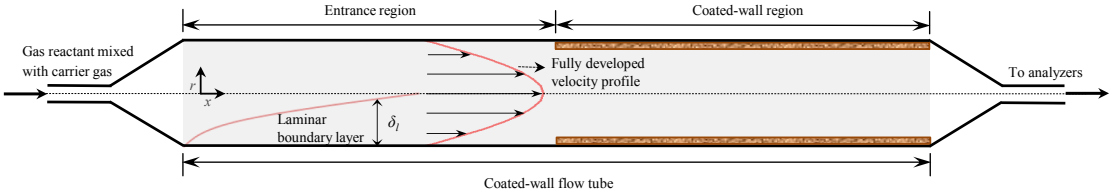

Figure 2. Development of laminar boundary layer and flow velocity profile within the coated-wall flow tube used for soil uptake experiments ($d = 7$ mm, $L = 250$ mm; Li et al., 2016).

near tube walls, and small-scale eddies would evolve from roughness elements. These roughness-induced eddies will give rise to local turbulence and hence corrupt the application of Brown/CKD/KPS methods for the correction of gas molecular diffusion effects and the determination of the uptake coefficient. The extent of these effects may depend on the coated film thickness and its surface roughness. It means that the roughness effects on flow conditions to a great extent rely on the various coating techniques applied by different operators, leading to disagreement of the experimental results.

In the present study, the surface roughness effects on laminar flow are quantitatively examined. In view of the special laminar boundary layer structure in flow tubes, we employ a critical height δ_c, which defines the smallest scale within which local turbulence can occur (i.e., for scales smaller than δ_c, local turbulence cannot exist; see Kolmogorov, 1991), to evaluate the influence of surface roughness on laminar flow patterns. By taking it into account in flow tube experimental design, it is feasible to satisfy the preconditions of merely radial molecular diffusion of gas reactants and therefore validate the application of Brown/CKD/KPS methods. The δ_c criterion provides an easy way of assessing and optimizing different flow tube configurations and operating conditions (tube diameter, tube length, flow velocity, coating thickness, etc.) with regard to (1) the applicability and validity of diffusion correction methods, and (2) the specific requirements of an individual flow tube experiment design. To illustrate the applicability of the δ_c criterion, we analyze and assess previous coated-wall flow tube studies with regard to potential roughness effects. Moreover, we develop modified CKD/KPS methods accounting for the maximum impact of local turbulence (CKD-LT/KPS-LT) to assess how much the real uptake coefficient may deviate from the value obtained with the original CKD/KPS methods assuming purely molecular diffusion.

2 Methods

2.1 Influence of surface roughness on laminar flow

According to the proverbial boundary layer theory proposed by Prandtl (1904), when a fluid (normally a gas mixture, a gas reactant mixed with a carrier gas, in uptake kinetic studies) enters the inlet of a flow tube with a uniform velocity, a laminar boundary layer (i.e., velocity boundary layer) will form very close to the tube wall (Fig. 2). This buildup of laminar boundary layer is because of the non-slip condition of the tube wall and the viscosity of the fluid; that is, viscous shearing forces between fluid layers are felt and dominant within the laminar boundary layer (Mauri, 2015). The thickness of laminar boundary layer δ_l will continuously increase in the flow direction (axial direction in Fig. 2) until at a distance (from the tube entrance) where the boundary layers merge. Beyond this distance, the tube flow is entirely viscous, and the axial velocity adjusts slightly further until the velocity along the axial direction does not change anymore. Then, a fully developed parabolic velocity profile is formed, characteristic of well-developed laminar flow (Mohanty and Asthana, 1979; White, 1998). The development and formation of this velocity profile are illustrated in Fig. 2. Normally, for coated-wall flow tube experiments, a chemically inert entrance region with smooth surface is designed to ensure the development of laminar flow before the reactive gas enters into the coated-wall region.

As demonstrated in previous studies using microchannels and pipes (Herwig et al., 2008; Gloss and Herwig, 2010; Zhang et al., 2010; Zhou and Yao, 2011), the roughness elements on flow tube coatings can have non-ignorable effects on laminar flow conditions even if these coatings are entirely submerged into the laminar boundary layer. In other words, the disturbance on well-developed laminar flow patterns can be artificially achieved by roughness elements of the tube coating. However, there is a critical height δ_c within which the roughness effects can become ignorable (Achdou et al., 1998).

Figure 3 shows a schematic of the structure of the δ_c and its related flow conditions in a coated-wall flow tube. When a roughness height δ_r (here in Fig. 3, the roughness height δ_r equates to the geometric coating thickness δ_g; see Sect. 2.3 for explanation) comes into the critical height δ_c where viscous effects overwhelmingly dominate, the flow very near the rough wall will tend to be Stokes-like or creeping, denoted as the laminar flow (LF) regime in Fig. 3a. This Stokes-like flow adjacent to the rough surfaces can avoid local turbulence between the roughness elements and guarantee perfect lam-

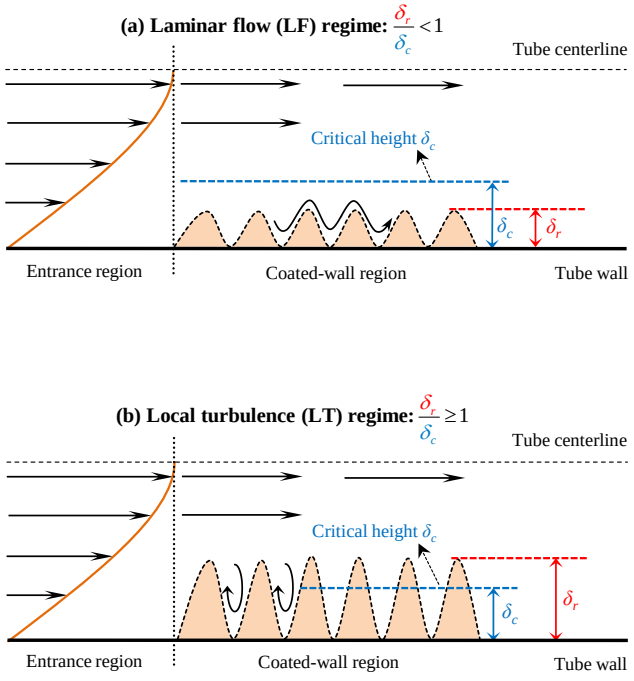

Figure 3. Schematic of the critical height δ_c and its related flow conditions in a flow tube with rough coatings. Upstream of the coated-wall region, the entrance region is designed to warrant well-developed laminar flow conditions. Two cases of tube coatings reflect different impacts of a roughness element with varying height δ_r on flow patterns.

inar flow conditions (i.e., only molecular diffusional transport of gas reactants to rough reactive coatings) throughout the whole flow tube volume. Thus, the LF regime satisfies the prerequisite for the diffusion correction methods used for flow tube experiments, i.e., $\delta_r / \delta_c < 1$. Nevertheless, when a roughness height is larger than the critical height δ_c, local eddies may occur in the spaces between the neighboring roughness elements (i.e., the local turbulence (LT) regime in Fig. 3b). Local turbulence induced by these roughness elements will enhance local transport of air masses within the scales of the roughness heights, which invalidates the assumption of solely molecular diffusion of gas reactants and therefore the application of diffusion correction methods for the determination of γ (Brown, 1978; Murphy and Fahey, 1987; Knopf et al., 2015). In the next section, we will show how to derive δ_c.

2.2 δ_c derivation

Achdou et al. (1998) proposed effective boundary conditions for a laminar flow over a rough wall with periodic roughness elements and observed that when $\delta_r/L_c < Re^{-1/2}$ (δ_r: roughness height; L_c: characteristic length, for a tube the characteristic length $L_c = d$) the roughness elements could be contained in the boundary layer. This means that, for their case, the boundary layer thickness is in the order of $L_c Re^{-1/2}$. Within the boundary layer, they found that local turbulence could occur between the roughness elements until $\delta_r/L_c < Re^{-3/4}$, where the viscous effects became dominated in roughness elements and then the flow near the rough wall tended to be creeping. This result coincides with Kolmogorov's theory (Kolmogorov, 1991), in which the critical length ratios between small-scale and large-scale eddies are also in the order of $Re^{-3/4}$, even though this theory only applies to turbulent flow with large Reynolds numbers. Here, we adopt this criterion to judge if local eddies could occur in the spaces between neighboring roughness elements. Thus, the critical height δ_c can be expressed as

$$\delta_c = d \times Re^{-3/4} = d^{1/4} \times \left(\frac{V_{avg}}{\nu}\right)^{-3/4}, \quad (2)$$

where d is diameter of the flow tube, Re is the Reynolds number, and V_{avg} and ν are average velocity and kinematic viscosity of the fluid, respectively.

With Eq. (2), for a specified experiment configuration (i.e., flow tube diameter, flow velocity, and fluid properties) the critical height δ_c can be determined, and therefore the effects of coating roughness on laminar flow can be estimated provided the roughness height δ_r is known.

2.3 Error estimation with modified CKD/KPS methods

The potential effects of coating roughness on laminar flow are described and classified into two regimes in Fig. 3 (Sect. 2.1), in which only the LF regime provides the ideal precondition ensuring that the diffusion correction methods (Brown/CKD/KPS methods) can be applied to obtain accurate γ through flow tube experiments. Regarding the LT regime, however, the roughness-induced effects can be quantitatively simulated, because local turbulence is constrained into the scale of the roughness height δ_r (Oke et al., 2017).

Hence, for the LT regime, in order to estimate the potential error of the uptake coefficient derived from molecular diffusion correction using the conventional CKD/KPS methods, we further develop modified CKD/KPS methods (denoted as CKD-LT/KPS-LT, illustrated in Fig. 4) to account for local turbulence impact. In the CKD-LT/KPS-LT methods, some basic assumptions are made: (1) the scale of a roughness element is much larger than the size of pores inside the bulk coating, and the macroscopic diffusion inside pores is not the domain of roughness-induced local eddies; (2) half of the surface roughness height is defined as the local-eddy-occurring region (i.e., $0.5\delta_r = R_m - R_g$); (3) the turbulent diffusion coefficient within the local-eddy-occurring region is infinitely large (i.e., the turbulent transport within it is extremely fast). When a coating is smooth, the mass-based coating thickness δ_m is equal to the geometric coating thickness δ_g. In this case, the radial molecular diffusion distance from the tube centerline is R_m, while with large surface roughness height, the radial molecular diffusion distance is reduced to R_g. With

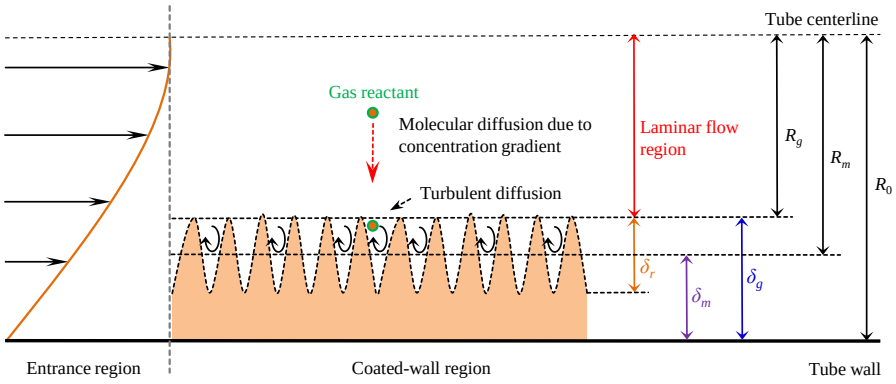

Figure 4. Illustration of the variables used for the CKD-LT and KPS-LT methods: δ_r, roughness height; δ_m, mass-based coating thickness; δ_g, geometric coating thickness; R_g, calculated flow tube radius based on δ_g; R_m, calculated flow tube radius based on δ_m; R_0, flow tube radius without coating.

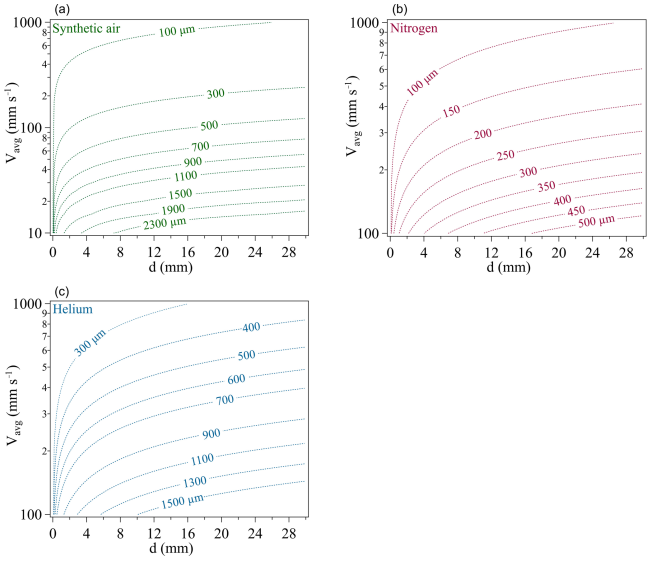

Figure 5. Calculated critical height δ_c (dash-dotted lines) versus varying tube diameter d and flow velocity V_{avg} in flow tube experiments with carrier gases of synthetic air **(a)**, nitrogen **(b)**, and helium **(c)**, respectively.

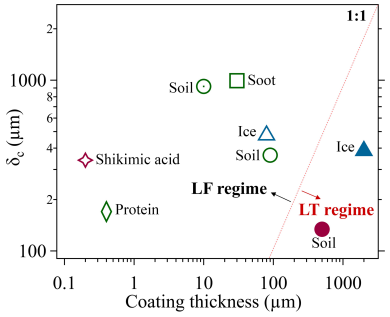

Figure 6. Representative coating thickness in previous coated-wall flow tube studies versus the calculated critical height δ_c (based on their experimentally adopted d and V_{avg}). The color of the symbols indicates the different types of carrier gases employed: synthetic air (green symbols), nitrogen (purple), and helium (blue). References for the coatings summarized here are diamond (Shiraiwa et al., 2011), square (Monge et al., 2010), open circle (Donaldson et al., 2014a, b), open circle with center (Wang et al., 2012), solid circle (Li et al., 2016), star (Steimer et al., 2015), solid triangle (McNeill et al., 2006), and open triangle (Petitjean et al., 2009). LF and LT refer to laminar flow and local turbulence, respectively.

the CKD-LT/KPS-LT methods, derivation of the uptake coefficient using R_g rather than R_m reflects an upper limit for the influence of local turbulence, as the turbulent diffusion coefficient in the local-eddy-occurring region is assumed to be infinitely large and turbulent transport occupies its whole volume. More details about CKD and KPS, and the derivations of γ_{CKD}, γ_{KPS}, γ_{CKD-LT}, and γ_{KPS-LT} can be found in Appendices C–E.

3 Results and discussion

3.1 Design of coated-wall flow tube experiments

The introduction of the critical height δ_c, into the field of gas uptake or reaction kinetic studies using coated-wall flow tubes, provides us the way for determining when the surface roughness effects can be negligible in flow tube experiments. That is, the roughness height δ_r of a coating film should be well within the domain of δ_c (LF regime in Fig. 3a). Only in this case, the free molecular diffusion of a gas reactant in the radial direction can be ascertained, and thus the Brown/CKD/KPS methods can be safely applied. Note that in real operations of flow tube coating design several techniques (stylus profiler, non-contact optical profiler, scan-

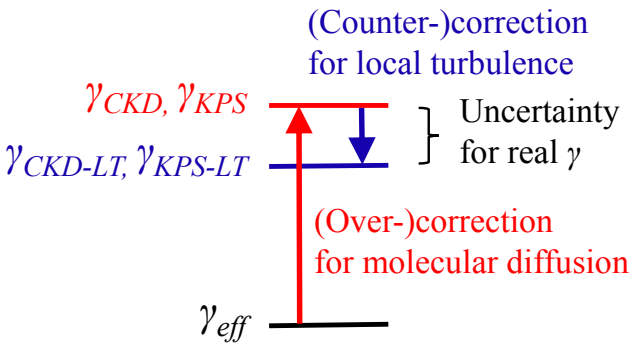

Figure 7. Schematic of different types of uptake coefficients and their divergences due to molecular diffusion and local turbulence effects. The uncertainty of γ is constrained by γ_{CKD} and $\gamma_{CKD\text{-}LT}$, or γ_{KPS} and $\gamma_{KPS\text{-}LT}$. Note that the degree of the divergences among these types of uptake coefficients depends on their magnitude; i.e., for lower uptake coefficient values, no corrections are needed (see Figs. 8 and 9). Similarly, γ_{CKD} and γ_{KPS}, or $\gamma_{CKD\text{-}LT}$ and $\gamma_{KPS\text{-}LT}$, may differ from each other depending on their magnitude (see Figs. 8 and 9, and Appendix C). The abbreviations and symbols are explained in Appendix A.

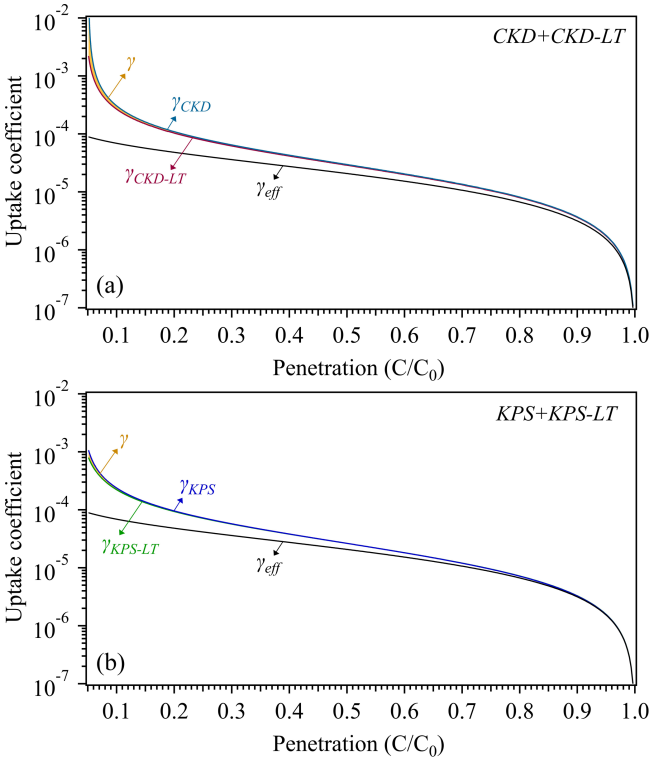

Figure 8. Schematic of different types of uptake coefficients versus the measured penetration (C / C_0), using both diffusion correction methods CKD **(a)** and KPS **(b)** as well as their modified versions, i.e., CKD-LT and KPS-LT, to evaluate roughness-induced local turbulence effects. The yellow shaded area shows the uncertainty range of γ. Derivation of the uptake coefficient is based on the specific experimental parameters in our previous study (Li et al., 2016): gas reactant, HCHO; carrier gas, N_2; volumetric flow rate $F = 1\,\mathrm{L\,min^{-1}}$ at 1 atm and 296 K; flow tube dimension, $d = 7$ mm, $L = 250$ mm. The δ_g and δ_r of the soil coating are estimated using scanning electron microscopy: $\delta_g / R_0 = 0.15$, $\delta_r / \delta_g = 0.2$.

ning electron microscopy and atomic force microscopy, etc.) are available for surface roughness examination (Poon and Bhushan, 1995). To simplify the discussion, here, we take the geometric thickness of a coating film δ_g as a maximum of its surface roughness and use the comparison between δ_g and δ_c as a reference for the design of flow tube coating thickness. Such treatment is more suitable for practical applications, because determination of coating film thicknesses can be simply achieved either by weighing the coating film mass (i.e., mass-based coating thickness δ_m) or by utilizing the scanning electron microscopy technique (i.e., geometric coating thickness δ_g), and the condition of $\delta_g / \delta_c < 1$ can definitely ensure the case of $\delta_r / \delta_c < 1$. As discussed in Sect. 2.3, for coatings with large surface roughness, their δ_g may be significantly larger than δ_m. In this case, the criterion of $\delta_g / \delta_c < 1$ is more appropriate to be adopted.

Figure 5 shows the calculated δ_c, with varying the tube diameter d and the average flow velocity V_{avg}. From Eq. (2), kinematic viscosity of a fluid (carrier gas in flow tubes) will affect δ_c. It is therefore necessary to classify the flow tube experiments according to the types of the utilized carrier gases, such as synthetic air (Fig. 5a), nitrogen (Fig. 5b), and helium (Fig. 5c). For future flow tube coating design, Fig. 5 can be used to eliminate the potential coating surface roughness effects. Figure 6 summarizes and evaluates the potential effects of surface roughness in previous flow tube experiments. To reflect the influence of inherent roughness of the inner surface of a flow tube wall itself, the mean wall roughness is also accounted for coating thickness calculation when using rough-wall flow tubes (e.g., sandblasted tubes), for example, in the protein coating experiment. As shown in Fig. 6, most of the coating thicknesses are well below the calculated values of δ_c (LF regime), implying that their surface roughness effects on laminar flow and on the calculated uptake coefficient are ignorable. A few coating thicknesses, however, are significantly larger than the calculated δ_c (LT regime), as shown by the solid symbols. As the thicknesses of these two coatings are reported in terms of geometric coating thickness δ_g (Li et al., 2016; McNeill et al., 2006), they may have had a potential influence on laminar flow pattern, and local turbulence may have occurred within the roughness-constructed spaces.

For most cases of flow tube experiments design, a coating layer cannot be thin enough due to requirements of reaction kinetics (bulk diffusion and surface reactions can both play important roles), and the thickness of a coating layer had been found to have an influence on gases uptake until a critical threshold was reached (Donaldson et al., 2014a; Li et al., 2016). This means that there is a need to comprehensively

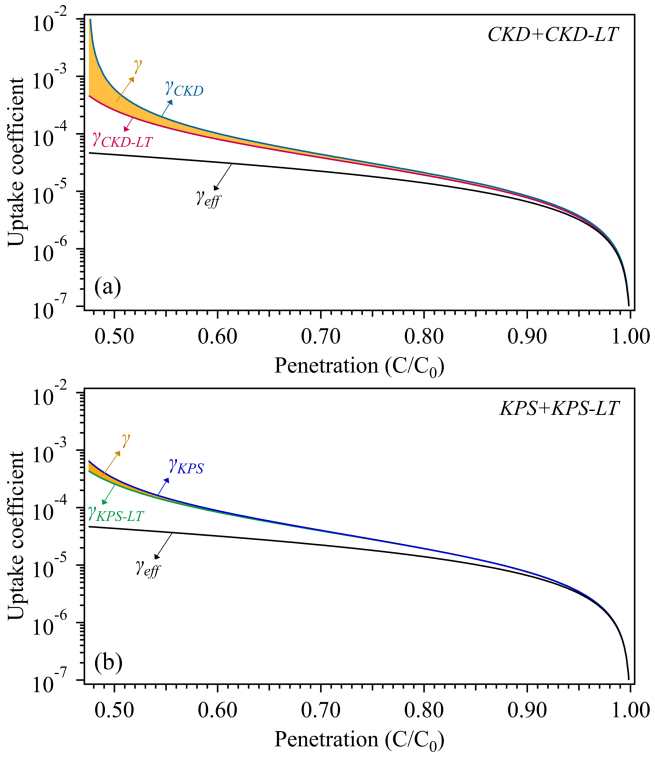

Figure 9. Schematic of different types of uptake coefficients versus the measured penetration (C / C_0), using both diffusion correction methods CKD **(a)** and KPS **(b)** as well as their modified versions, i.e., CKD-LT and KPS-LT, to evaluate roughness-induced local turbulence effects. The yellow shaded area shows the uncertainty range of γ. Derivation of the uptake coefficient is based on the following assumptions: gas reactant, O_3; carrier gas, N_2; volumetric flow rate $F = 5\,\mathrm{L\,min^{-1}}$ at 1 atm and 298 K; flow tube dimension, $d = 22$ mm, $L = 250$ mm. δ_g and δ_r of the coating material are defined by $\delta_g / R_0 = 0.2$, $\delta_r / \delta_g = 0.5$. The choice of 0.5 for δ_r / δ_g represents an extreme rough coating case.

consider all the parameters (coating thickness, tube diameter, tube length, flow velocity, etc.) and a compromise of each parameter for the others is necessary to finally ensure both the unaffected laminar flow conditions and the specific requirements for an individual flow tube design. Larger δ_c would allow a wider range of coating thickness δ_g without surface roughness effects. Based on Eq. (2), larger δ_c can be achieved either by increasing the tube diameter d or by decreasing the fluid average velocity V_{avg}. Under the conditions of fast uptake kinetics, relatively short residence time of gas reactants inside the coated-wall region is needed to allow for distinguishable penetration C/C_0 (i.e., the flow tube outlet concentration divided by the inlet concentration; see Fig. C1 for details). This requirement can be fulfilled by optimizing flow tube design. One can increase d or decrease V_{avg} to achieve larger δ_c, but this operation will inevitably extend the residence time of gas reactants. Then, this effect can be offset by reducing L, which could be easily achieved by adjusting the position of a movable injector inside the flow tube apparatus as in previous studies (Howard, 1979; Jayne et al., 1997; Pöschl et al., 1998; Kolb et al., 2010; VandenBoer et al., 2015).

3.2 Divergences between different types of uptake coefficients due to molecular diffusion and local turbulence effects

Normally, through coated-wall flow tube experiments, a penetration C/C_0 can be measured, and therefore an effective uptake coefficient γ_{eff} can be experimentally determined (see Eq. C1 in Appendix C) under the assumption that the loss process on the wall is first order. As discussed above, without roughness-induced local turbulence, the radial concentration gradient can give rise to molecular diffusion limitations of the gas reactant, which need to be corrected using the diffusion correction methods (i.e., Brown/CKD/KPS) to derive the real uptake coefficient γ. Thus, the deviation between γ_{eff} and γ is only caused by molecular diffusion effects under ideal laminar flow conditions (LF regime).

With roughness-induced local turbulence (LT regime), the preconditions of conventional molecular diffusion correction methods can be corrupted. Figure 7 displays a schematic of different types of uptake coefficients and their divergences due to molecular diffusion and local turbulence effects. For the LT regime, the conventional CKD or KPS may cause overcorrection of γ_{eff}, i.e., $\gamma_{CKD} \geq \gamma$ or $\gamma_{KPS} \geq \gamma$ (upper limit indicated in red in Fig. 7). In this case, the derived $\gamma_{CKD\text{-}LT}$ or $\gamma_{KPS\text{-}LT}$ (blue in Fig. 7) using our proposed CKD-LT or KPS-LT methods may serve as a lower limit of γ (see Sect. 2.3 for explanation), thus defining the uncertainty range of γ, as shown in Fig. 7.

To have a general cognition of the quantified divergence among the different types of uptake coefficients, we further present Figs. 8 and 9 as examinations of two specific experimental configurations. Each figure has two panels: Figs. 8a and 9a show the uptake coefficient corrected by the CKD and CKD-LT methods, and Figs. 8b and 9b by the KPS and KPS-LT methods. The derivation of γ_{eff} is based on Eq. (C1). For Fig. 8, the experimental configuration of the soil coating case (Li et al., 2016) in Fig. 6 (solid circle) is used as input parameters for the diffusion correction, while an assumed configuration with higher volumetric flow rate F and larger relative roughness height δ_r / R_0 (see caption for details) is adopted for Fig. 9. As shown in both figures, the uncertainty range of γ can be constrained by γ_{CKD} and $\gamma_{CKD\text{-}LT}$, or γ_{KPS} and $\gamma_{KPS\text{-}LT}$. In general, larger divergence, which corresponds to larger molecular diffusion and/or local turbulence effects, can be found at higher uptake coefficient magnitudes. The experimental configuration used for Fig. 8 results in a smaller difference of γ_{CKD} against $\gamma_{CKD\text{-}LT}$ and γ_{KPS} against $\gamma_{KPS\text{-}LT}$ than that for Fig. 9. This indicates that, for experiment design with rough coating, higher volumetric flow rate and/or larger relative roughness height will make the coating

surface roughness effects more prominent. The higher values of the uptake coefficient derived using CKD and CKD-LT than those using KPS and KPS-LT, respectively, can be due to the different algorithms employed for CKD and KPS (see Appendix C). At last, it should be noted that the whole discussion about surface roughness and the way the different diffusion correction methods are applied are linked to the assumption that first-order reaction kinetics are granted, as mentioned upfront.

4 Conclusions

In this study, a new criterion is proposed to eliminate/minimize the potential effects of coating surface roughness on laminar flow in coated-wall flow tube experiments. Employment of this criterion in future flow tube experiments design can validate the application of conventional diffusion correction methods for uptake coefficient calculations. While keeping a coating film thickness well within the critical height δ_c to exclude potential surface roughness effects, flexible coated-wall flow tube design can also be achieved. For example, one can increase δ_c by adjusting flow tube geometric parameters (i.e., tube diameter and tube length) or flow velocity V_{avg} to ensure not only an unaffected laminar flow pattern but also a situation-suitable residence time in flow tube reactors. We illustrate the application of this new criterion for previous investigations and demonstrate its effectiveness in optimizing flow tube design and consolidating kinetic experimental results. Moreover, based on the CKD/KPS methods, their modified versions (CKD-LT/KPS-LT) are proposed. The combinations of CKD/KPS and their modified versions can be used to quantify the maximum error of the calculated uptake coefficient (γ_{CKD} or γ_{KPS}) when roughness-induced local turbulence occurs, and the real uptake coefficient γ can be finally constrained by γ_{CKD} and $\gamma_{CKD\text{-}LT}$ (or γ_{KPS} and $\gamma_{KPS\text{-}LT}$).

Data availability. The Matlab code for CKD and CKD-LT is provided in Appendix E. The underlying research data can be accessed by contacting Yafang Cheng (yafang.cheng@mpic.de), Hang Su (h.su@mpic.de), or Guo Li (guo.li@mpic.de).

Appendix A: List of abbreviations and symbols

CKD	Cooney–Kim–Davis method for molecular diffusion correction (numerical solution)
CKD-LT	a modified CKD method to account for roughness-induced local turbulence effects
KPS	Knopf–Pöschl–Shiraiwa method for molecular diffusion correction (analytical approximation)
KPS-LT	a modified KPS method to account for roughness-induced local turbulence effects
γ	real uptake coefficient
γ_{CKD}	uptake coefficient derived using the CKD method
$\gamma_{\mathrm{CKD\text{-}LT}}$	uptake coefficient derived using the CKD-LT method
γ_{KPS}	uptake coefficient derived using the KPS method
$\gamma_{\mathrm{KPS\text{-}LT}}$	uptake coefficient derived using the KPS-LT method
γ_{eff}	experimentally determined effective uptake coefficient
Re	Reynolds number
ρ	density of the fluid passing through the flow tube
F	volumetric flow rate
V_{avg}	average velocity of the fluid (i.e., the volumetric flow rate divided by the cross-sectional area of the flow tube)
d	inner diameter of the coated-wall flow tube
μ	dynamic viscosity of the fluid
ν	kinematic viscosity of the fluid
δ_{r}	roughness height
δ_{l}	thickness of the laminar boundary layer
δ_{c}	critical height calculated using Eq. (2)
δ_{g}	geometric coating thickness
δ_{m}	mass-based coating thickness
L_{c}	characteristic length
L	coated-wall region length
R_0	flow tube radius without coating
R_{m}	flow tube radius calculated using δ_{m} (i.e., $R_{\mathrm{m}} = R_0 - \delta_{\mathrm{m}}$)
R_{g}	flow tube radius calculated using δ_{g} (i.e., $R_{\mathrm{g}} = R_0 - \delta_{\mathrm{g}}$)
LF regime	laminar flow regime shown in Figs. 3a and 6
LT regime	local turbulence regime shown in Figs. 3b and 6
C	gas reactant concentration at the flow tube outlet
C_0	gas reactant concentration at the flow tube inlet
C/C_0	penetration
$1 - C/C_0$	fractional loss
ω	mean molecular speed of the gas reactant
t	interaction time between the gas reactant and the coated wall (i.e., residence time)
$N_{\mathrm{Shw}}^{\mathrm{eff}}$	effective Sherwood number
Kn	Knudsen number
z^*	dimensionless axial distance
D	gas diffusion coefficient of the gas reactant
λ	mean free path of the gas reactant
C_{CKD}/C_0	penetration in the CKD generated table ($\mathrm{Table}_{\mathrm{CKD}}$)
$\gamma_{\mathrm{CKD},n}$	uptake coefficient in the CKD generated table ($\mathrm{Table}_{\mathrm{CKD}}$)
$(C_{\mathrm{CKD}}/C_0)_j$	penetration at the jth row in table ($\mathrm{Table}_{\mathrm{CKD}}$)
$\gamma_{\mathrm{CKD},j}$	uptake coefficient at the jth row in table ($\mathrm{Table}_{\mathrm{CKD}}$)
$C_{\mathrm{CKD-LT}}/C_0$	penetration in the CKD-LT generated table ($\mathrm{Table}_{\mathrm{CKD\text{-}LT}}$)
$\gamma_{\mathrm{CKD-LT},n}$	uptake coefficient in the CKD-LT generated table ($\mathrm{Table}_{\mathrm{CKD\text{-}LT}}$)
$(C_{\mathrm{CKD-LT}}/C_0)_k$	penetration at the kth row in table ($\mathrm{Table}_{\mathrm{CKD\text{-}LT}}$)
$\gamma_{\mathrm{CKD-LT},k}$	uptake coefficient at the kth row in table ($\mathrm{Table}_{\mathrm{CKD\text{-}LT}}$)

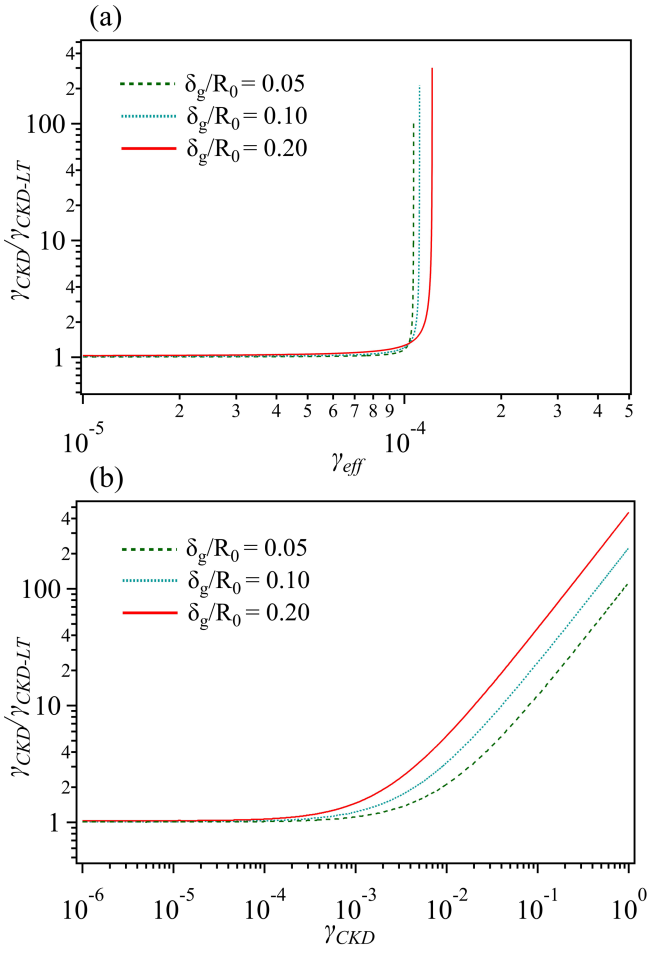

Figure B1. Maximum error of the CKD derived uptake coefficient (γ_{CKD}) relative to the CKD-LT derived uptake coefficient ($\gamma_{CKD\text{-}LT}$) versus changing γ_{eff} **(a)** and γ_{CKD} **(b)** for three cases with different ratio of the geometric coating thickness to tube radius (δ_g/R_0). For derivation of this plot, the specific experimental configuration includes gas reactant, O_3; carrier gas, N_2; volumetric flow rate $F = 1\,\mathrm{L\,min^{-1}}$ at 1 atm and 298 K; flow tube dimension, $d = 7$ mm, $L = 250$ mm. The choices of δ_g / R_0 cover the general ratio range in previous studies. The curves cannot be further extended due to reaching the limits of diffusion correction methods (see Appendix C).

Appendix B: Wall-roughness-induced error of γ_{CKD} in the LT regime: for previous flow tube studies

Local turbulence caused by rough surface coatings may introduce errors in the uptake coefficient derived from the Brown/CKD/KPS methods (e.g., calculated uptake coefficient γ_{CKD} or γ_{KPS} illustrated in Fig. 7). We show here an example illuminating how this error estimation can be accomplished by means of simulation under the predefined experimental configurations.

Figure B1 shows the maximum errors of γ_{CKD} as a function of varying γ_{eff} (Fig. B1a) and γ_{CKD} (Fig. B1b). There, three different cases of δ_g/R_0 are presented with all the other experimental configurations kept the same (see figure caption). For higher δ_g/R_0, the errors of γ_{CKD} are also larger, indicating that a thick and rough coating will generate more local turbulence and therefore have larger effects on derived uptake coefficients using the conventional molecular diffusion correction methods. Meanwhile, the errors are also closely related to the magnitude of γ_{CKD} and γ_{eff}: when they are smaller than10^{-4} the errors are inconspicuous, but beyond 10^{-4} the errors are apparent and considerably increase. The sharp increase of the error in Fig. B1a is due to the fact that there is a region where γ_{CKD} is very sensitive to variations of the measured penetration C/C_0 as γ_{CKD} gets close to 1 (i.e., the non-ideal region in Fig. C1). Compared to molecular diffusion, the roughness-induced turbulent transport may result in a lower C/C_0 which corresponds to a significant error of γ_{CKD}. In previous flow tube studies where local turbulence could not be avoided (LT regime), Fig. B1 can be used to estimate the potential maximum errors of the calculated γ_{CKD}. In order to guide flow tube designers to estimate the potential errors of their derived high uptake coefficient using our method, a tutorial derivation procedure for $\gamma_{CKD}/\gamma_{CKD\text{-}LT}$ versus γ_{CKD} or γ_{eff} is further presented in Appendix D.

Appendix C: Comparison between KPS and CKD

The KPS method is a recently developed analytical approximation method. The derivation of KPS is based on kinetic flux model framework and models describing interactions of gas species with aerosols in combination with the diffusion limitation theory for gas and particle uptake on a tube wall (Knopf et al., 2015, and references therein). This approximation method circumvents the complex operation procedures of previous numerical methods (e.g., the Brown and CKD methods) and therefore can be applied in a simpler way. As analyzed in KPS, the effective uptake coefficient γ_{eff} can be experimentally determined as (Knopf et al., 2015)

$$\gamma_{eff} = \frac{d}{\omega \times t} \ln\left(\frac{C_0}{C}\right), \tag{C1}$$

where d is flow tube diameter, ω is mean molecular speed of the gas reactant, t is residence time of the gas reactant within the coated-wall region, and C_0 and C are gas reactant concentration at the flow tube inlet and outlet, respectively. After correction for gas molecular diffusion effects, the real uptake coefficient γ is derived as

$$\gamma = \frac{\gamma_{eff}}{1 - \gamma_{eff}\frac{3}{2N_{Shw}^{eff} \times Kn}}, \tag{C2}$$

in which N_{Shw}^{eff} is the effective Sherwood number and Kn is the Knudsen number, which can be expressed, respectively,

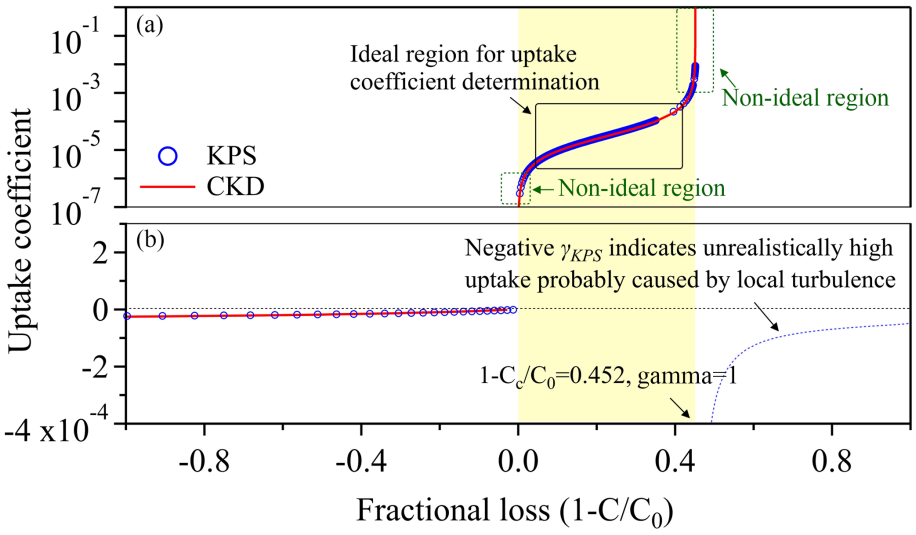

Figure C1. Comparisons between uptake coefficients (derived from KPS and CKD methods, respectively) versus the fractional loss. Panel **(a)** displays the derived positive uptake coefficients under the LF regime, and **(b)** the derived negative ones due to emission (left) or local turbulence effect (right). For derivation of this plot, the specific experimental configuration includes gas reactant, SO_2; carrier gas, synthetic air; volumetric flow rate $F = 4\,\mathrm{L\,min^{-1}}$ at 1 atm and 296 K; flow tube dimension, $d = 17$ mm, $L = 200$ mm.

as

$$N_{\mathrm{Shw}}^{\mathrm{eff}} = 3.6568 + \frac{0.0978}{z^* + 0.0154} \text{ with } z^* = L \times (\frac{\pi}{2}) \times \left(\frac{D}{F}\right), \quad \text{(C3)}$$

$$Kn = \frac{2\lambda}{d} \text{ with } \lambda = \frac{3D}{\omega}, \quad \text{(C4)}$$

where z^* is dimensionless axial distance, L is length of the coated-wall region, D is molecular diffusion coefficient of the gas reactant within the carrier gas at experimental conditions, F is volumetric flow rate of the fluid, and λ is mean free path of the gas reactant.

The CKD method in the present study is based on directly solving the differential equation, which is provided by Murphy and Fahey (1987) and used for description of the gas reactant concentration as a function of axial and radial position in a flow tube. Thus, this CKD method can possess higher accuracy than the previously used CKD interpolation method or the KPS method (Knopf et al., 2015; Li et al., 2016).

As shown in Fig. C1, with ideal laminar flow (i.e., without any local turbulence, LF regime) the KPS and CKD show perfect agreement for the derived uptake coefficient in the fractional loss range of 0.452 to 1 (shaded area in Fig. C1a). Due to the different algorithms employed, however, the CKD method (Murphy and Fahey, 1987; Cooney et al., 1974; Davis, 1973; Li et al., 2016) and the KPS method (Knopf et al., 2015) could derive contrasting uptake coefficient values when local turbulence occurs. If a fractional loss is larger than the critical fractional loss value (i.e., $1 - C/C_0 > 0.452$, in Fig. C1b), e.g., because of enhanced mass transport towards the coated wall due to local turbulence, the KPS results in a negative uptake coefficient (blue dashed line in Fig. C1) while the CKD has no solution. From Eq. (C1), it can be found that an unrealistically high fractional loss can lead to a high γ_{eff}, which may cause a negative denominator in Eq. (C2) and therefore a derived negative uptake coefficient. For a fractional loss value smaller than 0, both methods derive negative uptake coefficients implying emissions of gas reactants from the coating (i.e., $C/C_0 > 1$, in Fig. C1b).

Appendix D: Derivation procedure of $\gamma_{\mathrm{CKD}}/\gamma_{\mathrm{CKD\text{-}LT}}$ versus γ_{CKD} or γ_{eff}

Derivation of $\gamma_{\mathrm{CKD}}/\gamma_{\mathrm{CKD\text{-}LT}}$ versus $\gamma_{\mathrm{CKD\text{-}LT}}$ or γ_{eff} is based on a combination of the modified CKD method (CKD-LT) and the CKD method (a CKD-based method using Matlab) which was described in our previous study (Li et al., 2016). The derivation principle is shown in Fig. D1. For one specific experiment configuration, both CKD and CKD-LT can generate a correlation table (i.e., $\mathrm{Table_{CKD}}$ for CKD and $\mathrm{Table_{CKD\text{-}LT}}$ for CKD-LT) with its first column being penetration (i.e., C_{CKD}/C_0 or $C_{\mathrm{CKD-LT}}/C_0$) and the second column the corresponding uptake coefficient ($\gamma_{\mathrm{CKD,n}}$ or $\gamma_{\mathrm{CKD-LT,n}}$), and their one-to-one correspondence is indicated by the same subscripts (j,k, etc.), as shown in Fig. D1. The abbreviations and symbols are explained in Appendix A. With local turbulence, a penetration (C/C_0) obtained from flow tube experiments corresponds to one specific uptake coefficient: in $\mathrm{Table_{CKD}}$, this uptake coefficient is the calculated uptake coefficient γ_{CKD}, and in $\mathrm{Table_{CKD\text{-}LT}}$, it refers to the uptake coefficient $\gamma_{\mathrm{CKD\text{-}LT}}$. That is, with one identified C/C_0 the corresponding γ_{CKD} and $\gamma_{\mathrm{CKD\text{-}LT}}$ can be derived using CKD and CKD-LT, respectively, and $\gamma_{\mathrm{CKD}}/\gamma_{\mathrm{CKD\text{-}LT}}$ can thereafter be determined.

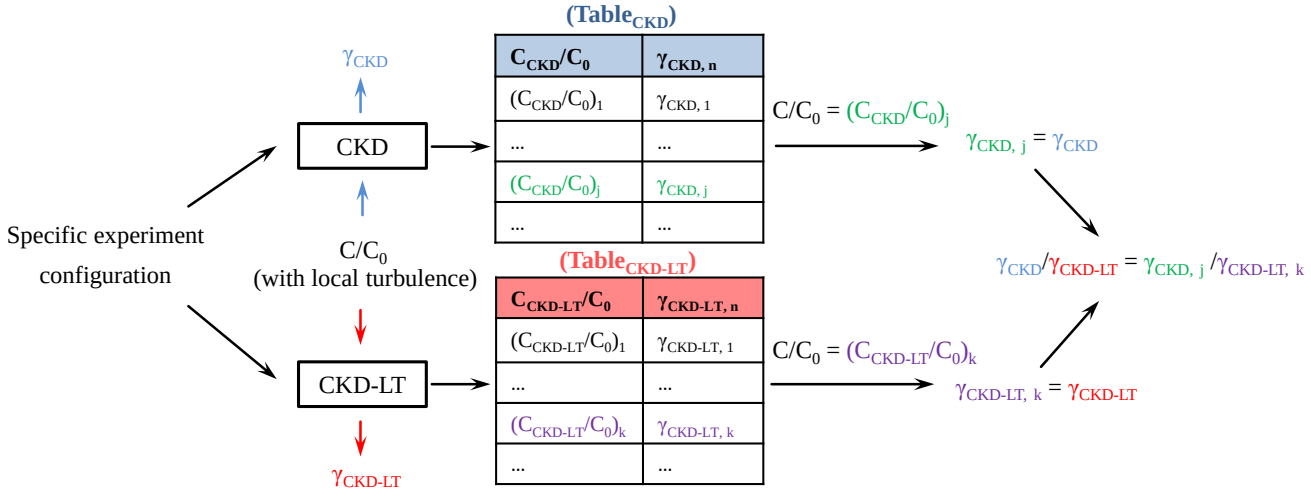

Figure D1. Schematic of the derivation principle for γ_{CKD} / $\gamma_{CKD\text{-}LT}$. The abbreviations and symbols are explained in Appendix A.

In order to facilitate flow tube designers to evaluate $\gamma_{CKD}/\gamma_{CKD\text{-}LT}$ basing on their own experiment configurations, a tutorial derivation procedure is shown as following, and the $\gamma_{CKD}/\gamma_{CKD\text{-}LT}$ versus γ_{CKD} derivation details of the case (the solid circle in Fig. 6) studied in the work by Li et al. (2016) are further elucidated as a derivation example.

1. In terms of input experimental parameters into CKD and CKD-LT models, for CKD and CKD-LT model calculation, the input parameters include coated-wall region length L, volume flow rate F, flow tube radius R_0, the ratio of geometric coating thickness to tube radius δ_g/R_0, the ratio of coating roughness height to geometric coating thickness δ_r/δ_g, experimental temperature T, experimental pressure P, mean molecular speed of the gas reactant ω, and diffusion coefficient of the gas reactant D. For example, $L = 0.25\,\text{m}$, $F = 1\times10^{-3}/60\,\text{m}^3\,\text{s}^{-1}$, $R_0 = 0.0035\,\text{m}$, $\delta_g/R_0 = 0.15$, $\delta_r/\delta_g = 0.2$, $T = 296\,\text{K}$, $P = 101\,\text{kPa}$, $\omega = 457.16\,\text{m}\,\text{s}^{-1}$ (gas reactant is HCHO), and $D = 1.77\times10^{-5}\,\text{m}^2\,\text{s}^{-1}$ (HCHO diffusion within nitrogen at 296 K and 101 kPa).

2. For models' output penetration versus uptake coefficient results, with CKD, the model calculation results are saved as an Excel file (i.e., Table$_{CKD}$ in Fig. D1), with its first column as the penetration C/C_0 (i.e., C_{CKD}/C_0) and the second column as the calculated uptake coefficient γ_{CKD} (i.e., $\gamma_{CKD,n}$). With CKD-LT, the model calculation results are saved as an Excel file (i.e., Table$_{CKD\text{-}LT}$ in Fig. D1), with its first column as the penetration C/C_0 (i.e., C_{CKD-LT}/C_0) and the second column as the uptake coefficient $\gamma_{CKD\text{-}LT}$ (i.e., $\gamma_{CKD-LT,n}$).

3. Regarding derivation of γ_{CKD} / $\gamma_{CKD\text{-}LT}$ versus γ_{CKD} or γ_{eff}, for previous flow tube experiments which might be influenced by coating surface roughness, a measured penetration C/C_0 can point to a corresponded calculated uptake coefficient γ_{CKD} using the CKD model generated table (Table$_{CKD}$). Meanwhile, this measured C/C_0 can also match an uptake coefficient $\gamma_{CKD\text{-}LT}$ using the CKD-LT model generated table (Table$_{CKD\text{-}LT}$). Then, γ_{CKD} / $\gamma_{CKD\text{-}LT}$ versus γ_{CKD} can be derived. On the other hand, the identified C/C_0 can be used for Eq. (C1) to derive γ_{eff}, and γ_{CKD} / γ_{CKD-L} versus γ_{eff} can be derived. For example, $C/C_0 = 0.34$, $\gamma_{CKD} = 5.50\times10^{-5}$, $\gamma_{CKD\text{-}LT} = 5.29\times10^{-5}$, $\gamma_{eff} = 4.83\times10^{-5}$, and $\gamma_{CKD}/\gamma_{CKD-LT} = 1.04$.

Appendix E: Matlab code for CKD and CKD-LT

E1 CKD

```
% Basic Information
%------------------------------------------------------------------------
% Model Name: CKD
% Model Description: Derive uptake coefficient under merely molecular
%                    diffusion conditions (molecular diffusion correction)
% Developed by: Guo Li, Yafang Cheng, Hang Su and Ulrich Pöschl
% Contact: guo.li@mpic.de
% Developed at: 25.October.2017
% References: Murphy, D. M. and Fahey, D. W., Analytical Chemistry, 1987
%             Li,G.,et al., Atmos.Chem.Phys.,2016;
%------------------------------------------------------------------------

% How to Use
%------------------------------------------------------------------------
% 1st step: Input parameters according to the experimental configuration
% 2nd step: Save and run the Main function
% 3rd step: After running the function, check the output Excel in the folder
%           where the code is located
%------------------------------------------------------------------------

function Main
% Main function
% Input Parameters
%************************************************************************
% The length of coated-wall flow tube L, m
L = 0.25;
% The sample volume flow rate F, m^3/s
F = 1*10^(-3)/60;
% Temperature at standard conditions T0, K
T0 = 273;
% Pressure at standard conditions P0, kPa
P0 = 101;
% Temperature at experimental conditions T, K
T = 296;
% Pressure at experimental conditions P, kPa
P = 101;
% The minimum value of the uptake coefficient g, g_min
g_min = 1e-7;
% The maximum value of the uptake coefficient g, g_max
g_max = 1e-4;
% The number of g between g_min and g_max, g_n
g_n = 1000;
% Mean molecular velocity of the gas analyte v, m/s
global v
v = 457.16;
% The ratio between geometric coating thickness δg and tube radius R0, a
global a
a = 0.15;
% The ratio between roughness height δr and geometric coating thickness δg, b
global b
b = 0.2;
% Flow tube radius without coating R0, m
global R0
R0 = 0.0035;
% The diffusion coefficient of gas analyte at T and P, D, m^2/s
global D
D = 0.0000177;
%************************************************************************
% Input END
t0=L*pi*D/(2*F)*(T0/T)*(P/P0);
Pdex1(t0,g_min,g_max,g_n)
%------------------------------------------------------------------------
```

```
function N = N_f(g)
% Sherwood Number
global R0
global a
global b
global v
global D
R = R0*(1-a+0.5*b*a);
N = 0.5*(v*R/D).*g./(2-g);
%--------------------------------------------------------------------------
function u0 = Pdex1ic(x)
% Initial conditions
u0 = 1;
%--------------------------------------------------------------------------
function [pl,ql,pr,qr] = Pdex1bc(xl,ul,xr,u,t)
% Boundary conditions
global g_i;
pl = 0;
ql = 0;
pr = N_f(g_i)*u;
qr = 1;
%--------------------------------------------------------------------------
function [c,f,s] = Pdex1pde(x,t,u,DuDx)
% Partial differential equation setting
c = 1-x^2;
f = DuDx;
s = 0;
%--------------------------------------------------------------------------
function Pdex1(t0,g_min,g_max,g_n)
% Partial differential equation
global g_i
global a
m = 1;
x = linspace(0,1,100);
t = linspace(0,t0,100);
g = linspace(g_min,g_max,g_n);
h = waitbar(0,'Please wait...');
steps = length(g);
for i=1:length(g)
    g_i = g(i);
    sol = pdepe(m,@Pdex1pde,@Pdex1ic,@Pdex1bc,x,t);
    u = sol(:,:,1);
    N_f(g(i))
    end_mean_u(i) = mean(u(end,:));
    waitbar(i / steps)
end
    A = [end_mean_u',g'];
close(h)
table_g = [end_mean_u',g'];

% Output Results
%--------------------------------------------------------------------------
xlswrite(['results',num2str(a),num2str(g_min),'.xls'], table_g);
%--------------------------------------------------------------------------
```

E2 CKD-LT

```
% Basic Information
%------------------------------------------------------------------------
% Model Name: CKD-LT
% Model Description: Derive uptake coefficient under molecular diffusion
%                    and surface-roughness-induced local turbulence
%                    conditions (for local turbulence effects estimation
%                    when combined with the CKD model)
% Developed by: Guo Li, Yafang Cheng, Hang Su and Ulrich Pöschl
% Contact: guo.li@mpic.de
% Developed at: 25.October.2017
% References: Murphy, D. M. and Fahey, D. W., Analytical Chemistry, 1987;
%             Li,G.,et al., Atmos.Chem.Phys.,2016;
%------------------------------------------------------------------------

% How to Use
%------------------------------------------------------------------------
% 1st step: Input parameters according to the experimental configuration
% 2nd step: Save and run the Main function
% 3rd step: After running the function, check the output Excel in the folder
%           where the code is located
%------------------------------------------------------------------------

function Main
% Main function
% Input Parameters
%************************************************************************
% The length of the coated-wall flow tube L, m
L = 0.25;
% The minimum value of the uptake coefficient g, g_min
g_min = 1e-7;
% The maximum value of the uptake coefficient g, g_max
g_max = 1e-4;
% The number of g between g_min and g_max, g_n
g_n = 1000;
% The sample volume flow rate F, m^3/s
global F
F = 1*10^(-3)/60;
% Temperature at standard conditions T0, K
global T0
T0 = 273;
% Pressure at standard conditions P0, kPa
global P0
P0 = 101;
% Temperature at experimental conditions T, K
global T
T = 296;
% Pressure at experimental conditions P, kPa
global P
P = 101;
% Mean molecular velocity of the gas analyte at T and P, v, m/s
global v
v = 457.16;
% The ratio between geometric coating thickness δg and tube radius R0, a
global a
a = 0.15;
% The ratio between roughness height δr and geometric coating thickness δg, b
global b
b = 0.2;
% Flow tube radius without coating R0, m
global R0
R0 = 0.0035;
```

```
% Diffusion coefficient of the gas analyte at T and P, D, m^2/s
global D
D = 0.0000177;
%*************************************************************************
% Input END
F1 = F*(1-a)^2/(1-a+0.5*a*b)^2;
t0 = L*pi*D/(2*F1)*(T0/T)*(P/P0);
Pdex1(t0,g_min,g_max,g_n)
%-------------------------------------------------------------------------
function N = N_f(g)
% Sherwood Number
global R0
global a
global v
global D
R = R0*(1-a);
N = 0.5*(v*R/D).*g./(2-g);
%-------------------------------------------------------------------------
function u0 = Pdex1ic(x)
% Initial conditions
u0 = 1;
%-------------------------------------------------------------------------
function [pl,ql,pr,qr] = Pdex1bc(xl,ul,xr,u,t)
% Boundary conditions
global g_i;
pl = 0;
ql = 0;
pr = N_f(g_i)*u;
qr = 1;
%-------------------------------------------------------------------------
function [c,f,s] = Pdex1pde(x,t,u,DuDx)
% Partial differential equation setting
c = 1-x^2;
f = DuDx;
s = 0;
%-------------------------------------------------------------------------
function Pdex1(t0,g_min,g_max,g_n)
% Partial differential equation
global g_i
global a
m = 1;
x = linspace(0,1,100);
t = linspace(0,t0,100);
g = linspace(g_min,g_max,g_n);
h = waitbar(0,'Please wait...');
steps = length(g);
for i=1:length(g)
    g_i = g(i);
    sol = pdepe(m,@Pdex1pde,@Pdex1ic,@Pdex1bc,x,t);
    u = sol(:,:,1);
    N_f(g(i))
    end_mean_u(i)= mean(u(end,:));
    waitbar(i / steps)
end
close(h)
table_g = [end_mean_u',g'];

% Output Results
%-------------------------------------------------------------------------
xlswrite(['results',num2str(a),num2str(g_min),'.xls'], table_g);
%-------------------------------------------------------------------------
```

Competing interests. The authors declare that they have no conflict of interest.

Acknowledgements. This study was supported by the Max Planck Society (MPG) and National Natural Science Foundation of China (grant nos. 41330635 and 91644218). Guo Li acknowledges the financial support from the China Scholarship Council (CSC). Yafang Cheng and Hang Su conceived the study. Guo Li., Yafang Cheng, Hang Su, and Ulrich Pöschl developed the methods. Guo Li performed data analysis. Yafang Cheng, Hang Su, Ulrich Pöschl, Uwe Kuhn, Markus Ammann, and Min Shao discussed the results. Guo Li, Yafang Cheng, and Hang Su wrote the manuscript with inputs from all coauthors.

The article processing charges for this open-access publication were covered by the Max Planck Society.

Edited by: Aijun Ding
Reviewed by: two anonymous referees

References

Achdou, Y., Pironneau, O., and Valentin, F.: Effective Boundary Conditions for Laminar Flows over Periodic Rough Boundaries, J. Comput. Phys., 147, 187–218, https://doi.org/10.1006/jcph.1998.6088, 1998.

Bartels-Rausch, T., Huthwelker, T., Gaggeler, H. W., and Ammann, M.: Atmospheric pressure coated-wall flow-tube study of acetone adsorption on ice, J. Phys. Chem. A, 109, 4531–4539, 2005.

Bedjanian, Y., Romanias, M. N., and El Zein, A.: Interaction of OH Radicals with Arizona Test Dust: Uptake and Products, J. Phys. Chem. A, 117, 393–400, 2013.

Brown, R. L.: Tubular Flow Reactors With First-Order Kinetics, J. Res. Natl. Bur. Stand., 83, 1–8, 1978.

Chu, L. T., Diao, G. W., and Chu, L.: Kinetics of HOBr uptake on NaBr and NaCl surfaces at varying relative humidity, J. Phys. Chem. B, 106, 5679–5688, 2002.

Cooney, D. O., Kim, S.-S., and James Davis, E.: Analyses of mass transfer in hemodialyzers for laminar blood flow and homogeneous dialysate, Chem. Eng. Sci., 29, 1731–1738, https://doi.org/10.1016/0009-2509(74)87031-4, 1974.

Davies, J. A. and Cox, R. A.: Kinetics of the heterogeneous reaction of HNO_3 with NaCl: Effect of water vapor, J. Phys. Chem. A, 102, 7631–7642, 1998.

Davis, E. J.: Exact solutions for a class of heat and mass transfer problems, Can. J. Chem. Eng., 51, 562–572, https://doi.org/10.1002/cjce.5450510506, 1973.

Donaldson, M. A., Berke, A. E., and Raff, J. D.: Uptake of Gas Phase Nitrous Acid onto Boundary Layer Soil Surfaces, Environ. Sci. Technol., 48, 375–383, 2014a.

Donaldson, M. A., Bish, D. L., and Raff, J. D.: Soil surface acidity plays a determining role in the atmospheric-terrestrial exchange of nitrous acid, P. Natl. Acad. Sci. USA, 111, 18472–18477, 2014b.

El Zein, A. and Bedjanian, Y.: Reactive Uptake of HONO to TiO_2 Surface: "Dark" Reaction, J. Phys. Chem. A, 116, 3665–3672, 2012.

Fernandez, M. A., Hynes, R. G., and Cox, R. A.: Kinetics of $ClONO_2$ Reactive Uptake on Ice Surfaces at Temperatures of the Upper Troposphere, J. Phys. Chem. A, 109, 9986–9996, https://doi.org/10.1021/jp053477b, 2005.

Gloss, D. and Herwig, H.: Wall roughness effects in laminar flows: an often ignored though significant issue, Exp. Fluids, 49, 461–470, 2010.

Herwig, H., Gloss, D., and Wenterodt, T.: A new approach to understanding and modelling the influence of wall roughness on friction factors for pipe and channel flows, J. Fluid. Mech., 613, 35–53, 2008.

Howard, C. J.: Kinetic measurements using flow tubes, The Journal of Physical Chemistry, 83, 3–9, https://doi.org/10.1021/j100464a001, 1979.

Hynes, R. G., Mössinger, J. C., and Cox, R. A.: The interaction of HCl with water-ice at tropospheric temperatures, Geophys. Res. Lett., 28, 2827–2830, 10.1029/2000GL012706, 2001.

Hynes, R. G., Fernandez, M. A., and Cox, R. A.: Uptake of HNO_3 on water-ice and coadsorption of HNO_3 and HCl in the temperature range 210–235 K, J. Geophys. Res.-Atmos., 107, 4797, https://doi.org/10.1029/2001JD001557, 2002.

Jayne, J. T., Pöschl, U., Chen, Y.-m., Dai, D., Molina, L. T., Worsnop, D. R., Kolb, C. E., and Molina, M. J.: Pressure and Temperature Dependence of the Gas-Phase Reaction of SO_3 with H_2O and the Heterogeneous Reaction of SO_3 with H_2O/H_2SO_4 Surfaces, J. Phys. Chem. A, 101, 10000–10011, 10.1021/jp972549z, 1997.

Khalizov, A. F., Cruz-Quinones, M., and Zhang, R. Y.: Heterogeneous Reaction of NO_2 on Fresh and Coated Soot Surfaces, J. Phys. Chem. A, 114, 7516–7524, 2010.

Knopf, D. A., Pöschl, U., and Shiraiwa, M.: Radial Diffusion and Penetration of Gas Molecules and Aerosol Particles through Laminar Flow Reactors, Denuders, and Sampling Tubes, Anal. Chem., 87, 3746–3754, 2015.

Kolb, C. E., Cox, R. A., Abbatt, J. P. D., Ammann, M., Davis, E. J., Donaldson, D. J., Garrett, B. C., George, C., Griffiths, P. T., Hanson, D. R., Kulmala, M., McFiggans, G., Pöschl, U., Riipinen, I., Rossi, M. J., Rudich, Y., Wagner, P. E., Winkler, P. M., Worsnop, D. R., and O'Dowd, C. D.: An overview of current issues in the uptake of atmospheric trace gases by aerosols and clouds, Atmos. Chem. Phys., 10, 10561–10605, https://doi.org/10.5194/acp-10-10561-2010, 2010.

Kolmogorov, A. N.: The Local Structure of Turbulence in Incompressible Viscous Fluid for Very Large Reynolds Numbers, Proc.: Math. Phys. Sci., 434, 9–13, 1991.

Landy, J. C., Isleifson, D., Komarov, A. S., and Barber, D. G.: Parameterization of Centimeter-Scale Sea Ice Surface Roughness Using Terrestrial LiDAR, IEEE T. Geosci. Remote Sens., 53, 1271–1286, 2015.

Li, G., Su, H., Li, X., Kuhn, U., Meusel, H., Hoffmann, T., Ammann, M., Pöschl, U., Shao, M., and Cheng, Y.: Uptake of gaseous formaldehyde by soil surfaces: a combination of adsorption/desorption equilibrium and chemical reactions, Atmos. Chem. Phys., 16, 10299–10311, https://doi.org/10.5194/acp-16-10299-2016, 2016.

Mauri, R.: General Features of Fluid Mechanics, in: Transport Phenomena in Multiphase Flows, edited by: André Thess, R. M., Springer International Publishing, Switzerland, 39–48, 2015.

McCabe, J. and Abbatt, J. P. D.: Heterogeneous Loss of Gas-Phase Ozone on n-Hexane Soot Surfaces: Similar Kinetics to Loss on Other Chemically Unsaturated Solid Surfaces, J. Phys. Chem. C, 113, 2120–2127, 2009.

McNeill, V. F., Loerting, T., Geiger, F. M., Trout, B. L., and Molina, M. J.: Hydrogen chloride-induced surface disordering on ice, P. Natl. Acad. Sci. USA, 103, 9422–9427, 2006.

Mohanty, A. K. and Asthana, S. B. L.: Laminar-Flow in the Entrance Region of a Smooth Pipe, J. Fluid. Mech., 90, 433–447, 1979.

Monge, M. E., D'Anna, B., Mazri, L., Giroir-Fendler, A., Ammann, M., Donaldson, D. J., and George, C.: Light changes the atmospheric reactivity of soot, P. Natl. Acad. Sci. USA, 107, 6605–6609, 2010.

Murphy, D. M., and Fahey, D. W.: Mathematical Treatment of the Wall Loss of a Trace Species in Denuder and Catalytic-Converter Tubes, Anal. Chem., 59, 2753–2759, 1987.

Nikuradse, J.: Laws of flow in rough pipes, NACA Technical Memorandum, 1292, 1–62, 1950.

Oke, T. R., Mills, G., Christen, A., and Voogt, J. A.: Airflow, in: Urban Climates, 1st ed., Cambridge University Press, 77–121, 2017.

Onstott, R. G.: SAR and Scatterometer Signatures of Sea Ice, in: Microwave Remote Sensing of Sea Ice, American Geophysical Union, Washington, USA, 73–104, 2013.

Petitjean, M., Mirabel, P., and Le Calve, S.: Uptake Measurements of Acetaldehyde on Solid Ice Surfaces and on Solid/Liquid Supercooled Mixtures Doped with HNO_3 in the Temperature Range 203–253 K, J. Phys. Chem. A, 113, 5091–5098, 2009.

Poon, C. Y. and Bhushan, B.: Comparison of surface roughness measurements by stylus profiler, AFM and non-contact optical profiler, Wear, 190, 76–88, 1995.

Pöschl, U., Canagaratna, M., Jayne, J. T., Molina, L. T., Worsnop, D. R., Kolb, C. E., and Molina, M. J.: Mass Accommodation Coefficient of H_2SO_4 Vapor on Aqueous Sulfuric Acid Surfaces and Gaseous Diffusion Coefficient of H_2SO_4 in N_2/H_2O, J. Phys. Chem. A, 102, 10082–10089, https://doi.org/10.1021/jp982809s, 1998.

Prandtl, L.: Über Flüessigkeitsbewegung bei sehr kleiner Reibung, Verhandl. III, Intern. Math. Kongr., Heidelberg, 484–491, 1904.

Qiu, C., Wang, L., Lal, V., Khalizov, A. F., and Zhang, R. Y.: Heterogeneous Reactions of Alkylamines with Ammonium Sulfate and Ammonium Bisulfate, Environ. Sci. Technol., 45, 4748–4755, 2011.

Shiraiwa, M., Ammann, M., Koop, T., and Pöschl, U.: Gas uptake and chemical aging of semisolid organic aerosol particles, P. Natl. Acad. Sci. USA, 108, 11003–11008, 2011.

Shiraiwa, M., Pöschl, U., and Knopf, D. A.: Multiphase Chemical Kinetics of NO_3 Radicals Reacting with Organic Aerosol Components from Biomass Burning, Environ. Sci. Technol., 46, 6630–6636, 2012.

Steimer, S. S., Berkemeier, T., Gilgen, A., Krieger, U. K., Peter, T., Shiraiwa, M., and Ammann, M.: Shikimic acid ozonolysis kinetics of the transition from liquid aqueous solution to highly viscous glass, Phys. Chem. Chem. Phys., 17, 31101–31109, 2015.

Stemmler, K., Ammann, M., Donders, C., Kleffmann, J., and George, C.: Photosensitized reduction of nitrogen dioxide on humic acid as a source of nitrous acid, Nature, 440, 195–198, 2006.

Symington, A., Leow, L. M., Griffiths, P. T., and Cox, R. A.: Adsorption and Hydrolysis of Alcohols and Carbonyls on Ice at Temperatures of the Upper Troposphere, J. Phys. Chem. A, 116, 5990–6002, https://doi.org/10.1021/jp210935b, 2012.

Taylor, J. B., Carrano, A. L., and Kandlikar, S. G.: Characterization of the effect of surface roughness and texture on fluid flow – past, present, and future, Int. J. Therm. Sci., 45, 962–968, 2006.

VandenBoer, T. C., Young, C. J., Talukdar, R. K., Markovic, M. Z., Brown, S. S., Roberts, J. M., and Murphy, J. G.: Nocturnal loss and daytime source of nitrous acid through reactive uptake and displacement, Nat. Geosci., 8, 55–60, 2015.

Wang, L., Wang, W. G., and Ge, M. F.: Heterogeneous uptake of NO_2 on soils under variable temperature and relative humidity conditions, J. Environ. Sci.-China, 24, 1759–1766, 2012.

White, F. M.: Viscous flow in ducts, in: Fluid Mechanics, edited by: Holman, J. P. and Lloyd, J., McGraw-Hill Higher Education, Columbus, USA, 325–426, 1998.

Zhang, C. B., Chen, Y. P., and Shi, M. H.: Effects of roughness elements on laminar flow and heat transfer in microchannels, Chem. Eng. Process., 49, 1188–1192, 2010.

Zhou, G. B. and Yao, S. C.: Effect of surface roughness on laminar liquid flow in micro-channels, Appl. Therm. Eng., 31, 228–234, 2011.